AN *IN SITU* FTIR-DRIFTS STUDY ON BIMETALLIC CDRM CATALYSTS

by

Salih Emre Demirel

B.S., Chemical Engineering, Boğaziçi University, 2013

Submitted to the Institute for Graduate Studies in
Science and Engineering in partial fulfillment of
the requirements for the degree of
Master of Science

Graduate Program in Chemical Engineering
Boğaziçi University

2015

to my family

ACKNOWLEDGEMENTS

First, I would like to express my truthful gratitude to my thesis supervisor Prof. Ahmet Erhan Aksoylu who did not hesitate to share his wisdom and expertise in catalysis with me. It was privilege for me to work with him during my thesis. I am deeply grateful to Prof. Aksoylu for his support and encouragement during my thesis.

I would like to express my sincere appreciations for the members of my thesis committee, Prof. Ramazan Yıldırım and Assoc. Prof. Hasan Bedir, who devoted their valuable time to read and comment on my thesis in such a short notice.

I would like to thank my dear friends Özgür Yaşar Çağlar, Serhat Erşahin, Serdar Özsezen, Elif Topal and Onur Yanardağ for their undertanding and support during my hard times and for their presence in my happy memories. I will always remember them with great warmth in my hearth. I also thank to Barış Burnak and Coşar Doğa Demirhan for their help during my thesis. I am highly excited for the next four years that we will spend together in Texan deserts.

I would like to also thank to Elif x (Can+Erdinç+Gençtürk), Begüm Alaybeyoğlu and Manouchehr Nadjafi for their endless support and friendship all the time. Without them, it would be much harder to complete this thesis. They will remain as the indispensable members of my 'favorite' group.

Very special thanks to Bilge Kerem Aksakal, Ali Uzun, Aybüke Leba, Utku Deniz, Burcu Karagöz, Melis Yıldırım, Merve Eropak, Sinan Koç, Özgü Özer, Fidan Sümbül, Zeynep Kürkçüoğlu, Fabian Huneke and Volkan Erinç for their friendship and for giving me support and motivation during my studies.

Special thanks to Aysun İpek Paksoy who guided me whenever I needed her help and thaught me the art of spectroscopy. It would be much harder to complete this thesis without her support. I also want to thank Melek Selcen Başar and ali Uzun for their valuable time that they spent on helping me. Also, very special thanks to Coşar Doğa

Demirhan and Serhat Erşahin for their help and valuable time that they spared for my experimental work.

Cordial thanks are for Yakup Bal for his technical assistance during my thesis. I would also like to thank Bilgi Dedeoğlu, Başak Ünen and Melike Gürbüz for their friendly attitude.

Finally, I want to thank to my dear parents who has supported me during my educational life and encouraged me to pursue an academic career. Without them, I would not be able to write this thesis. Also, I want to thank my beloved sisters, Zeynep Merve Demirel and Elif Demirel who have been and will always be in my heart. I also want to thank to my dear grandfather Selahattin Olcay and grandmother Semiha Olcay for their encouragement and prayings during my educational life.

Financial support provided by TUBITAK through Project 111M144 is greatly acknowledged.

ABSTRACT

AN *IN SITU* FTIR-DRIFTS STUDY ON BIMETALLIC CDRM CATALYSTS

The purpose of this research was to gain a deeper insight into the difference between the micro-structural and kinetic properties of two bimetallic catalysts, i.e. 0.3Pt10Ni/Al_2O_3 and 0.2Pt15Ni/Al_2O_3, which have been previously studied and shown to have different kinetic behaviors in CDRM reaction. In this context, CO characterization, CO-TPD, CO_2 and CH_4 adsorption and *in situ* reaction experiments by using FTIR-DRIFTS system were conducted. CO characterization studies conducted at room temperature revealed that dispersion of Ni on the sample containing higher amount of Pt, i.e. 0.3Pt10Ni, was better than that on the 0.2Pt15Ni sample. CO adsorption experiments performed at 300 °C showed that the lower Ni:Pt ratio of the 0.3Pt10Ni sample resulted in a higher extent of reduction. FTIR-DRIFTS-CO-TPD experiments revealed that CO species adsorb in linear fashion were more thermally stable on 0.3Pt-10Ni sample than the ones adsorbed on 0.2Pt15Ni sample. Furthermore, more multicentered CO species remaining on the surface of 0.2Pt15Ni sample after desorption indicates that decrease in the Ni:Pt ratio causes a decrease in thermal stability of these species. CO_2 adsorption experiments conducted at 300 °C revealed that more formate species were formed on 0.3Pt10Ni sample indicating its higher activity in CO_2 utilization. In the CH_4 adsorption experiments, CO formation was observed on both samples showing that the support also has a role in the course of the CDRM reaction. Due to the lower dispersion of 0.2Pt15Ni sample, there formed fewer amounts of formate species on this sample. *In situ* reaction tests revealed that more gaseous CO and more formate type species were formed on 0.3Pt10Ni sample. Differences in the CO adsorption behavior, CO_2 utilization and CH_4 adsorption characteristics of the two samples proves the previous findings on the two catalysts indicating there are significant differences among two samples in terms of the CDRM reaction pathways on them.

ÖZET

BİMETALİK METANIN KARBONDİOKSİT REFORMLAMASI (CDRM) KATALİZÖRLERİ ÜZERİNDE FTIR-DRIFTS ÇALIŞMASI

Bu çalışmanın amacı, Metanın Karbondioksit Reformlaması Reaksiyonu (CDRM) için daha önce çalışılmış ve farklı kinetik davranışlar sergilemiş bimetalik 0.3Pt10Ni/Al_2O_3 ve 0.2Pt15Ni/Al_2O_3 katalizörleri üzerine daha derin bir bakış açısı kazanmaktır. Bu amaçla, FTIR-DRIFTS sistemi kullanılarak CO karakterizasyonu, CO-TPD, CO_2 ve CH_4 adsorpsiyon ve reaksiyon deneyleri yapılmıştır. Oda sıcaklığında gerçekleştirilen CO adsorpsiyon deneyleri, Ni metal dağılımının, daha fazla Pt metali içeren 0.3Pt10Ni katalizörünün üzerinde daha iyi olduğunu göstermiştir. 0.3Pt10Ni katalizörünün daha az Ni:Pt oranına sahip olmasının 300 °C sıcaklığında yapılan CO adsorpsiyon deneylerinde bu ürünün daha iyi indirgenmesini sağladığı gözlemlenmiştir. FTIR-DRIFTS-CO-TPD deneyleri, yüzeye doğrusal olarak bağlanan CO moleküllerinin ısıya karşı dayanıklılıklarının 0.3Pt10Ni katalizörü üzerinde 0.2Pt15Ni katalizörüne kıyasla daha yüksek olduğu gözlenmiştir. Ayrıca, 0.2Pt15Ni katalizörünün üzerinde desorpsiyon sonucu daha fazla çok-merkezli bağlanmış CO moleküllerinin gözlenmesi, Ni:Pt oranının azalmasının yüzeye çok-merkezli yapıda bağlanan CO moleküllerinin stabilitelerinde azalmaya neden olduğunu göstemiştir. 300 °C sıcaklıkta gerçekleştirilen CO_2 adsorpsiyon deneylerinde, 0.3Pt10Ni katalizörü üzerinde daha çok format oluşumu gözlemlenmiştir. Daha fazla format oluşumu, bu katalizörün CO_2 kullanımında daha etkin olduğunu göstermiştir. CH_4 adsorpsiyonu deneyleri sırasında gözlemlenen CO oluşumu, katalizör desteğinin de Metanın Karbondioksit Reformlaması Reaksiyonu sırasında etkin olduğunu göstermiştir. Ni metal dağılımı daha az olduğu için 0.2Pt15Ni katalizörü üzerinde daha az format oluşumu gözlemlenmiştir. Reaksiyon deneyleri sırasında 0.3Pt10Ni katalizörü üzerinde daha çok CO ve format oluşumu gözlemlenmiştir. CO adsorpsiyon davranışlarında, CO_2 kullanımlarında ve CH_4 adsorpsiyon karakterlerinde gözlenen farklar, bu iki katalizör üzerinde daha önce yapılan araştırmaları doğrulayarak, Metanın Karbondioksit Reformlaması Reaksiyonunun bu iki katalizör üzerinde farklı reaksiyon mekanizmaları izlediğini göstermiştir.

TABLE OF CONTENTS

ACKNOWLEDGEMENTS iv
ABSTRACT vi
ÖZET vii
LIST OF FIGURES x
LIST OF TABLES xiii
LIST OF SYMBOLS xiv
LIST OF ACRONYMS/ABBREVIATIONS xv
1. INTRODUCTION 1
2. LITERATURE SURVEY 4
2.1. Catalysts for Carbon Dioxide Reforming of Methane 5
2.2. Kinetic and Mechanistic Studies on CDRM 10
2.2.1. CH_4 Activation 11
2.2.2. CO_2 Activation 13
2.2.3. Reaction Mechanisms for Catalytic Dry Reforming of Methane 14
2.3. FTIR-DRIFTS Studies 20
2.3.1. CO Adsorption and Surface Characterization 22
2.3.2. CO_2 Adsorption 27
2.3.3. CH_4 Adsorption and *In situ* Reaction Tests 28
3. EXPERIMENTAL WORK 31
3.1. Materials 31
3.1.1. Chemicals 31
3.1.2. Gases and Liquids 31
3.2. Experimental Systems 32
3.2.1. Catalyst Preparation Systems 32
3.2.2. Catalyst Characterization and Reaction System 33
3.3. Catalyst Preparation and Pretreatment 34
3.4. Catalyst Characterization and Reaction Tests 35
3.4.1. Pretreatment Tests 35
3.4.2. Adsorption and Reaction Tests 37
4. RESULTS AND DISCUSSIONS 40

4.1. Effect of Pretreatment 41
4.2. CO Adsorption Experiments 43
4.2.1. CO Adsorption Experiments at Room Temperature 43
4.2.2. CO Adsorption Experiments at 300 °C 48
4.2.3. Temperature Programmed CO Desorption Tests 50
4.3. CO_2 Adsorption Experiments 54
4.3.1. CO_2 Adsorption Experiments at Room Temperature 54
4.3.2. CO_2 Adsorption Experiments at 300 °C 57
4.4. CH_4 Adsorption Experiments 59
4.4.1. CH_4 Adsorption Experiments at Room Temperature 59
4.4.2. CH_4 Adsorption Experiments at 300 °C 61
4.5. *In situ* Reaction Experiments 65
5. CONCLUSIONS AND RECOMMENDATIONS 69
5.1. Conclusions 69
5.2. Recommendations 70
REFERENCES 72

LIST OF FIGURES

Figure 2.1. Gibbs free energy values as a function of temperature for (a) Carbon Dioxide Reforming of Methane (b) Methane Decomposition (c) Reverse Water Gas Shift (d) CO Disproportionation. 5

Figure 2.2. Carbonaceous species frequently encountered in FTIR-DRIFTS studies (Köck *et al.*, 2013; Collins *et al.*, 2006). 21

Figure 3.1. Schematic diagram of the impregnation system (Akın, 1996). 33

Figure 3.2. Schematic representation of FTIR-DRIFTS system (Çağlayan, 2011). 34

Figure 4.1. Spectra obtained upon 30 min 1% CO adsorption on 0.3Pt10Ni/Al_2O_3 catalysts at room temperature with *in situ* pretreatment 1 (a), pretreatment 2 (b), pretreatment 3 (c) and pretreatment 4 (d). 41

Figure 4.2. Spectra obtained upon 30 min 1% CO adsorption followed by 30 min He flush on 0.3Pt10Ni/Al_2O_3 catalysts at room temperature with *in situ* pretreatment 1 (a), pretreatment 2 (b), pretreatment 3 (c) and pretreatment 4 (d). 42

Figure 4.3. Spectra obtained on 0.3Pt10Ni/Al_2O_3 catalyst upon 30 min 1% CO adsorption followed by 30 min He flush at room temperature. 44

Figure 4.4. Spectra obtained on 0.2Pt15Ni/Al_2O_3 catalyst upon 30 min 1% CO adsorption followed by 30 min He flush at room temperature. 47

Figure 4.5. Spectra obtained on 0.3Pt10Ni/Al_2O_3 catalyst upon 30 min 1% CO adsorption followed by 30 min He flush at 300 °C. 48

Figure 4.6. Spectra obtained on 0.2Pt15Ni/Al_2O_3 catalyst upon 30 min 1% CO adsorption followed by 30 min He flush at 300 °C. 49

Figure 4.7. Spectra obtained on 0.3Pt10Ni (left) and 0.2Pt15Ni (right) after 30 min CO flow at 25 °C (a), 30 min He flow at 25 °C (b), followed by 30 min He flow at 100 °C (c), at 200 °C (d), and at 300 °C (e). 50

Figure 4.8. Spectra obtained on 0.3Pt10Ni after 30 min 1% CO flow at 25 °C (a), 30 min He flow at 25 °C (b), after 30 min 1% CO flow at 300 °C (c), 30 min He flow at 100 °C (d), at 200 °C (e), and at 300 °C (f). 53

Figure 4.9. OCO stretching region of the spectra obtained on 0.3Pt10Ni (bottom two) and 0.2Pt15Ni (top two) after 30 min 10% CO_2 flow at 25 °C (a), 30 min He flow at 25 °C (b). 55

Figure 4.10. C-H and OH stretching region of the spectra obtained on 0.3Pt10Ni (bottom two) and 0.2Pt15Ni (top two) after 30 min 10% CO_2 flow at 25 °C (a), followed by 30 min He flow at 25 °C (b). 56

Figure 4.11. Metal carbonyl region of the spectra obtained on 0.3Pt10Ni (bottom two) and 0.2Pt15Ni (top two) after 30 min 10% CO_2 flow at 300 °C (a), followed by 30 min He flow at 300 °C (b). 57

Figure 4.12. C-H stretching region (left) and OCO region (right) of the spectra obtained on 0.3Pt10Ni (bottom two) and 0.2Pt15Ni (top two) after 30 min 10% CO_2 flow at 300 °C (a), followed by 30 min He flow at 300 °C (b). 58

Figure 4.13. Spectra obtained on 0.3Pt10Ni (bottom) and 0.2Pt15Ni (top) after 30 min 10% CH_4 flow at 25 °C. 60

Figure 4.14. Spectra obtained on 0.3Pt10Ni (bottom) and 0.2Pt15Ni (top) 30 min He flow at 25 °C. 61

Figure 4.15. Spectra obtained on 0.3Pt10Ni (bottom) and 0.2Pt15Ni (top) after 30 min 10% CH_4 flow at 300 °C. 62

Figure 4.16. Spectra obtained on 0.3Pt10Ni (bottom) and 0.2Pt15Ni (top) after 30 min He flow at 300 °C. 64

Figure 4.17. Spectra obtained on 0.3Pt10Ni (bottom four spectra) and 0.2Pt15Ni (top four spectra) after 10 minutes (a), 30 minutes (b), 60 minutes of exposure to 40% CO_2 40% CH_4 and 20% He flow at 300 °C (c), 30 minutes of He flow at 300 °C (d). 66

Figure 4.18. Spectra obtained on 0.3Pt10Ni (gray) and 0.2Pt15Ni (black) after 10 minutes (a), 30 minutes (b), 60 minutes (c) of exposure to 40% CO_2 40% CH_4 and 20% He flow at 300 °C. 67

LIST OF TABLES

Table 2.1. Band assignments of CO on Ni/Al_2O_3 (adapted from Gökaliler, 2012). 23

Table 2.2. Band assignments of CO on Pt/Al_2O_3 (adapted from Gökaliler, 2012). 24

Table 3.1. Chemicals used for catalyst preparation. 31

Table 3.2. Specifications and applications of the gases used. 32

Table 3.3. Specifications and applications of the liquids used. 32

Table 3.4. Pretreatment procedures. 36

Table 3.5. List of FTIR-DRIFTS experiments. 38

LIST OF SYMBOLS

K	Equilibrium Constant
T	Temperature
ν	Stretching vibration
δ	Bending vibration
ΔH	Standard Enthalpy of Reaction
$\Delta\nu_3$	Difference between asymmetric and symmetric vibrations

LIST OF ACRONYMS/ABBREVIATIONS

BOS	Birleşik Oksijen Sanayi
CDRM	Carbon Dioxide Reforming of Methane
DI	Deionized Water
DRIFTS	Diffuse Reflectance Infreared Fourier Transform Spectroscopy
ER	Eley-Rideal
FTIR	Fourier Transform Infra Red
GC	Gas Chromatograph
IPCC	Intergovernmental Panel of Climate Change
IR	Infra Red
LHHW	Langmuir-Hinshelwood-Hougen-Watson
MCT	Mercury-Cadmium-Telluride
Me	Metal
MS	Mass Spectrometer
RWGS	Reverse Water-Gas Shift
TOS	Time-on-Stream
TPD	Temperature-Programmed-Desorption
TPR	Temperature-Programmed-Reduction

1. INTRODUCTION

There are strong evidences in the Intergovernmental Panel of Climate Change (IPCC) 5th assessment report showing that the most important reason of global temperature rise is the increasing concentrations of greenhouse gasses -especially CO_2 owing to its *thermodynamic* stability- in the atmosphere due to manmade activities.

Carbon dioxide reforming of methane (CDRM) is the first step in utilization of two most stable greenhouse gasses, carbon dioxide and methane, in producing valuable chemical products. CDRM reaction converts methane and CO_2 into syngas (CO and H_2), which can be converted further via Fischer-Tropsch reaction to olefins, parafins, alcohols, etc. (Özkara-Aydınoğlu *et al.*, 2009):

$$CH_4 + CO_2 \leftrightarrow 2CO + 2H_2 \qquad \Delta H^0_{298} = +247\ \mathrm{kj/mol}$$

CDRM is a highly endothermic reaction requiring high operating temperatures and its side reactions produce coke deposits causing catalyst deactivation. Hence, the design and development for highly active and coke deposition resistant CDRM catalysts has become a research focus (Ni *et al.*, 2013).

Ni/γ-Al_2O_3 is the most frequently used catalyst for the reforming reactions due to its low cost and high catalytic activity (Son *et al.*, 2014). Yet, although coke formation on Ni metal can be mitigated by using excess steam in steam reforming reaction, this is not possible for the dry reforming reaction due to absence of steam. Trace amount of noble metal addition to Ni based catalysts have been shown to result in better CDRM activity and stability (Steinhauer *et al.*, 2009).

Understanding the structure–activity relationships at the molecular and atomic scale is of significant importance in assisting the improvement of existing catalytic processes as well as developing new catalytic ones. Furthermore, it is highly important to investigate the kinetics and mechanistic steps of a reaction in order to understand the rate determining steps which primarily determine the performance of a catalyst. *In situ* spectroscopic

methods are advanced tools of catalysis science providing fundamental information about catalytic structure and surface species under controlled environments. The developments in analysis systems have allowed major advances in catalysis science towards the rational design of new and efficient catalysts (Banares, 2005). Diffusive Reflectance Infrared Fourier Transform Spectroscopy, also known as FTIR-DRIFTS, is a Fourier transform infrared spectroscopy (FTIR) method which makes use of the phenomenon of diffuse reflectance, and is used primarily on powders and other solid samples (Ryczkowski, 2001). In this sense, catalysis community has been using this method for several years in order to understand the reaction mechanisms and surface interactions between the catalysts and the reactants under reaction conditions. Additionally, some researchers used FTIR-DRIFTS in order to identify the surface characteristics of the catalysts by using probe molecules, i.e. CO, NO, CH_3CN, pyridine, NH_3 etc. (Vindigni *et al.*, 2012).

In a previous study conducted in our group, performance of the bimetallic 0.3-0.5 wt. % Pt and 10-15 wt. % catalysts were investigated, and the catalyst with the lowest Ni:Pt ratio was shown to have both high CDRM activity and stability (Özkara-Aydinoğlu and Aksoylu, 2011). A following kinetic study revealed that kinetic parameters and models differed significantly by the change in Ni:Pt ratio (Özkara-Aydinoğlu and Aksoylu, 2013). In this study, FTIR-DRIFTS spectroscopy was used in order to gain a deeper insight into the structural and reaction mechanistic differences between these two bimetallic catalysts. Bimetallic $0.3Pt10Ni/Al_2O_3$ and $0.2Pt15Ni/Al_2O_3$ catalysts were characterized first with the help of CO adsorption experiments on FTIR-DRIFTS both at room temperature and at elevated temperatures, 300 °C. Following the characterization studies, FTIR-DRIFTS analysis was performed on the freshly reduced forms of both PtNi catalysts under the flow of individual reactants, under the flow of He-diluted CO_2 and He-diluted CH_4, both at room temperature and at 300 °C, aiming to understand the adsorption properties of the reactants and products on the active sites. As the last part of this study, *in situ* reaction tests were performed by feeding both of the reactants into the IR cell in order to observe the changes on the active sites and the species formed on the catalyst surface under the flow of the reactant gasses.

In Chapter 2, theoretical background of CDRM reaction, its kinetics and proposed mechanisms in the literature, with a special emphasis on the activation mechanisms of the

reactants, and literature data on the FTIR-DRIFTS studies are given. The experimental systems and procedures used in the current study are presented in Chapter 3. Experimental results and related discussions can be found in Chapter 4. Finally, Chapter 5 includes the conclusions drawn from the present study and recommendations for future work.

2. LITERATURE SURVEY

Carbon dioxide reforming of methane (CDRM) reaction converts methane and carbon dioxide catalytically into CO and H_2:

$$CH_4 + CO_2 \leftrightarrow 2CO + 2H_2 \quad \Delta H^0_{298} = +247 \text{ kj/mol} \tag{2.1}$$

CDRM is a highly endothermic reaction requiring temperatures as high as 800 ^{0}C. Carbon deposition is a common deactivation mechanism observed for CDRM catalysts. There are mainly two reactions leading to carbon deposition:

$$CH_4 \leftrightarrow C + 2H_2 \tag{2.2}$$

$$2CO \leftrightarrow C + CO_2 \tag{2.3}$$

The first reaction is known as methane decomposition while the second one is called CO disproportionation (Yang, *et al.*, 2010). Other than those two reactions, there are other side reactions occurring simultaneously with CDRM (Gallego *et al.*, 2008):

(Reverse Water Gas Shift) $$H_2 + CO_2 \leftrightarrow CO + H_2O \tag{2.4}$$

(CO_2 Methanation) $$4H_2 + CO_2 \leftrightarrow CH_4 + 2H_2O \tag{2.5}$$

(Steam Reforming of Methane) $$CH_4 + H_2O \leftrightarrow CO + 3H_2 \tag{2.6}$$

(CO Methanation) $$CO + 3H_2 \leftrightarrow CH_4 + H_2O \tag{2.7}$$

(Coke Gasification) $$C + H_2O \leftrightarrow CO + H_2 \tag{2.8}$$

Among these side reactions, methane decomposition, reverse water gas shift reaction and CO disproportionation are the ones that have more significance in the course of the CDRM. A thermodynamic analysis of these reactions by using standard free energies is given in Figure 2.1.

As standard free energy turns to negative at 640 °C, CDRM starts to proceed in the forward direction. A significant side reaction that affects the H_2/CO ratio of the product stream, reverse water gas shift reaction, is favored until 820 °C. Carbon formation via methane decomposition can occur above 557 °C, whereas its formation via CO disproportionation is favored below 700 °C (Pakhare and Spivey, 2014).

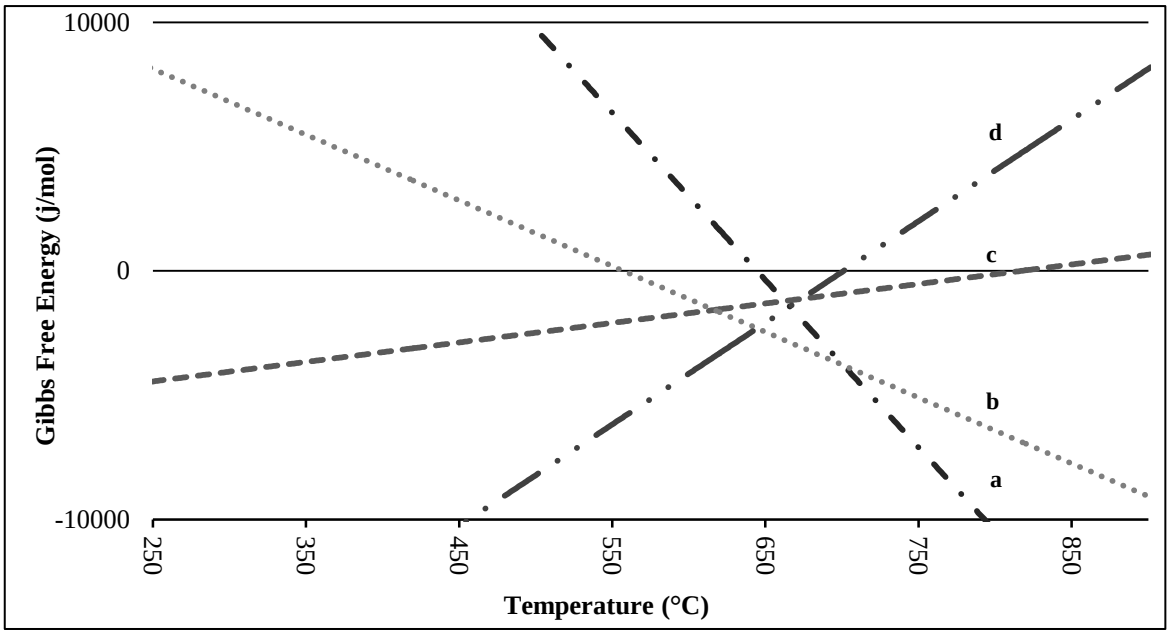

Figure 2.1. Gibbs free energy values as a function of temperature for Carbon Dioxide Reforming of Methane (a), Methane Decomposition (b), Reverse Water Gas Shift (c), CO Disproportionation (d).

2.1. Catalysts for Carbon Dioxide Reforming of Methane

An active catalyst for CDRM reaction should be thermally stable and should be resistant to carbon deposition. First study on CDRM was done by Fischer and Tropsch in 1928 over Co and Ni catalysts, and they reported severe carbon deposition on these catalysts (Pakhare and Spivey, 2014). Since then, there has been extensive work in the scientific community for design and development a cheap transition metal catalyst by utilizing mono- and multi-metallic formulations comprised of either noble metals or combination of transition metals, and/or by incorporating promoters to the supports aiming to enhance the activity and carbon deposition resistance. In the literature, noble metal catalysts Pt, Rh, Ru, Pd and first row of Group VIII transition metals Ni, Co and Fe on

both irreducible and reducible oxide supports like Al_2O_3, SiO_2, ZrO_2, La_2O_3, CeO_2, and TiO_2 were investigated for the CDRM reaction (Son *et al.*, 2014; Özkara-Aydinoğlu and Aksoylu, 2013; Sutthiumporn *et al.*, 2012; Özkara-Aydinoğlu and Aksoylu, 2011; Özkara-Aydınoğlu and Aksoylu, 2010; Özkara-Aydınoğlu *et al.*, 2009).

Alumina is used as a support in several different catalytic reactions, and also for CDRM, due to its thermal stability and coexistence of both acidic and basic sites on it. Additionally, its defective spinel structure contains a certain fraction of cation vacancies which facilitates interaction of the active component with the support. Depending on the precursors used and the conditions of pretreatment, alumina can be in different crystal phases, denoted by Greek letters χ, δ, ε, γ, η, κ, θ and ρ. Yet, due to its high surface area, γ-Al_2O_3 is the most commonly used alumina structure in heterogeneous catalysis (Hattori and Ono, 2015; Ivanova *et al.*, 2010).

Among the metals belonging to the first row of Group VIII transition metals, i.e. Ni, Co and Fe, Ni shows the highest CDRM activity according to the several studies in which γ-Al_2O_3 was used as the support material. Apart from those, monometallic noble catalysts Rh, Pd, Ru, Pt and Ir were all reported as active in CDRM reaction. In addition, noble metal catalysts have higher selectivity for carbon-free operation than those of Co, Ni and Fe due to lower carbon dissolutions in them leading to much lower carbon formation rates (Wang *et al.*, 1996; Faroldi *et al.*, 2009). Yet, limited availability of the noble metals and high costs associated with them have led the search for cheaper alternatives for the stable CDRM operation. Ni/γ-Al_2O_3 is the most frequently used catalyst for the reforming reactions due to its low cost and high catalytic activity (Son *et al.*, 2014). Yet, although coke formation on Ni metal can be mitigated by using excess steam in steam reforming reaction, this is not possible for the dry reforming reaction due to absence of steam. Hence, in order to overcome the carbon deposition problem observed on Ni/γ-Al_2O_3 catalysts and to design and develop more active and stable catalyst for CDRM reaction, several different modifications have been proposed in the literature.

Among the different modifications proposed for the Ni/γ-Al_2O_3 catalysts, there are several studies regarding the addition of alkali and alkali earth metals (such as K, Na, Ca and Mg) as promoters. These alkali and alkali earth metals affect electronic properties and

dimensions of the Ni clusters. They also modify the acidity of the surface and enrich the surface in terms of CO_2 by stabilizing surface carbonate species. Furthermore, Walter *et al.* reported that surface CH_x species react preferentially with surface OH groups rather than the surface O groups. Hence, by using alkali and alkali earth metals as promoters, surface basicity of Ni/Al_2O_3 can be improved and removal of the CH_x fragments from the surface can be fastened (Walter *et al.*, 1994; Hou *et al.*, 2003).

Another modification for the improved CDRM performance of Ni-based catalysts is the addition of non-noble metals to form bimetallic catalysts. Zhang *et al.* investigated the effect of different non-noble metals on the Ni-Me-Al-Mg-O composite prepared by co-precipitation (Me=Co, Fe, Cu or Mn). They found that Ni-Co bimetallic catalyst was the most stable and active configuration among the metals studied and the catalyst with 3.6% Ni and 4.9% Co (molar percent) did not lose its catalytic activity for 250 hours (Zhang *et al.*, 2007).

Trace amount of noble metal addition to Ni based catalysts have been also studied for the CDRM reaction in order to combine the high activity of noble metals with Ni and to eliminate the problems associated with coke deposition on Ni without significantly changing the catalyst cost (Steinhauer *et al.*, 2009). Several studies have shown that adding Pt to Ni-based catalysts can improve the CDRM activity and stability. Platinum can increase activity by increasing the reducibility of NiO species in close proximity to Pt in Pt-Ni system; H and CO form on Pt, and spillover to Ni sites to reduce NiO. Additionally, Pt has been shown to limit coking, so that more active surface area becomes available for reaction. Islands of Pt on the Ni surface or Pt in a surface alloy decrease the ensemble size of Ni regions and thus limit coking, which is more prevalent on larger Ni particles. Platinum also limits the amount of carbon whisker growth due to both low solubility of carbon in Pt and the low adsorption strength of carbon on Pt compared to Ni (Gould *et al.*, 2015).

De Miguel *et al.* aimed to investigate the effect of trace amount of Pt addition to 10 wt% $Ni/\gamma\text{-}Al_2O_3$ on CDRM activity for long term reactions. Bimetallic $0.5Pt10Ni/\gamma\text{-}Al_2O_3$ and monometallic 0.5 wt. % Pt and 10 wt. % Ni containing catalysts were tested for CDRM activity for 6500 min at 750 °C. Although all catalysts started with ca. 70%

methane conversion, CH_4 conversion for 0.5Pt/γ-Al_2O_3 catalyst decreased rapidly to 30% within 24 hours and stayed constant. 0.5Pt10Ni/γ-Al_2O_3 and 10Ni/γ-Al_2O_3 showed stable operation for 6500 min, and bimetallic Pt-Ni catalyst had slightly higher CH_4 conversion and higher H_2/CO selectivity than the monometallic Ni catalyst. Both H_2 chemisorption and cyclohexane dehydrogenation tests showed that Pt addition to Ni led to a decrease in the number of accessible sites for H_2 on Ni. Additionally, cyclohexane dehydrogenation tests on the used catalysts showed that there was a significant drop in the cyclohexane dehydrogenation rate for 0.5Pt catalyst showing that the activity decrease in monometallic Pt catalyst was a result of sintering instead of carbon deposition. On the other hand, amount of deposited carbon was 22 wt. % for monometallic Ni and only 7 wt. % for Pt-Ni catalyst showing the stabilizing effect of trace amount of Pt addition (De Miguel *et al.*, 2012).

Mahoney *et al.* studied the effect of Pt addition to the $CeZrO_2$ and Al_2O_3 supported Ni catalysts by conducting Temperature Programmed Reaction (TPR) tests. In CH_4 pulse tests, 50 µl of methane was injected to the reactor at 800 °C. They observed there is an induction period on the 15Ni/$CeZrO_2$ catalyst to reach the methane conversion values of the 0.2Pt-15Ni/$CeZrO_2$. They stated that the induction period required for the 15Ni/$CeZrO_2$ catalyst resulted from the time required for Ni catalyst to be completely reduced as the experiments were performed without prior reduction. On the other hand, Pt containing catalyst did not need such a time for the complete reduction as the Pt addition already increased the reducibility of the catalyst. In their TPR tests, which were also performed without any prior reduction and with a stoichiometric feed of CH_4 and CO_2, they measured produced H_2 amounts as the temperature of the reactor gradually increased. The onset temperature for the H_2 production was lower on Pt containing catalysts; it is 475 °C for the Pt-Ni/Al_2O_3 while it was 575 °C for the Ni/Al_2O_3 (Mahoney *et al.*, 2014).

Pawelec *et al.* studied the effect of Ni content on the surface, and catalytic behavior of bimetallic Pt-Ni catalysts supported on ZMS-5. Bimetallic catalysts were prepared by sequential impregnation with 0.3-0.5 wt. % Pt and 1-12 wt. % Ni on zeolite. According to their XRD patterns, as Pt loading increased NiO particle size decreased showing the positive effect of Pt addition on the metal dispersion. According to their TPR studies on catalysts loaded with 0.5Pt and varying Ni contents in the range of 1-12 wt. %, Ni particle

size of the bimetallic catalyst affected the reduction temperature. As the Ni particle size increased, the interphase between the Ni particle and the support decreased leading to easier reduction of Ni particles. Catalytic performance tests conducted at 773 and 873 K showed that the performance of the bimetallic catalysts increased with the increasing Ni content and 0.5Pt12Ni catalyst gave the highest CH_4 and CO_2 conversions with the highest H_2/CO ratio. Yet, highest stability was achieved with 0.5Pt6Ni catalyst. Increasing the Ni content above 6% decreased the stability of the catalysts. Superior activity of the 0.5Pt6Ni/ZMS-5 catalyst was explained by the existence of the smaller Ni particles on the surface caused by the dilution effect of Pt (Pawelec *et al.*, 2007).

Özkara-Aydınoğlu and Aksoylu also studied on Pt-Ni bimetallic catalysts and worked for optimizing the Ni:Pt ratio. They prepared 0.3 wt. % Pt/δ-Al_2O_3, 10 wt. % Ni/δ-Al_2O_3 monometallic catalysts by pore volume impregnation and bimetallic catalysts with 0.2-0.3 wt. % Pt and 10-15 wt. % Ni by sequential impregnation. Their XPS results showed that the relative intensity of Ni^{+2} for 0.2Pt15Ni/δ-Al_2O_3 was 0.78, whereas it was 0.60 for the 0.3Pt10Ni sample. Based on their XPS results on freshly reduced catalysts, they inferred that low Ni:Pt ratio of the 0.3P10Ni catalyst led to a relatively stronger synergetic interaction between metallic phases and easy reduction on NiO species. Furthermore, XRD tests showed that Ni particle size was 12.6 nm for the 0.3Pt10Ni/δ-Al_2O_3 sample, 19.8 nm for the 0.2Pt15Ni/δ-Al_2O_3 catalyst and 14 nm for the monometallic 10Ni/δ-Al_2O_3. The lower particle size of the sample having lower Ni:Pt ratio indicated a higher dispersion of the Ni metal induced by higher amount of Pt addition. Spent catalysts were also tested by XRD and no increase in the Ni metal size was observed indicating no sintering took place during the reaction tests. All the samples were tested for the CDRM activity at 923 K with varying feed compositions for 4 hours, and 0.3Pt10Ni/δ-Al_2O_3, which has the lowest Ni:Pt ratio, was found to be the most active and stable composition. According to their TGA/TDA analysis on the spent samples, weight loss of 0.3Pt10Ni sample was only ca. 15 wt. %, whereas 0.2Pt15Ni sample lost ca. 45 wt. % of its weight, pointing out to higher coking resistance of the 0.3Pt10Ni catalyst, which can be explained by the higher oxygen utilization activity caused by well dispersed Pt particles all over the Ni-covered surface. Their investigation of the used samples by electron microscopy revealed no difference between the two samples in terms of the morphology of the carbon

formed on the surface, and the carbon was in the form of filamentous carbon whiskers (Özkara-Aydinoğlu and Aksoylu, 2011).

2.2. Kinetic and Mechanistic Studies on CDRM

There are four main steps in the CDRM reaction. First step is the dissociation and activation of CH_4 and CO_2. Second step is the adsorption of elemental and intermediate C, H and O species on active metal sites. Third and fourth steps are the formation of products through surface reactions and their subsequent desorption from the surface (Kathiraser *et al.*, 2015). There are significant amount of studies in the literature in which activation of reactant gasses, especially methane dissociation step, are termed as rate determining steps. Hence, activation mechanisms for both of the reactants should be carefully addressed and investigated (Fan *et al.*, 2009).

Power-law type rate expressions provide a rough estimation of the effect of the parameters used in the experiment and form a reliable basis for further studies aiming to obtain detailed mechanistic expressions. A kinetic study on 0.3Pt10Ni/Al_2O_3 and 0.2Pt15Ni/Al_2O_3, which were also used in this study, conducted by Özkara-Aydinoğlu and Aksoylu in the temperature range of 853-893 K. Power-law type rate expression was applied to both of the catalysts and the reaction order of CH_4 was found to be close to unity for them both. On the other hand, reaction order for CO_2 was 0.87 for 0.3Pt10Ni, whereas it was 1.40 for the 0.2Pt15Ni catalyst. Higher reaction order of CH_4 compared to the order of CO_2 over 0.3Pt10Ni sample suggested that CO_2 adsorbs more strongly than CH_4, and methane surface coverage is relatively lower for 0.3Pt10Ni sample. Higher reaction order of CO_2 on 0.2Pt15Ni compared to that of 0.3Pt10Ni showed that the reaction rate on 0.2Pt15Ni was more sensitive to CO_2 signifying the importance of Pt in the cleaning of the surface carbon via CO_2 utilization. They also investigated the effect of CO inhibition and found that CO addition in the mixed feed tests resulted in lower reaction rates for both of the catalyst configurations, and the inhibition was more pronounced on 0.2Pt15Ni. However, upon the addition of H_2 to the feed, reaction rate initially declined for 0.2Pt15Ni sample whereas it was slightly enhanced for 0.3Pt10Ni sample. It should be noted that, further H_2 addition gave no further change in the reaction rates indicating an equilibrium

state between the gas phase hydrogen and hydrogen coordinated to Ni (Özkara-Aydinoğlu and Aksoylu, 2013).

There are mainly two types of mechanisms proposed in the literature for the CDRM reaction according to whether support material has a part on the activation mechanisms of the reactants or not. In the mono-functional mechanism, methane and carbon dioxide are both activated on the active metal and support has no part in the activation mechanism. The mono-functional mechanism is valid for the inert supports like SiO_2. On the other hand, it has been shown that participation of the support into the reaction either by activation of methane or carbon dioxide is an important part of the several proposed reaction mechanisms. The essential role of metal-support interface on the activation of the reactants has been also mentioned (Ferreira-Aparicia *et al.*, 2000a). Hence, a second mechanism, i.e. bi-functional mechanism, in which support material also takes part in the course of the reaction, has been proposed by many authors. In this mechanism, CH_4 is not only but mainly activated on the active metal whereas CO_2 is activated on the support material (Pakhare and Spivey, 2014; Bitter *et al.*, 2000).

2.2.1. CH_4 Activation

CH_4 is activated on the active metals by dissociation to form CH_x and adsorbed hydrogen atoms, which later form hydrogen molecule and desorbs from the surface (Fan *et al.*, 2009). In the literature, there are 2 mechanisms proposed for the dissociation of methane on transition metal surfaces. While one mechanism suggests a direct dissociation of methane, second mechanism supposes an indirect dissociation of methane by means of CH_x or formyl groups formation. Molecular beam studies on several metal surfaces (W(110), Ni(111), Ni(100), Pt(111), Pt(110), Pd(110), Ir(110), Ir(111)) indicated that methane activation mechanism is temperature dependent. At lower temperatures, methane is activated by forming intermediates, whereas at higher temperatures the direct dissociation begins (Bradford and Vannice, 1999a; Seets *et al.*, 1997; Pakhare and Spivey, 2014).

Support also has a role on the methane activation. Zhang and Verykios studied CDRM reaction on Ni catalysts supported on Al_2O_3 and La_2O_3. Their time-on-stream

(TOS) tests conducted at 750 °C showed that initial rates for Ni supported on alumina were higher than that on supported on La_2O_3. Yet, as time passed, alumina supported catalyst deactivated significantly and the rate of reaction decreased continuously until 5 hours TOS. On the other hand, rate of CDRM on La_2O_3 supported catalyst increased and reached a steady-state which corresponded to a higher activity level than that observed over the alumina supported catalyst. Higher initial activity of the alumina supported catalyst was explained by the acidic nature of alumina support by which the activation of methane was favored. Promotion of methane decomposition by the acidity of the support was also reported by Garcia-Dieguez *et al.* (Garcia-Dieguez *et al.*, 2010a). Faster deactivation of alumina supported catalyst when compared with that of Ni/La_2O_3 suggested that alumina was not as active as La_2O_3 in CO_2 activation, and in its further utilization in the oxidation of surface carbon due to its less basic nature (Zhang and Verykios, 1996).

Hu and Ruckenstein employed an isotope pulse-GC-MS method in order to identify whether removal of the lattice oxygen of the NiO/MgO or the C-H cleavage of methane is the rate determining step in the reaction between methane and lattice oxygen (NiO). In their pulse experiments, although the rate of CH_4 dissociation was calculated as two times that of the rate of CD_4 dissociation, both CH_4 and CD_4 conversions were found as nearly equal indicating that C-H cleavage of CH_4 was not the rate determining step. They concluded that the rate determining step in the reaction between methane and lattice oxygen was the removal of lattice oxygen by methane (Hu and Ruckenstein, 1999).

Staag *et al.* also performed pulse experiments on Pt/ZrO_2 catalyst at 800 °C with $^{13}CH_4$. Though, they observed H_2, ^{13}CO and a small amount of $^{13}CO_2$ formation, the amounts produced decreased in each consecutive $^{13}CH_4$ pulses. Since the only source of O was the support, they suggested that some of the carbon produced from $^{13}CH_4$ was able to partially reduce the oxide support near the perimeter of the particle. The reduction in the production of H_2 and ^{13}CO in each consecutive pulse was explained by the production of $^{13}CH_x$ species on Pt metal which caused blocking of the active sites (Staag *et al.*, 1998). CO formation under methane flow was also observed by Bradford and Vannice. In their FTIR-DRIFTS experiments conducted on TiO_2 supported Pt and Rh catalysts at 423 K, CO formation on Rh and Pt was observed upon CH_4 flow. However, no CO formation was observed on the catalysts containing Pd, Ni and Cu metals and TiO_2 support alone

(Bradford and Vannice, 1999b). Similarly, CO formation under methane flow induced by the O present on the support was also observed by Garcia-Dieguez *et al.* in their Transient-Response-Method experiments (Garcia-Dieguez *et al.*, 2010a).

Methane dissociation is also reported as a surface structure dependent process. Beebe *et al.* performed methane adsorption experiments on 3 different single Ni crystal surfaces. They found that Ni reactivity increased in the order of Ni(111)<Ni(100)<Ni(110). They also reported that the reactivity towards methane is a strong function of surface coverage for the Ni(111) and Ni(100) surfaces; whereas there seemed no such inhibition on Ni(110) surface (Beebe *et al.*, 1987). Furthermore, according to Bradford and Vannice, CH_x fragments are preferentially located at a site that completes their tetravalancies, signifying the geometric constraints on methane adsorption. Hence, decomposition of CH_4 into CH_x fragments on active metal, requires a concomitant occupation of the metal sites according to the following equation:

$$CH_{x+1} - (3 - x)M + 2M \rightarrow CH_x - (4 - x)M + H - M \qquad (2.9)$$

where M signifies a surface metal atom (Bradford and Vannice, 1998).

2.2.2. CO_2 Activation

In addition to the active metal surfaces, CO_2 activation mostly occurs on the support materials and/or at the interfacial sites between support and active metal (Fan *et al.*, 2009). Hence, activation mechanism can be different depending on the nature of the support. CO_2 is an acidic molecule and it interacts easily with the basic supports (Nagaoka *et al.*, 2001). On acidic supports CO_2 is activated by formation of formates and bicarbonates with the surface hydroxyls, whereas on basic supports its activation is through formation oxy-carbonates (Pakhare and Spivey, 2014; Staag *et al.*, 1998).

CO_2 activation in the presence of methane may result in a different process than the CO_2 activation on an unmodified surface. For instance, Staag *et al.* performed $^{13}CH_4$ pulse experiments on Pt/ZrO_2 at 800 °C followed by $^{12}CO_2$ pulses. Upon $^{12}CO_2$ pulses, they observed both ^{12}CO and ^{13}CO in the product stream. In the experiments performed by using only ZrO_2 support, no CO_2 dissociation was observed indicating the need of Pt metal

for the dissociation. Hence, they suggested that CO_2 dissociation occurred near the metal-support interface or it occurred on oxygen vacancies generated during the previous reduction of the support by the methane pulses suggesting a redox cycle (Staag *et al.*, 1998). A similar conclusion was derived by Garcia-Dieguez *et al.* who suggested that the presence of H_2 and CH_x species on the surface enhanced the CO_2 activation (Garcia-Dieguez *et al.*, 2010a).

Ruckenstein and Hu performed a transient response analysis on NiO/MgO solid solution catalysts at 800 °C. Their response curves showed that two kinds of oxygen were formed over the catalyst during the CDRM reaction: adsorbed and lattice type oxygens. They proposed that oxygen was formed on the surface rapidly by CO_2 dissociation. This surface O either oxidized Ni^0 to NiO (lattice oxygen), which was subsequently reduced by C species slowly to Ni^0 and CO, or oxidized the surface carbon species directly, which was termed as a faster process than the former. They proposed a dynamic redox process for the lattice oxygen formation by CO_2 adsorption on Ni^0 and its following consumption in the reduction of the NiO by the surface carbon species (Ruckenstein and Hu, 1998).

2.2.3. Reaction Mechanisms for Catalytic Dry Reforming of Methane

In order to develop an active and stable catalyst for the CDRM reaction, it is highly important to understand the reaction mechanism and to determine the rate determining step (RDS) that primarily determines the performance of the catalyst.

There are both Langmuir Hinshelwood-Hougan-Watson (LHHW) and Eley-Rideal (ER) type models in the literature. Among the few ER type models proposed in the literature, Akpan *et al.* studied CDRM kinetics over Ni/CeO_2-ZrO_2 catalyst and they considered four different steps as the RDS: Adsorption and/or dissociation of methane, surface reaction of solid carbon with lattice oxygen of the support, surface reaction of reduced site with the gaseous CO_2 and surface reaction between two adsorbed hydrogen atoms. Between those, their kinetic model showed that RDS of CDRM was the methane dissociation (Akpan *et al.*, 2007). Becerra *et al.* also performed a mechanistic study on Ni/Al_2O_3 by using an ER model assuming non-dissociative adsorption of methane and

found that the reaction between adsorbed species and the gaseous CO_2 was the RDS (Becerra *et al.*, 2003).

A general mechanism for CDRM reaction on Ni-based catalysts was given by Bradford and Vannice where the following steps were suggested for the CDRM reaction (Bradford and Vannice, 1998):

- reversible dissociation of CH_4;

$$CH_4 + * \leftrightarrow CH_x * + ((4 - x)/2)\, H_2 \tag{2.10}$$

- un-dissociative adsorption of CO_2 on the support;

$$2[CO_2 + * \rightleftharpoons CO_2 *] \tag{2.11}$$

- H-assisted dissociation of CO_2 in the metal-support interfacial region;

$$H_2 + 2 * \rightleftharpoons 2H * \tag{2.12}$$

$$2\,[CO_2 * + H * \rightleftharpoons CO * + OH *] \tag{2.13}$$

- reaction between CH_x and OH (or O) species to yield CH_xO species;

$$OH * + H * \rightleftharpoons H_2O + 2 * \tag{2.14}$$

$$CH_x * + OH * \rightleftharpoons CH_xO * + H * \tag{2.15}$$

- CH_xO decomposition in the metal support region to H_2 and CO;

$$CH_xO * \rightarrow CO + (x/2)\, H_2 \tag{2.16}$$

$$3\,[CO * \rightleftharpoons CO + *\,] \tag{2.17}$$

Cheng *et al.* studied the role of support on Ni/γ-Al_2O_3 and conducted TPR and H_2-TPD experiments on the catalysts on which different degrees of reductions were applied.

Based on a H spillover from Ni^0 to the support, they proposed a modification to the mechanism proposed by Bradford and Vannice (Cheng *et al.*, 2001):

- reversible dissociation of CH_4 to yield CH_x species and H on Ni^0 with a large portion of H spilt over onto the support;

$$Al - O + H_{sp} \rightarrow Al - OH \tag{2.18}$$

  where H_{sp} is the spilt over hydrogen.

- H-promoted CO_2 dissociation on the support;

$$Al - OH + CO_2 + * \rightarrow Al - COOH + O* \tag{2.19}$$

$$Al - COOH \rightarrow Al - OH + CO \tag{2.20}$$

$$O* + H_{sp} \rightarrow *OH \tag{2.21}$$

$$2\,Al - OH \rightarrow Al - H_2O + Al - O \tag{2.22}$$

$$2*OH \rightarrow *H_2O + O* \tag{2.23}$$

  where * denotes the oxygen vacancy.

- Reaction of CH_x species with H_2O to yield CH_xO species and H_2, and CH_xO decomposition to CO and H_2 on the metal-support interfacial region. H_2O mainly comes from the support and migrates to the metal-support interfacial region.

A more detailed mechanism on the basis of participation of the surface O and OH groups of the alumina in the reaction mechanism was proposed by Ferreira-Aparicio and coworkers. Based their findings by in situ FTIR spectroscopic examination on Rh/Al_2O_3 catalyst, they proposed the following mechanism (Ferreira-Aparicio *et al.*, 2000b):

- CH_4 is activated on the ruthenium surface yielding adsorbed hydrogen and CH_x species similar to the reactions given by Equation 2.10 and Equation 2.12;

- while migration of surface OH groups of alumina takes part in the oxidation of the carbon deposits;

$$2\,OH_{(Al_2O_3)} \leftrightarrow OH_{(Ru-ads)} \tag{2.24}$$

$$OH_{(Ru-ads)} \leftrightarrow O_{(Ru-ads)} + H_{(Ru-ads)} \tag{2.25}$$

$$H_{(Ru-ads)} + OH_{(Ru-ads)} \leftrightarrow H_2O_{(g)} \tag{2.26}$$

$$CH_{x\,(Ru-ads)} + O_{(Ru-ads)} \leftrightarrow CO_{(Ru-ads)} + xH_{(Ru-ads)} \tag{2.27}$$

$$CO_{(Ru-ads)} \leftrightarrow CO_{(g)} \tag{2.28}$$

- CO_2 is activated on the support to form carbonates by reaction given in Equation 2.30 and bicarbonates by reaction given in Equation 2.31;

$$CO_{2\,(g)} \leftrightarrow CO_{2\,(Al_2O_3-ads)} \tag{2.29}$$

$$CO_{2\,(Al_2O_3-ads)} + O^{2-}_{(Al_2O_3)} \leftrightarrow CO^{2-}_{3\,(Al_2O_3-ads)} \tag{2.30}$$

$$CO_{2\,(Al_2O_3-ads)} + OH^{-}_{(Al_2O_3)} \leftrightarrow HCO^{-}_{3\,(Al_2O_3-ads)} \tag{2.31}$$

- Hydrogen adsorbed on the active metal, through methane dissociation or by reaction given in Equation 2.25, is diffused to the alumina surface;

$$2\,H_{(Ru-ads)} \leftrightarrow 2\,H_{(Al_2O_3-ads)} \tag{2.32}$$

- Hydrogen diffused through the surface reacts with surface carbonates and bicarbonates to give formate species;

$$CO^{2-}_{3\ (Al_2O_3-ads)} + \ 2\ H_{(Al_2O_3-ads)} \leftrightarrow \ HCO^{-}_{2\ (Al_2O_3-ads)} + OH^{-}_{(Al_2O_3)} \quad (2.33)$$

$$HCO^{-}_{3\ (Al_2O_3-ads)} + \ 2\ H_{(Al_2O_3-ads)} \leftrightarrow \ HCO^{-}_{2\ (Al_2O_3-ads)} + \ H_2O_{(Al_2O_3-ads)} \quad (2.34)$$

- then, these formates are decomposed into CO and surface OH;

$$HCO^{-}_{2\ (Al_2O_3-ads)} \leftrightarrow \ CO_{(\ Al_2O_3-ads)} + \ OH^{-}_{(Al_2O_3)} \quad (2.35)$$

$$CO_{(Al_2O_3-ads)} \leftrightarrow \ CO_{\ (g)} \quad (2.36)$$

- meanwhile, surface groups of the alumina goes under the following equilibrium reactions;

$$2\ OH^{-}_{(Al_2O_3)} \leftrightarrow \ H_2O_{\ (Al_2O_3-ads)} + \ O^{2-}_{(Al_2O_3)} \quad (2.37)$$

$$H_2O_{\ (Al_2O_3-ads)} \leftrightarrow \ H_2O_{\ (g)} \quad (2.38)$$

Recently, Kathiraser *et al.* published a comprehensive review on CDRM reaction kinetics over Ni-based catalysts (Kathiraser *et al.*, 2015). Among the studies based on single rate determining step, Wei and Iglesia suggested C-H bond cleavage of methane as the only rate determining step for Ni/MgO catalyst (Wei and Iglesia, 2004). Methane activation on Ni metal was also termed as the only kinetically relevant step by Wang and Au who studied on Ni/SiO_2 catalyst (Wang and Au, 1996). Osaki *et al.* performed pulse surface reaction rate analysis on Al_2O_3, TiO_2, SiO_2 and MgO supported Ni catalysts and suggested that surface reaction between CH_x and adsorbed O is the rate determining step in CDRM reaction (Osaki *et al.*, 1996). Kroll and coworkers proposed that the reaction between the adsorbed carbon and oxygen is the sole kinetically relevant step on Ni/SiO_2 catalyst as it requires surface migration of those species (Kroll *et al.*, 1996). On the basis of activation energies, Wang *et al.* suggested that reverse Boudouard reaction producing CO from adsorbed carbon and adsorbed CO_2 molecule was the rate determining step on Ni/Al_2O_3 (Wang and Lu, 1999).

There are also studies in which two rate determining steps are proposed. Nandini *et al.* performed a kinetic study on 13.5Ni-2K/10CeO_2-Al_2O_3. On the basis of a mechanism involving irreversible methane dissociation to CH_x fragments, non-dissociative CO_2 adsorption, promotion of CO_2 dissociation on the surface by the surface hydrogen atoms and interaction of CH_x fragments with surface hydroxyl groups which produces CH_xO species; they proposed a LHHW type rate mechanism with methane decomposition to CH_x species and decomposition of CH_xO species to CO and H_2 as the rate determining steps, and achieved a high confidence in parameter estimation by using the experimental data (Nandini *et al.*, 2006). Furthermore, there are dual site mechanisms that suggest two different rate determining steps occurring on two different sites. For instance, CH_4 activation by metal Ni and C gasification by adsorbed CO_2 on the support were proposed as possible rate determining steps for the CDRM reaction on La_2O_3 supported Ni catalysts (Moradi *et al.*, 2010)

In their kinetic study on 0.3Pt10Ni/Al_2O_3 and 0.2Pt15Ni/Al_2O_3, Özkara-Aydinoğlu and Aksoylu considered 8 different models in order to find reliable kinetic expression(s) for each catalyst and to understand the effect of Ni:Pt ratio on the reaction mechanism of CDRM reaction. According to their model discrimination based on variance values obtained upon non-linear regression analysis, an ER type model (designated as model 1), which assumes that CO_2 is adsorbed on the catalyst surface and reacted with the gaseous or weakly adsorbed CH_4, gave the lowest squared error for the 0.3Pt10Ni/Al_2O_3 catalyst. A very close squared error was also obtained for the model (model 2) which is based on a stepwise mechanism, where in methane is decomposed to hydrogen and active carbon followed by the reaction of this active carbon with CO_2 to 2CO. In this model, equilibrium constant for CO_2 was larger than that of CH_4 indicating that 0.3Pt10Ni catalyst has the ability to utilize CO_2 as the oxygen source. Model that was obtained by adding CO inhibition term to the denominator of the model 1 (Model 6), gave higher squared errors than the model 1 showing that 0.3Pt10Ni catalyst did not suffer significantly from CO inhibition (Özkara-Aydinoğlu and Aksoylu, 2013).

For the 0.2Pt15Ni catalyst, Özkara-Aydinoğlu and Aksoylu found that the best fitting two models (model 8 and 6) were the ones in which inhibiting effect of CO was considered. Hence, they proposed that 0.2Pt15Ni catalyst was strongly affected by the CO

inhibition. The only common model between the two catalyst samples was the one which assumed that CH_4 and CO adsorbed on the same site while CO_2 was adsorbed on a different site (model 5). In this model, adsorption coefficients increased in the following sequence: $K_{CH4}<K_{CO}<K_{CO2}$ for 0.3Pt10Ni sample and $K_{CH4}< K_{CO2}< K_{CO}$ for 0.2Pt15Ni sample. For the 0.3Pt10Ni sample, higher K value obtained for CO_2 compared to that of obtained for CH_4 showed that the utilization of CO_2 was strong on this sample. The highest K value obtained on 0.2Pt15Ni sample was the equilibrium constant of CO indicating that a very strong CO inhibition effect was observed on 0.2Pt15Ni sample. In fact, K_{CO} for the 0.2Pt15Ni sample was five times higher than that of 0.3Pt10Ni sample revealing the difference among the samples in their relative vulnerability to CO inhibition (Özkara-Aydinoğlu and Aksoylu, 2013).

2.3. FTIR-DRIFTS Studies

Diffusive Reflectance Infrared Fourier Transform Spectroscopy, also known as FTIR-DRIFTS, is a Fourier transform infrared spectroscopy (FTIR) method which makes use of the phenomenon of diffuse reflectance, and is used primarily on powders and other solid samples. In diffuse reflectance spectroscopy, electromagnetic radiation reflected from dull surfaces is collected and analysed. Hence, this method is highly useful in examining the surface of the catalysts during heterogeneous reactions to observe the possible intermediate species that may evolve in the course of the reaction and thus, is commonly used in the catalysis community (Ryczkowski, 2001).

There are several carbonaceous species form when CH_4, CO_2 or CO is adsorbed on the catalyst surface: Carbonates, bicarbonates (hydrogen carbonates), carboxylates, which can be classified as strongly perturbed CO_2 species, and formates. These species are observable by IR spectroscopy and frequently encountered in FTIR-DRIFTS studies. Naming of these compounds differ according to their geometric orientation and the that they bind to the surface sites. When one specie is bounded to two surface sites, it is called bridged; when two atoms of specie is bounded to one single surface site; it is called bidentate. These carbonaceous species with their different orientations are shown in the Figure 2.2.

The exact assignment of these species in the spectra is not straightforward; yet there are some rules that can help for their identification. Formates are the least challenging ones to identify as they give rise to C-H stretching band around 2900 cm^{-1} (Rethwisch and Dumesic, 1986). Carbonates and bicarbonates give rise to the asymmetric and symmetric OCO stretching bands in 1700-1100 cm^{-1} region. Bicarbonates also have OH group in their structure which produces OH stretching, ν(OH), and OH bending bands, δ(OH). Carboxylates give rise to both asymmetric and symmetric ν(CO_2) bands. Apart from the wavenumber of the IR signal, thermal stability of these carbonate type species may help to identify them. For instance, thermal stability of the bridged carbonates is suggested to be higher than that of carboxylates. Also, polydentate carbonates are much more stable than the other bidentate and bridged carbonates, and then the carboxylates and bicarbonates as well. Among the mono- and bidentate carbonates, bidentate carbonates are reported to be less stable (Collins *et al.*, 2006; Holmgren *et al.*, 1999).

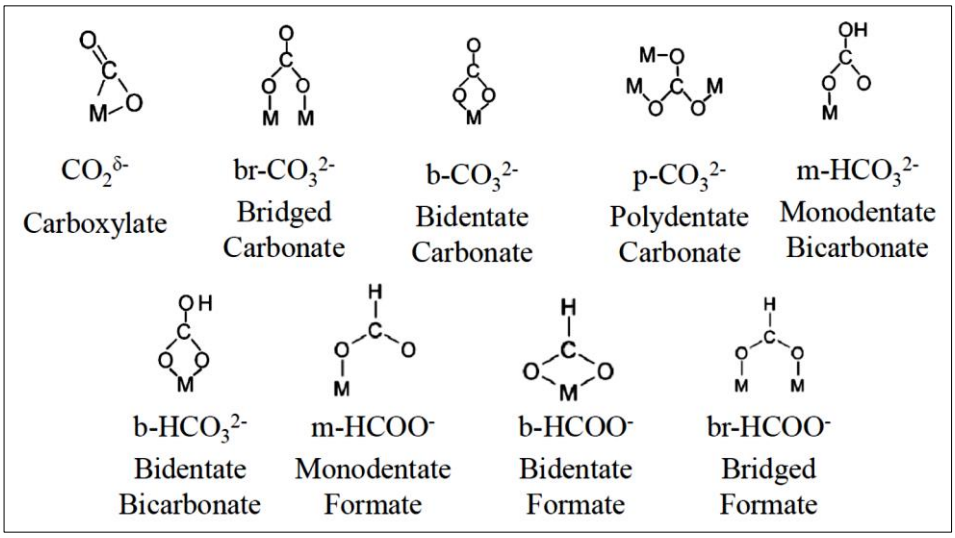

Figure 2.2. Carbonaceous species frequently encountered in FTIR-DRIFTS studies (Köck *et al.*, 2013; Collins *et al.*, 2006)

Width of the ν_3 band (stretching mode) splitting ($\Delta\nu_3$) is also suggested to be an indication of a surface group. For instance, $\Delta\nu_3$ is higher than 400 cm^{-1} for the bridged carbonates. Additionally, while bidentate carbonates have $\Delta\nu_3$ around 300 cm^{-1}, $\Delta\nu_3$ for those of monodentate and polydentate carbonates are less than 100 cm^{-1}. $\Delta\nu_3$ for monodentate and bidentate bicarbonates are smaller than 200 cm^{-1} while $\Delta\nu_3$ for the

bidentate form is smaller than that for the monodentate form. For bridged bicarbonates, $\Delta\nu_3$ is suggested to be larger than 400 cm^{-1}. As for the formates, frequency separation for monodentate formates is larger than 250 cm^{-1}, while $\Delta\nu_3$ for bidentate formates is lower than 250 cm^{-1} (Pan *et al.*, 2014; Collins *et al.*, 2006).

2.3.1. CO adsorption and Surface Characterization

IR spectroscopy of adsorbed CO reveals information on the composition and structure of surface compounds, the nature of the bonds between adsorbate and support surface, the existence of various types of surface compounds and active surface sites, and the degree of metal dispersion of the supported catalysts (Poncelet *et al.*, 2005). CO is a weak base and can make bonds to the acidic sites with different strengths. This feature is different from other bases used for characterization purposes, i.e. ammonia and pyridine. Ammonia and pyridine, having stronger basic characteristics, are adsorbed strongly on both strong and weak acid sites, and the bands associated with these adsorptions are not distinctly different. The precise frequency of the CO metal bond depends on the nature of the metal, its surface structure and CO coverage (Hattori and Ono, 2015).

In case of the CO adsorption on alumina, driving force for the adsorption is the σ-donation from 5σ CO-orbital to the empty 3p orbitals of the unsaturated Al atoms. As the 5σ CO-orbital is slightly antibonding, the CO-bond becomes stronger upon adsorption and the CO frequency shifts to higher frequencies than the gaseous CO stretching. CO adsorption on alumina results in four bands denoted as band A (between 2240-2200 cm^{-1}), band B (between 2200-2190 cm^{-1}), band C (between 2165-2155 cm^{-1}) and band D (between 2150-2140 cm^{-1}). Band D denotes physically adsorbed or H-bonded CO to the OH groups of alumina. Band C is due to the octahedral Al atoms and band B is due to CO adsorbed to the tetrahedral Al atoms. Band A is due to the CO adsorbed on Al atom at the surface defects, (Hattori and Ono, 2015; Zecchina *et al.*, 1987). CO adsorption studies on alumina also revealed the acidity of the OH groups of alumina. OH groups on alumina surface are observed in the 3600-3800 cm^{-1} region. Knözinger and Ratnasamy found that the OH band at lower frequency (3725 cm^{-1}) disappeared upon CO adsorption, while the bands at 3785 and 3775 cm^{-1} were not affected by CO indicating that the band at lower

frequency was stronger Bronsted acid than the other two appearing at higher frequencies (Knözinger and Ratnasamy, 1978).

Table 2.1. Band assignments of CO on Ni/Al_2O_3 (adapted from Gökaliler, 2012).

Species	**Adsorption Site**	**IR Frequency (cm^{-1})**	**Comment**
CO—NiO	Ni^{1+} and Ni^{2+}	2200 - 2120	Unreduced
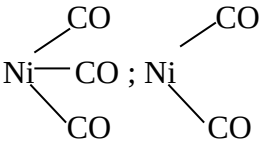	Ni^0 and $Ni^{\delta+}$	2120 - 2050	Highly Dispersed
CO—Ni	Ni^0	2065 - 2020	Moderately Dispersed
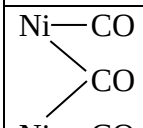	Ni^0 or $Ni^{\delta+}$	1990-1940	Crystalline
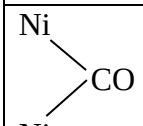	Ni^0 or $Ni^{\delta+}$	1940-1850	Crystalline

Upon CO adsorption on Ni, two main regions are observed in the metal carbonyl bond range of the spectrum: Linearly bound mono- or multiple carbonyl(s) are observed between 2000-2100 cm^{-1}, and bridged carbonyls are observed between 2000-1750 cm^{-1}. Infrared spectroscopy of adsorbed CO gives an insight on the type of the Ni atom on the surface. Bands at higher wavenumbers (2120-2050 cm^{-1}) are indicative of lower reduction level and higher dispersion, while those below 2050 cm^{-1} signify moderately to poorly dispersed Ni^0 (Zhu *et al.*, 2008). Bands above 2120 cm^{-1} indicate presence of unreduced nickel (Poncelet *et al.*, 2005). The low frequency band at 2000-1750 cm^{-1} is attributed to crystalline structure of the metal with a lower extent of dispersion. For instance, CO adsorption yielding peaks at 1956 cm^{-1} and 1939 cm^{-1} were shown to indicate the presence

of Ni(100) and Ni(111) surfaces, respectively (Yate and Garland, 1961; Damyanova *et al.*, 1996). In terms of geometry of coordination, CO preferentially bonds linearly to defect sites, whereas bridge bonding (two- or three-fold) is more favorable at close packed plane sites (Anderson *et al.*, 1993). Geometrical representations of these species are summarized in Table 2.1.

Table 2.2. Band assignments of CO on Pt/Al_2O_3 (adapted from Gökaliler, 2012).

Species	**Adsorption Site**	**IR Frequency (cm^{-1})**	**Comment**
CO—PtO	$Pt^{\delta+}$	2200 - 2100	Unreduced
Pt Pt Pt — CO Pt Pt	Pt^0	2090-2080	Terrace Site
CO—Pt	Pt^0	2080-2040	Edge Site
Pt—CO CO Pt—CO	Pt^0	1860-1780	

The IR spectra obtained upon CO adsorption on Pt/Al_2O_3 shows two distinct regions depending on the nature of the bonding. Linearly bonded CO on one Pt atom gives rise to a band between 2040-2090 cm^{-1}; while bridge bonded CO molecules are observed in the range between 1860-1780 cm^{-1}. Linear region spectrum also indicates the type of the Pt surface on which CO is adsorbed. Greenler *et al.* found that three bands appearing at 2081, 2070 and 2063 cm^{-1} are indication of CO adsorbed on face, corner and edge atoms, respectively (Greenler *et al.*, 1985). Dependence of the IR band of CO on the extent of the reduction and the particle size of the Pt metal was also reported in the literature. It has been suggested that CO adsorption on oxidized Pt (PtO) yields a band above 2090 cm^{-1}, and CO adsorbed on reduced Pt produces peaks at lower frequencies. Furthermore, as the particle

size of the Pt decreases, frequency of the CO adsorption also decreases; the corresponding band of linear CO gets broader and a shoulder appears at the lower frequencies (De Menorval *et al.*, 1997; Holmgren *et al.*, 1999; Garcia-Dieguez *et al.*, 2010). Representations of the adsorbed CO species with their frequency intervals are given in Table 2.2.

CO adsorption based FTIR studies on Pt-Ni bimetallic catalysts revealed that the adsorption characteristics of the catalyst surface are strongly affected by the metal present in a relatively higher amount. For instance, Lonetgan *et al.* performed IR-CO experiments on three bimetallic catalysts with different Pt:Ni ratios (1:1,1:3,1:10). They observed that at lower Ni loadings (Pt:Ni=1:1,1:3), the peaks associated with bridge-bound CO appeared at frequencies similar to the CO bridge binding sites on 1 wt. % Pt/γ-Al_2O_3, suggesting that CO was adsorbed on Pt atoms. However, on 1Pt10Ni/γ-Al_2O_3, the bridge-bound CO frequency was similar to that on 10Ni/γ-Al_2O_3, suggesting that CO is most likely adsorbed on Ni atoms (Lonetgan *et al.*, 2010). However, some changes in the peak intensities are reported to occur depending on the metal loading. Li *et al.* performed IR-CO tests on 0.1-0.2 wt. % Pt and 0.9-2.6 wt. % Ni catalysts and observed that as the loading of Ni increased, bands indicating bridge bonded CO species appeared on the spectrum (Li *et al.*, 2007).

Although the CO adsorption spectrums of the bimetallic catalysts are strongly shaped by the metal with the higher loading, there are some shifts in the frequencies and changes in the relative absorbance of the bands induced by the addition of a second metal. Pawelec *et al.* studied the effect of Ni content on the surface characteristics and catalytic behavior of bimetallic Pt-Ni catalysts supported on ZMS-5. Bimetallic catalysts were prepared by sequential impregnation of 0.3-0.5 wt. % Pt and 1-12 wt. % Ni on zeolite. In CO adsorption DRIFT spectroscopy, they observed high-frequency band shifts from 2092 to 2085 cm^{-1} and decrease in intensity after introduction of Pt to Ni sample. They associated this band shift with the change of the electronic state of the metal atoms, which can be attributed to a subsequent reduction of the partially oxidized $Ni^{\delta+}$ atoms in the presence of Pt (spill-over effect of Pt). They also explained the decrease in intensity by the dilution effect of Pt, which results in more uniform distribution of Ni particles on the catalyst surface (Pawelec *et al.*, 2007).

Pt addition can also alter the stability of the metal-CO bonds. Parizotto *et al.* conducted CO adsorption and TPD-CO tests on $15Ni/Al_2O_3$ and $0.05Pt\text{-}15Ni/Al_2O_3$ by using FTIR spectroscopy. They observed 2 bands around ca. 2074 (HF1) and 2037 (HF2) cm^{-1} at high frequency region and 2 bands around ca. 1939 (LF1) and 1903 cm^{-1} (LF2) at low frequency region. They attributed the band at ca. 2037 cm^{-1} to linear bonded CO to Ni atoms and bands at 1939 and 1903 cm^{-1} to the compressed and isolated bridged bonded carbonyls, respectively. After 10 min N_2 purge, they observed a decrease in the intensity of the band around 2074 cm^{-1} (HF1) for both catalysts and claimed that this high frequency peak is related to the subcarbonyl species adsorbed on low-coordinated Ni sites which are less thermally stable than others. After N_2 purge, they observed that the band at ca. 2037 cm^{-1} got more apparent with the presence of Pt and band ratio of HF/LF increased slightly. They also performed Temperature-Programmed-Desorption (TPD) tests after CO adsorption at room temperature under N_2 flow and ranked the thermal stability of the bands as HF1<HF2<LF1<LF2. They found that TPD-CO of $0.05Pt\text{-}15Ni/Al_2O_3$ showed a slight increase in intensity of the HF2 band and a decrease in intensity of the low frequency bands when the temperature was increased from 100 to 150 °C. They suggested that Pt caused a decrease in the thermal stability of the CO adsorbed in the bridged form or there was a reconstruction of the Ni surface induced by the presence of CO and Pt. On the basis of TPD-CO results, they mentioned that presence of trace amount of Pt resulted in a change of the superficial structure of Ni metal (Parizotto *et al.*, 2009).

A DFT study on Ni(111) and PtNi(111) surfaces performed in our group revealed that CO adsorption was strong at all the surface configurations studied (atop, bridge, HCP and FCC); while it was the strongest on the HCP sites, and oxygen molecule was found stably adsorbed on the hollow sites. The frequency analysis of adsorbed CO on Ni(111) surface showed that the stretching frequencies of CO coordinated at atop, bridge, FCC and HCP sites are at 2099, 1971, 1975 and 1987 cm^{-1}, respectively, for the 1/2 MLE surface concentration. The frequencies obtained for 1/4 MLE surface coverage of CO were 2125, 2025, 1975 and 1987 cm^{-1} for atop, bridge, FCC and HCP coordinated CO, respectively. On PtNi(111), stretching frequencies of CO adsorbed at different sites were studied for 1/6 MLE surface concentration by replacing CO at several different initial configurations. The calculated stretching frequencies upon energy optimization were in the range of 2140-2035

cm^{-1} for the terrace sites, 2140-2017 cm^{-1} for bridge sites, 2122 cm^{-1} for the FCC sites and 2008-1971 cm^{-1} for the HCP sites (Ayvaz, 2010).

2.3.2. CO_2 Adsorption

As mentioned earlier, CO_2 activation mainly occurs on the support materials and at the interfacial sites between support and active metal. Additionally, CO_2 is activated on acidic supports via formation of formates and bicarbonates with the surface hydroxyl; while on basic supports, it is activated by forming oxy-carbonates (Fan *et al.*, 2009; Pakhare and Spivey *et al.*, 2014; Staag et. al, 1998). Hence, it is important to understand how CO_2 reacts with the support material in order to gain an insight for the CO_2 adsorption spectra.

The spectra of CO_2 adsorption on γ-Al_2O_3 at room temperature generates a peak at 2359 cm^{-1} which is attributed to the physisorbed CO_2 species. In addition, there appears a broad region between 1200-1700 cm^{-1} which is attributed to the CO_2 molecules adsorbed in a linear configuration on the cations (υ_2 band), or in a non-linear (or 'bent') manner in the form of carbonate/bicarbonate ions. These species are termed as carbonaceous species and their formation is found strongly depends on the degree of dehydration of the alumina surface. It is reported in the literature that heat treatment below 673 K results in a surface full of OH groups, and adsorption of CO_2 on these sites yields the formation of bicarbonate species and linear bonded CO_2. If the heat treatment applied is above 673 K, oxide ions and exposed Al ions exist together with OH groups, and upon CO_2 adsorption, linear CO_2, bridged, bidentate and monodentate carbonates and bicarbonates form on the surface. As OH groups are needed for the formation of bicarbonate species, in order to have bidentate and bridged carbonate species on the surface, the presence of both exposed Al ion and coordinatively unsaturated O ion are needed. For the linear CO_2, coordinatively unsaturated Al atom of tetrahedral coordination or of octahedral coordination are required (Hattori and Ono, 2015; Rege and Yang, 2001).

Parkyns *et al.* investigated the effect of degassing temperature on the adsorption spectra of the CO_2 coordinated on alumina. According to him, when the applied heat treatment is below 500 °C, mostly bicarbonate species appear in the spectrum signified by

a peak around 3610 ± 5 cm^{-1}, which is the indication of the hydroxyl stretching of a surface bicarbonate group, and bands at 1640, 1480 and 1232 cm^{-1}, which are all different modes of bicarbonate species. When the heat treatment is above 800 °C, bicarbonate bands are no longer observed and several carbonate species become more apparent. His tentative assignments were as follows: uncoordinated carbonate ion in the range 1445-1470 cm^{-1}, unidentate at 1530 and 1370 cm^{-1}, and bidentate at 1660 and 1230 (or 1270 cm^{-1}) (Parkyns, 1971). Ferreira-Aparicio *et al.* also studied CO_2 adsorption on Rh/Al_2O_3 catalyst at 873 K. They observed adsorbed CO on Rh metal and bicarbonate ions, which yield frequencies of 3614, 1636, 1485 and 1235 cm^{-1} (Ferreira-Aparicio *et al.*, 2000b).

Miyao *et al.* studied effect of chlorine addition on selective CO methanation reaction over Ni-Al mixed oxide catalyst by conducting in-situ FTIR-DRIFTS analysis. Upon CO_2 flow over the unmodified Ni-Al mixed oxide catalyst at 230 °C, they observed bands at 2014 and 1844 cm^{-1}, which were assigned to linear and bridge bonded CO indicating the dissociation of CO_2 to CO on Ni sites. They also observed carbonate and bicarbonate species at 1648 cm^{-1}, 1447 cm^{-1}, 1360 cm^{-1}, 1230 cm^{-1}, which were formed on alumina, and carboxylate at 1533 cm^{-1} formed on Ni sites (Miyao *et al.*, 2014).

A DFT study on Ni(111) and PtNi(111) surfaces performed in our group proposed that CO_2 adsorption was the most stable on bridge sites, and CO_2 molecule originally replaced on other sites diffused to the bridge sites. On the other hand, oxygen molecule was found to be stable on the hollow sites (Ayvaz, 2010).

2.3.3. CH_4 Adsorption and In-situ Reaction Tests

It has been reported in the literature that methane activation, i.e. hydrogen and surface carbon formation, occurs on the active metal. Yet, CO formation on the active metal by the interaction between the CH_4 and the surface OH groups of alumina has been reported for several Al_2O_3 supported catalysts; i.e. Co, Ni, Ru, Rh and Ir (Bradford and Vannice, 1999). In addition, methane flow at temperatures higher than 573 K was found results in CO and H_2 formation on these alumina supported catalysts (Ferreiara-Aparicio *et al.*, 1997).

Bradford and Vannice conducted CH_4 adsorption tests on several metals including Cu, Ni, Pd, Rh and Pt supported on SiO_2 and TiO_2. Upon CH_4 adsorption on SiO_2 at 293 K, strong interaction between CH_4 and the OH groups of the support, silanols, was observed indicated by the loss of the band at 3744 cm^{-1}, which was attributed to the isolated OH groups on SiO_2. Upon the CH_4 adsorption tests conducted at 423 K on TiO_2 supported transition metals, Ti-O bond cleavage was observed by the loss of the band at 930 cm^{-1}, accompanied by formation of OH bands at 3669 and 3680 cm^{-1}. On all metals, a sharp band at ca. 1690 cm^{-1} was observed and it was assigned to the $H_2C{=}O$ species, which are strongly coordinated at Lewis acidic (Ti^{+n}) sites. In addition, adsorbed CO was observed on Rh and Pt catalysts with a decrease in their $H_2C{=}O$ band intensity. They attributed this decrease in the intensity to the consumption of these species to produce CO, and concluded that $H_2C{=}O$ can be a precursor to CO formation on the metal surface (Bradford and Vannice, 1999b).

In a DFT study on Ni(111) and PtNi(111) surfaces performed in our group, frequency analysis of CH_x-Ni(111) system yields frequencies in the range of 3500-3000 cm^{-1} for the C-H bond of the coordinated CH_3 molecule both at 1/2 and 1/4 MLE surface concentrations. For the adsorbed CH_2, this range was lower and narrower by being 3243-2859 cm^{-1} for 1/2 MLE surface concentrations, and 2741-2690 cm^{-1} for the 1/4 MLE surface concentrations. For the coordinated CH molecule, C-H stretching frequencies were calculated in the range of 2978-2968 cm^{-1} for 1/2 MLE and 2875-2858 cm^{-1} for 1/4 MLE surface concentrations. In these studies, a decrease in C-H stretching frequency was observed with the change in adsorption type from atop to bridge. On PtNi(111), C-H stretching frequencies calculated for the CH_3 molecule were in the range of 3000-3500 cm^{-1}, similar to the Ni(111) surface. For the CH_2 adsorbed molecule, this range was 2800-2600 cm^{-1}, and that for the CH molecule, it was 2950-2730 cm^{-1} (Ayvaz, 2010).

FTIR-DRIFT spectroscopy was also employed by the researchers for monitoring the CDRM reaction. Son *et al.* investigated the effect of MgO addition on the CDRM performance of the bimetallic Co-Ni/Al_2O_3 catalysts. They conducted FTIR-DRIFTS study under 100 ml/min flow of CH_4, CO_2, N_2 at 300 °C. For CH_4-CO_2 co-feeding conditions, large amounts of formate and carbonate species were observed. They found that with the addition of MgO, the adsorption of formate species was increased indicating that the MgO

addition fastened the decomposition/dissociation of CH_4 and CO_2 resulting in an increase in the formation of formate intermediates (Son *et al.*, 2014).

Garcia-Dieguez *et al.* performed a FTIR-DRIFTS study at 500 °C on Pt/Al_2O_3 catalysts supported on nanofibrous-structured alumina. The composition of the feed mixture was changed in a cyclical manner. First, CO_2 and CH_4 were fed together and a strong band at 2057 cm^{-1} corresponding to the linearly adsorbed CO was observed. A band at 1980 cm^{-1}, which they did not observe in their CO adsorption tests conducted at the same temperature, also appeared. They explained the existence of this band by the CO adsorption on Pt with increased electronic density promoted by the presence of CH_x and H_2 species. After 15 minutes, they also observed formate species (at 1380, 1598 and 2908 cm^{-1}) together with carbonate, bicarbonate and carboxylate species. Secondly, only CH_4 was fed to the system and no change in the surface species was observed except for a decrease in the gaseous CO band. After a third cycle for which both reactants were co-fed again, a fourth cycle, with only CO_2 feed, was introduced. At this cycle, bands related with formate species and a band assigned to the CH_x and H_2-promoted CO adsorption on Pt metal were disappeared while the intensities of the bands yielded by the carbonate and bicarbonate species were increased. A decrease in the intensity of the band belongs to linearly adsorbed CO on Pt, at 2057 cm^{-1}, was also observed. These changes in the spectra led the authors to propose that the presence of H_2 and CH_x species were definitely enhances CO_2 activation (Garcia-Dieguez *et al.*, 2010a).

Kroll *et al.* also conducted in situ FTIR-DRIFTS analysis over Ni/SiO_2 during CDRM reaction. At 500 °C, they observed linear and multibonded CO species at 2012 and 1855 cm^{-1}, respectively. They also observed a sharp band at 3718 cm^{-1}, which was assigned to the terminal silanol groups (Si-OH). At 700 °C, they could not observe adsorbed CO species or hydroxyl bands. They only observed broad and weak bands in the 2700-3000 cm^{-1} region, which developed by time on stream and are assigned to the C-H species. After 22 hours of reaction, this C-H region was narrowed and they assigned bands at 2965, 2928, and 2860 cm^{-1} to the $–CH_3$, $=CH_2$ and $\equiv CH$ species, respectively (Kroll *et al.*, 1996).

3. EXPERIMENTAL WORK

3.1. Materials

3.1.1. Chemicals

The chemicals used for catalyst preparation and background spectrum for FTIR-DRIFTS studies are presented in Table 3.1. All the chemicals used are research grade with high purity.

Table 3.1. Chemicals used for catalyst preparation.

Chemicals	Formula	Specification (%)	Source	Molecular Weight (g/mol)
Aluminum Oxide	γ-Al_2O_3	99.98	Alfa Aesar	101.96
Nickel(II) nitrate hexahydrate	$Ni(NO_3)_2$.6H2O	99	Merck	290.81
Tetraammineplatinum (II) nitrate	$Pt(NH_3)_4(NO_3)_2$	99.995+	Aldrich	387.22

3.1.2. Gases and Liquids

All of the gases used in this study were bought from Birleşik Oksijen Sanayi (BOS) A.Ş. and Linde Group, Istanbul. Liquid nitrogen was supplied by HABAŞ. Table 3.2 and Table 3.3 show the specifications and applications of the liquids and gases used in this study.

Table 3.2. Specifications and applications of the gases used.

Gas	Specification (%)	Application
Argon	99.995	DRIFT Cell
Carbon dioxide	99.995	Reactant
Carbon monoxide	99.999	Reactant
Helium	99.999	Inert
Hydrogen	99.995	Reducing Agent
Methane	99.995	Reactant

Table 3.3. Specifications and applications of the liquids used.

Liquid	Specification	Application
Nitrogen	HABAŞ	MCT Detector
Water	Deionized (DI)	Aqueous solutions

3.2. Experimental Systems

3.2.1. Catalyst Preparation Systems

Catalysts used in this study were prepared by incipient-to-wetness impregnation method which has three steps:

- Evacuating the support,
- Contacting the support with the precursor solution, and
- Drying.

In this method, certain amount of support was placed in the Buchner erlenmeyer and kept under vacuum both before and during the addition of precursor solution in order to remove trapped air in pores and let the precursor solution to penetrate into pores. First, the support material was mixed with ultrasonic mixer for 30 min. A MasterFlex computerized-

drive peristaltic pump was used to add the precursor solution to the vacuum flask at a rate of 0.5 ml/min through silicone tubing. The slurry was mixed during and after impregnation for an extra 90 min for uniform metal dispersion. The thick slurry obtained was dried overnight to remove water.

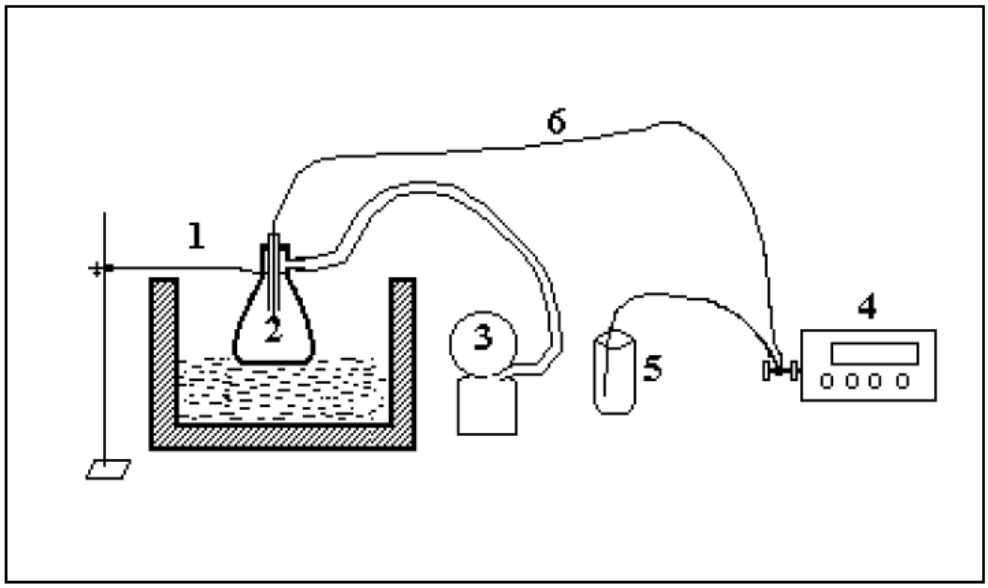

Figure 3.1. Schematic diagram of the impregnation system (Akın, 1996).
1. Ultrasonic mixer, 2. Büchner flask, 3.Vacuum pump, 4. Peristaltic pump, 5. Reactant storage tank, 6. Silicone Tubing.

3.2.2. Catalyst Characterization and Reaction System

A schematic representation of the FTIR-DRIFTS system is given in Figure 3.2. The FTIR transmittance/absorbance spectra have been collected on a Bruker Vertex 70V equipped with a Mercury-Cadmium-Telluride (MCT) detector. PIKE Technologies DRIFTS cell with ZnSe window with PIKE Technologies temperature controller and Brooks mass flow controllers allowed thermal treatments under controlled atmospheres and spectrum scanning at controlled temperatures (20-320 °C).

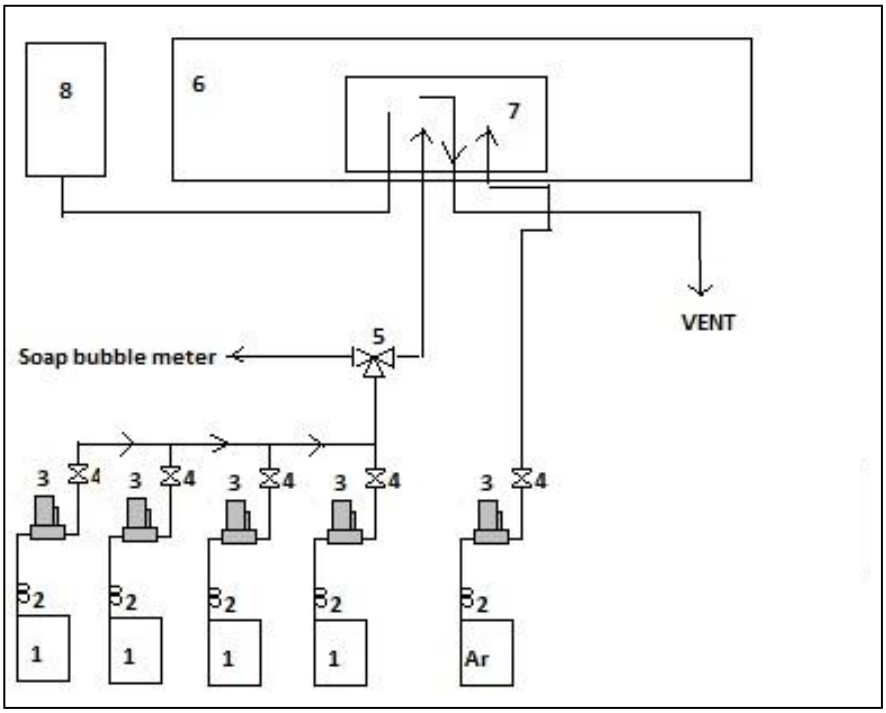

Figure 3.2. Schematic representation of FTIR-DRIFTS system (Çağlayan, 2011). 1.Gas cylinders, 2. Gas Regulator, 3. Mass flow controller, 4. On-off valve, 5. Three-way valve, 6. FTIR, 7. DRIFTS cell, 8. Heating chamber.

The feed section was composed of mass flow control systems, 1/4", 1/8" and 1/16" stainless steel tubing and fittings for feeding gaseous species, i.e. carbon monoxide, carbon dioxide, methane, helium, argon and hydrogen. The high purity gases were supplied by pressurized cylinders and were passed through the gas flow regulators. The flow rates of the gasses were controlled by Brooks Instrument mass flow controllers and the set values of were adjusted by two Brooks Instrument 0154 series control boxes. On-off valves were placed in front of the mass flow controllers to protect them from possible back-pressure fluctuations. In order to meter the flow of individual species and adjust desired feed ratios, each gas was fed from an independent line.

3.3. Catalyst Preparation and Pretreatment

In this thesis, two catalysts, 0.2Pt15Ni/δ-Al_2O_3 and 0.3Pt10Ni/δ-Al_2O_3, which were previously studied in our group for their CDRM performance and reaction kinetics and shown to have different CDRM mechanisms, were used.

Pellet form γ-Al_2O_3 support material was crushed and sieved to 250-354 μm (45-60 mesh) particle size. After drying γ-Al_2O_3 at 150 °C for 2 h and then calcining it at 900 °C for 4 h in a muffle furnace, thermally stable δ-Al_2O_3 support was obtained.

A sequential impregnation route was applied in the preparation of bimetallic Pt-Ni/δ-Al_2O_3, in which Pt solution was impregnated over initially prepared and calcined Ni/δ-Al_2O_3 catalyst. Ni was impregnated on δ-Al_2O_3 support using an aqueous solution of $Ni(NO_3)_2.6H_2O$ precursor as explained in Section 3.2.1. The precursor solutions were prepared by dissolving the calculated amount of the precursor salt in deionized water with the ratio of ca. 1 ml solution/g support. The resulting slurry was then dried overnight at 120 °C and calcined at 600 °C for 4 h to obtain NiO/δ-Al_2O_3. Similarly, Pt solution prepared using $Pt(NH_3)_4(NO_3)_2$ as a precursor was added to NiO/δ-Al_2O_3 and the resulting slurry was dried overnight at 120 °C and calcined at 500 °C for 4 h. In order to obtain the same surface characteristics of the bimetallic PtNi catalysts as that were used by Özkara-Aydinoğlu in her performance and kinetic experiments, an *ex situ* reduction with 50 ml/min H_2 flow was performed for 2 h at 500 °C.

3.4. Catalyst Characterization and Reaction Tests

3.4.1. Pretreatment Tests

In order to activate the catalyst, an *in situ* reduction pretreatment was conducted prior to the FTIR-DRIFTS experiments. Four different pretreatment procedures were applied as given in Table 3.4. All the pretreatments were performed on 0.3Pt10Ni/δ-Al_2O_3. After the *in situ* pretreatment, 30 min of 1% CO adsorption and a following 30 min of He flush was used to understand the effect of pretreatment on the catalyst surface as CO is a widely used probe molecule for surface characterization purposes.

In pretreatment 1, catalyst sample prereduced *ex situ* was heated to 393 K with 20 K/min heating rate under 45 ml min^{-1} He flow. Then, sample was flushed 45 ml min^{-1} He flow at 393 K for 20 minutes followed by cooling to the room temperature under He flow.

In pretreatment 2, catalyst sample prereduced *ex situ* was heated to 573 K with 20 K/min heating rate under 45 ml min^{-1} He flow. Then, the sample was flushed 45 ml min^{-1} He for one hour at 573 K and cooled down to the room temperature under the same flow.

In pretreatment 3, catalyst sample prereduced *ex situ* was heated to 573 K with 20 K/min heating rate under 45 ml min^{-1} He flow. Then, the sample was reduced under 10% H_2/He mixture of 45 ml min^{-1} He flow for one hour at 573 K and cooled down to the room temperature under 45 ml min^{-1} He flow.

In pre-treatment 4, catalyst sample prereduced *ex situ* was heated to 573 K with 20 K/min heating rate under 45 ml min^{-1} He flow. Then, the sample was reduced under 50 ml min^{-1} 10% H_2/He mixture of 45 ml min^{-1} He flow for one hour at 573 K. Then, H_2 flow was stopped and the temperature was increased to 593 K in one minute. At 593 K, sample was flushed with 45 ml min^{-1} He for one hour and cooled down to the room temperature under the same flow.

Table 3.4. Pretreatment procedures.

Pretreatment	**Procedure**
1	20 min He flow at 393 K
2	One hour He flow at 573 K
3	One hour reduction under 10% H_2/He flow at 573 K
4	One hour reduction under 10% H_2/He flow at 573 K followed by one hour He flush at 593 K

After performing the pretreatment procedures and the sample cooled down to the room temperature under He flow, CO adsorption experiments were conducted with 1% CO/He mixture for a He flow of 45 ml/min. Finally, He flush was applied under 45 ml/min of He flow at room temperature for 30 minutes.

3.4.2. Adsorption and Reaction Tests

The FTIR-DRIFTS system described in Section 3.2.2 was used for conducting adsorption and reaction experiments. The catalyst samples were firstly reduced *ex situ* at 500 °C for 2 h using flowing 50 mL min^{-1} H_2. In the case of CO/He adsorption and FTIR-DRIFTS-TPD-CO studies, the ex situ reduced catalyst sample in a very fine powder form was diluted with dry KBr (1:10 w/w) in order to improve signal-to-noise ratio. Dilution rate for the CO_2, CH_4 and reaction tests were 1:5 (w/w). Signal averaging was set to 128 scans per spectrum, and the spectra were collected at a 4 cm^{-1} resolution in the 4000-600 cm^{-1} range.

In CO adsorption studies, *ex situ* reduced catalyst sample in a very fine powder form was diluted with dry KBr (1:10 wt/wt) for improved S/N ratio. In accordance with the results obtained from the pretreatment tests, an *in situ* pretreatment following the procedure of pretreatment 4 was applied prior to all experiments. The background spectrum of the solid catalyst was taken after the *in situ* pretreatment at the adsorption temperature under He flow. CO adsorption experiments were conducted both at room temperature and at 573 K under 1% CO/He mixture for a He flow of 45 ml min^{-1} for 30 minutes. Following 30 min of adsorption, CO flow was stopped and the sample was flushed with of 45 ml min^{-1} He flow 30 minutes in order to observe the species strongly adsorbed on the catalyst surface. In the adsorption tests conducted at 573 K, catalyst sample that was heated to 593 K after reduction at 573 K was cooled to the test temperature under He flow. Spectrum of the catalyst was taken in 10 minute intervals and a total of 8 spectra were obtained. The spectrum of the solid catalyst taken after the pre-treatment was subtracted from the spectrum of the catalyst obtained after exposure to the adsorption mixture.

Same procedure was followed for the CO_2 and CH_4 adsorption tests which were also conducted both at room temperature and 573 K. Yet, dilution rate of the sample was decreased to 1:5 wt/wt and the experiments were conducted under 10% CO_2/He or 10% CH_4/He mixture with a He flow of 45 ml/min.

For the FTIR-DRIFTS-CO-TPD tests, first a CO adsorption test at room temperature was conducted. After a 30 min of He flow, temperature was increased to 100 °C with 20 K/min heating rate under 45 ml min^{-1} He flow. Four spectra were taken with 10 min interval and temperature was increased to 200 °C with 20 K/min heating rate. Similarly, four spectra were taken with 10 min intervals and temperature was increased further to 300 °C under same flow and heating rate. An additional four spectra were taken at this temperature.

Table 3.5. List of FTIR-DRIFTS experiments.

Experiment	**Catalyst**	**Temperature**	**Feed Composition (%) with He as balance**		
			CH_4	**CO_2**	**CO**
CO adsorption	0.2Pt15Ni	298 K	-	-	1
CO adsorption	0.3Pt10Ni	298 K	-	-	1
CO adsorption	0.2Pt15Ni	573 K	-	-	1
CO adsorption	0.3Pt10Ni	573 K	-	-	1
CO-TPD	0.2Pt15Ni	298-573 K	-	-	1
CO-TPD	0.3Pt10Ni	298-573 K	-	-	1
CO_2 Adsorption	0.2Pt15Ni	298 K	-	10	-
CO_2 Adsorption	0.3Pt10Ni	298 K	-	10	-
CO_2 Adsorption	0.2Pt15Ni	573 K	-	10	-
CO_2 Adsorption	0.3Pt10Ni	573 K	-	10	-
CH_4 Adsorption	0.2Pt15Ni	298 K	10	-	-
CH_4 Adsorption	0.3Pt10Ni	298 K	10	-	-
CH_4 Adsorption	0.2Pt15Ni	573 K	10	-	-
CH_4 Adsorption	0.3Pt10Ni	573 K	10	-	-
Reaction	0.2Pt15Ni	573 K	40	40	-
Reaction	0.3Pt10Ni	573 K	40	40	-

In situ reaction tests were conducted at 573 K under 50 ml min^{-1} of 40% CO_2-40% CH_4-20% He mixture. Reaction experiments were performed for one hour and followed by

a He flush at 573 K with 45 ml min^{-1} for 30 min. Spectrum of the catalyst sample was taken in 10 minute intervals and a total of 11 spectra were obtained.

All the experiments performed in the adsorption and reaction studies are summarized in Table 3.5.

4. RESULTS AND DISCUSSION

CDRM is one of the most well-known and used hydrogen (or syngas) production route having an advantage of converting two greenhouse gasses, CO_2 and CH_4, into valuable products. The aim of the current work is to understand the routes and mechanistic steps of the CDRM on the active sites of the bimetallic catalysts that had been designed and shown to have high activity and selectivity in CDRM reaction. Ni/Al_2O_3 catalysts are known to be highly active for the CDRM, yet they are also prone to carbon deposition which limits their use in possible industrial CDRM applications. Incorporating Ni catalysts with small amounts of noble metals has been shown to improve the performance of the Ni based catalysts. In a previous study performed in our group, performance of the bimetallic 0.3-0.5 wt. % Pt and 10-15 wt. % catalysts were investigated and the catalyst with the lowest Ni:Pt ratio was shown to have both high CDRM activity and stability (Özkara-Aydinoğlu and Aksoylu, 2011). A following kinetic study revealed that kinetic parameters and models differed significantly by the change in Ni:Pt ratio (Özkara-Aydionğlu and Aksoylu, 2013). In this study, FTIR-DRIFTS spectroscopy was used in order to gain a deeper insight into the difference between these two bimetallic catalysts. Bimetallic $0.3Pt10Ni/Al_2O_3$ and $0.2Pt15Ni/Al_2O_3$ catalysts were characterized first with the help of CO adsorption experiments on FTIR-DRIFTS. Characterization tests were performed both at room temperature and at elevated temperatures, 300 °C, in order to observe the effect of temperature on the catalyst surface. As CO is also a product of the CDRM reaction, CO adsorption experiments are useful to observe the effect of product on the catalytic sites. Following the characterization studies, FTIR-DRIFTS analysis was performed on the freshly reduced forms of both PtNi catalysts under the flow of individual reactants, under the flow of He-diluted CO_2 and He-diluted CH_4, both at room temperature and at 300 °C, aiming to understand the adsorption properties of the reactants and products on the active sites. As the last part of the studies, *in situ* reaction tests were performed by feeding both of the reactants into the IR cell in order to observe the changes on the active sites under the flow of the reactant gasses.

4.1. Effect of Pretreatment

Prior to the experiments, all catalyst samples were *ex situ* reduced at 500 °C for 2 hours under %100 H_2 flow. A further *in situ* pretreatment procedure was performed in order to activate the sample. It is highly possible that some hydroxyl species may form on the catalyst surface during the catalyst preparation prior to the FTIR DRIFTS experiment, and these species may deactivate the surface. Hence, as summarized in Table 3.4, four different pretreatments were conducted and the resulting surface was characterized by 1% CO adsorption tests in order to find the most suitable pretreatment procedure. Resulting spectra taken after 30 minutes of CO adsorption and after the following additional 30 minute He flush are shown in the Figure 4.1 and Figure 4.2, respectively.

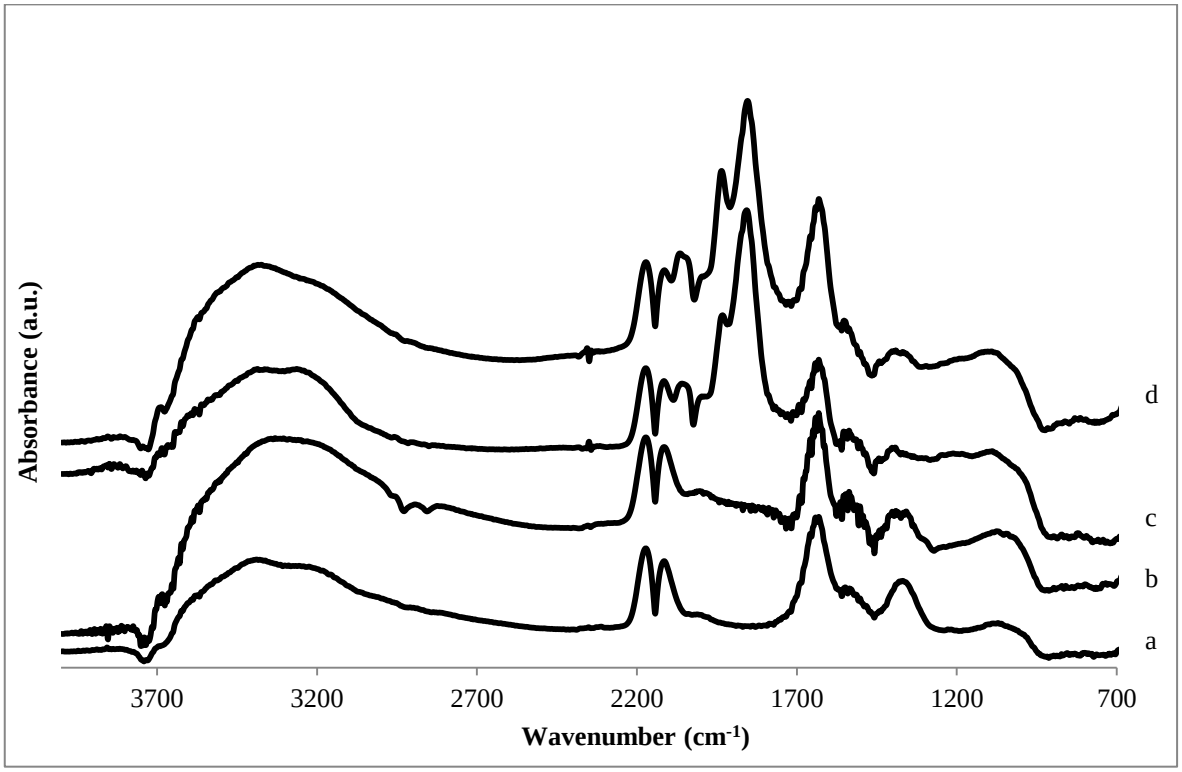

Figure 4.1. Spectra obtained upon 30 min 1% CO adsorption on 0.3Pt10Ni/Al_2O_3 catalysts at room temperature with *in situ* pretreatment 1 (a), pretreatment 2 (b), pretreatment 3 (c) and pretreatment 4 (d).

After pretreatment 1, apart from gaseous CO observed at 2181 cm^{-1} and 2015 cm^{-1}, a wide but weak band was observed in the 2000-2100 cm^{-1} region which can be assigned to the CO adsorbed on Pt and Ni particles mostly in linear fashion. Only strong bands are due to those of carbonaceous species in the 1200-1800 cm^{-1} region and to those of hydroxyl groups at 3000-3800 cm^{-1}. Yet, after He flush, bands associated with linearly adsorbed CO were all removed showing that they were not strongly chemisorbed on the surface.

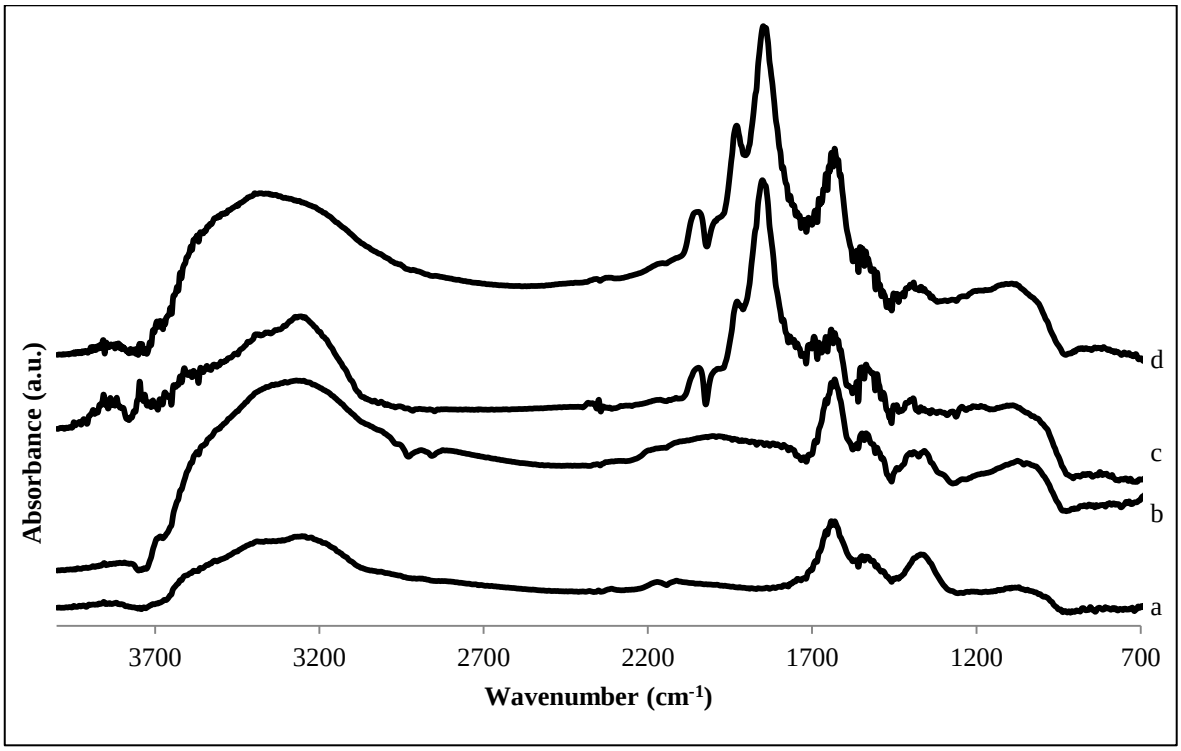

Figure 4.2. Spectra obtained upon 30 min 1% CO adsorption followed by 30 min He flush on 0.3Pt10Ni/Al_2O_3 catalysts at room temperature with *in situ* pretreatment 1 (a), pretreatment 2 (b), pretreatment 3 (c) and pretreatment 4 (d).

When the inert flow temperature is increased to 300 °C in pretreatment 2, both carbonaceous and OH bands were increased in intensity. Similar to the pretreatment 1, a very wide band in the metal-carbonyls region (1800-2300 cm^{-1}) was appeared but they were more apparent this time with some bridged CO species appearing around 1960 cm^{-1}. Furthermore, these chemisorbed CO species were not removed after He flow. Spectra upon He flush also revealed that there was a wide region in the 2220-2120 region cm^{-1}, which can be assigned to CO adsorbed on unreduced Ni atoms (Poncelet *et al.*, 2005).

Performing an additional *in situ* reduction process at 300 °C (pretreatment 3), there appeared four different bands in the metal carbonyl region indicating that the inactivity towards CO for the pretreatments 1 and 2 was a result of metal oxidation and they were removed by the hydrogen treatment. Also, these species were stabilized on the surface indicated by their presence after He flow.

A further inert flow after reduction at 320 °C (pretreatment 4), resulted in a spectrum with a better quality; showing increase in the intensity of the linearly, bridged and multi-bonded CO bands. Hence pretreatment 4 was chosen as the pretreatment procedure and all the following FTIR-DRIFTS experiments were conducted by following pretreatment 4.

Carbonaceous species are produced upon the contact between the flowing gas and the alumina support. Surface OH groups of the alumina are known to exist on the surface when the pretreatment temperature is below 500 °C (Parkyns, 1971). Since, both *ex situ* and *in situ* reductions were not performed at temperatures higher than 500 °C, it is certain that there existed certain amount of –OH groups on the surface and they were involved in the formation of the carbonaceous species. The negative peaks in the 3600-3800 cm^{-1} region which belong to the surface hydroxyls of alumina shows that some of the –OH groups were consumed by the gaseous CO in the formation of carbonaceous species.

The spectral region corresponding to the carbonaceous species did not seem to be altered significantly by the change in the pretreatment procedure. This result indicates that the main effect of the pretreatment was on the active metals and the *in situ* reduction removed oxygen from NiO and PtO particles giving way to the metallic Ni and Pt.

4.2. CO Adsorption Experiments

4.2.1. CO Adsorption Experiments at Room Temperature

CO adsorption tests performed in FTIR-DRIFTS at room temperature are frequently used for characterization purposes. Metal carbonyl region of the obtained spectra upon CO adsorption at room temperature for 0.3Pt10Ni and 0.2Pt15Ni catalysts are given in Figure

4.3 and Figure 4.4, respectively. First 4 spectra from the below belongs to the spectrum taken after 0, 10, 20 and 30 minutes of adsorption test; while the other top 4 spectra belongs to the spectra taken after 0, 10, 20 and 30 minutes of He flush.

CO adsorption experiments on both of the catalysts show that there is a broad band between 2090 and 2020 cm^{-1} indicating moderately to highly dispersed Ni^0 species. Bands below 2000 cm^{-1} are indication of bridged CO and low dispersed Ni sites (Poncelet *et al.*, 2005). As Poncelet *et al.* proposed a reduction temperature between 450-550 °C leads to enhancement of the mobility of the nickel species and increases the probability of forming ensembles composed of several adjacent nickel atoms. These adjacent Ni atoms set the surface for the formation of bridged and multibonded CO (Poncelet *et al.*, 2005).

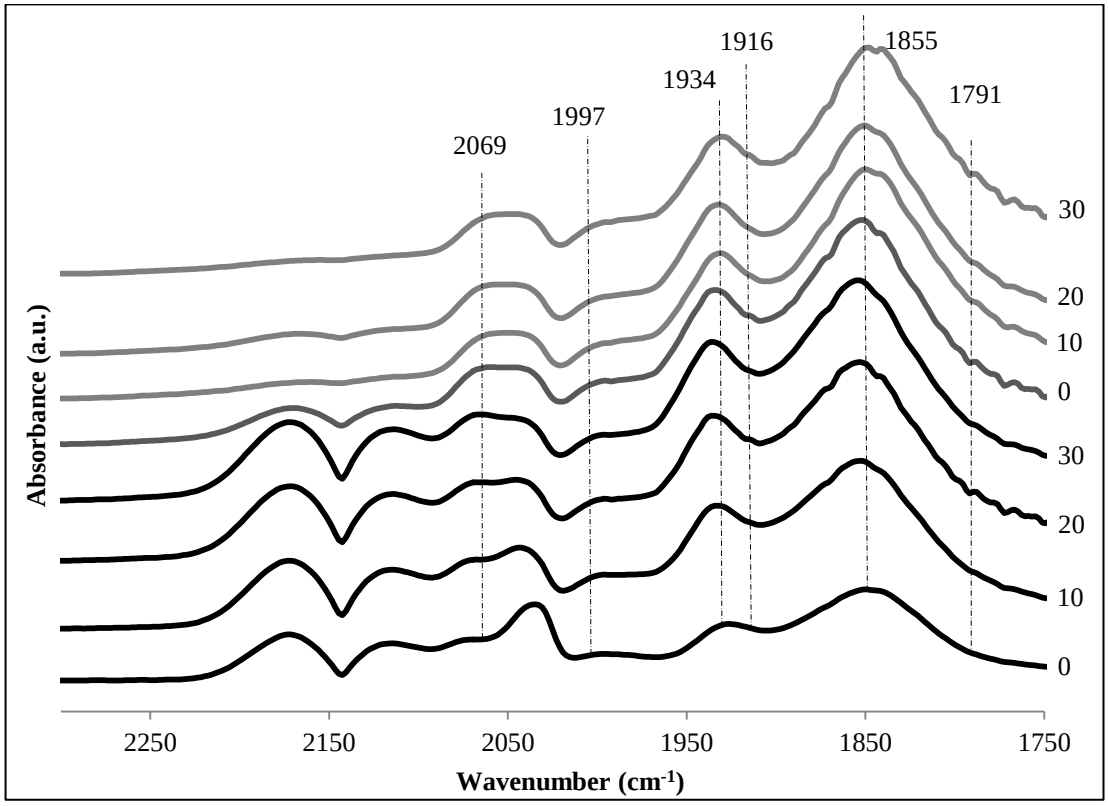

Figure 4.3. Spectra obtained on 0.3Pt10Ni/Al_2O_3 catalyst upon 30 min 1% CO adsorption followed by 30 min He flush at room temperature.

Absence of any bands above 2090 cm^{-1} reveals that there are no significant unreduced Ni sites prevalent on the catalyst or they are hindered by the gaseous CO peak.

However, absence of these unreduced sites on the spectra of the both of the samples does not mean that both of the samples were completely reduced. Kester *et al.* showed that there are two different Ni^{2+} species formed during the catalyst preparation and reduction, with distributions varying with the Ni content: one was Ni^{2+} in tetrahedral sites of alumina (Ni_T^{2+}), the other one was Ni^{2+} in octahedral positions (Ni_{Oc}^{2+}). While nickels positioned on octahedral sites are reducible and participates in the CO adsorption, nickels in tetrahedral environment are not reducible at 500 °C and do not adsorb CO molecules (Kester *et al.*, 1986). Hence, the presence of Ni^{+2} atoms at the tetrahedral positions should not be excluded as they cannot be observed by the IR-CO experiments (Poncelet *et al.*, 2005; Damyanova, 1996). Furthermore, some CO adsorbed on unreduced Ni species can be observed if the reduction of a specie is not complete, by judging from the adsorption tests conducted with pretreatment 2 (see Figure 4.2). When only the Ni atoms that are positioned at octahedral positions, and hence already reducible ones, are considered by inspecting the relative sizes of the bands, it can be inferred that the amount of unreduced NiO sites (Ni^{+2} or Ni^{+} species) are insignificant when compared with other reduced adsorption sites. Thus, absence, or very little amount, of unreduced Ni sites is consistent with the literature on Pt-Ni bimetallic catalysts as Pt addition to Ni metal is known to lead an easier reduction of the Ni metal (Mahoney *et al.*, 2014; Gould *et al.*, 2015).

On 0.3Pt10Ni sample, strong band at 1934 cm^{-1} and a shoulder at 1916 cm^{-1}, which is strongly covered by the former, indicate bridged CO molecules bonded to the Ni(111) and Ni(100) surfaces, respectively (Dias and Assaf, 2004). At 1855 cm^{-1} and 1791 cm^{-1} multibonded CO molecules adsorbed with different geometrical configurations (HCP and FCC) are also observed. The width and high intensity of these bands indicate that large amounts of Ni^0 crystallites were present on the surface leading to bridged or multibonded CO species.

A DFT study conducted in our group revealed that CO adsorption frequency on Ni(111) was 1975 cm^{-1} for FCC and 1987 cm^{-1} for HCP sites (Ayvaz, 2010). Although their frequencies seem to be shifted to the higher wavenumbers in the DFT study, by judging from their respective ranking, it can be inferred that the band around 1855 cm^{-1} refers to the HCP sites, whereas the band at 1791 cm^{-1} signifies the CO adsorbed on FCC

sites. They also found that the strongest chemisorption occurred at HCP sites; which is in accordance with the higher intensity observed for the band at 1855 cm^{-1}.

A closer inspection into the metal carbonyl region revealed that there are two bands that evolve by the time on stream: A band around 2069 cm^{-1} and another around 1997 cm^{-1}. The band around 2069 cm^{-1} probably corresponded to the linear CO adsorption on Pt metal as it was more pronounced on the sample with higher Pt loading. Its broad nature, comprising up to 2060 cm^{-1}, suggests CO adsorption on different Pt sites. According to Greenler *et al.*, band at 2069 cm^{-1} belongs to the CO adsorbed on corner atom, while band at 2060 cm^{-1} indicates CO adsorbed on an edge Pt atom (Greenler *et al.*, 1985). The gradual increase of this band could be attributed to the low interaction between those species at low surface concentrations (Yates and Garland, 1961).

Another band around 1997 cm^{-1}, which also developed during time on stream, belonged to the CO adsorbed on Ni metals in bridged form. This band can be attributed to the bridge type bonding which occurs between two adjacent Ni sites which both have one linearly bonded CO molecule to each (similar to the species reported to be observed in 1990-1940 cm^{-1} region in Table 2.1). As these species requires linearly bonded CO molecules to form, their intensities grew in the later stages of the adsorption.

Spectra obtained on 0.2Pt15Ni sample have the very similar bands to the 0.3Pt10Ni sample in the bridged and multibonded CO region. However, linear bonded CO region shows some discrepancies. In this region, spectrum seems to be centered around the band at 2028 cm^{-1} which was not detected on the 0.3Pt10Ni sample. This may be due to the higher Ni content of the 0.2Pt15Ni sample giving rise to the more types of Ni crystallographic structures to appear on the surface. Those two bands growing during time on stream, at 2069 and 1997 cm^{-1}, also appears on 0.2Pt15Ni sample. Yet, the band at 2069 cm^{-1} is much weaker which can be a result of the lower Pt content.

No quantitative analysis on the intensity of the adsorption bands was performed in this study. Yet, as the gaseous CO concentration was 1% for both of the adsorption experiments, its intensity can be used as a reference to compare the relative intensities of the other bands. The most striking result is that the intensity of the bands above 2000 cm^{-1}

on the 0.3Pt10Ni catalyst is higher than the intensity of the gaseous CO; whereas intensity of the bands above 2000 cm^{-1} on the 0.2Pt15Ni sample is lower than the gaseous CO. As the bands above 2000 cm^{-1} indicates well dispersed metal particles, it can be concluded that dispersion of the Ni on the sample containing higher amount of Pt, i.e. 0.3Pt10Ni, was better than on the 0.2Pt15Ni sample. This result was also confirmed by XRD results performed on 0.2Pt15Ni and 0.3Pt10Ni catalysts. While the Ni size was found to be 12.6 nm for 0.3Pt10Ni sample, it was found as 19.8 nm for the 0.2Pt15Ni sample. This was suggested to be due to the intimate interaction between the Pt and Ni sites in the closed vicinity (Özkara-Aydinoğlu and Aksoylu, 2011).

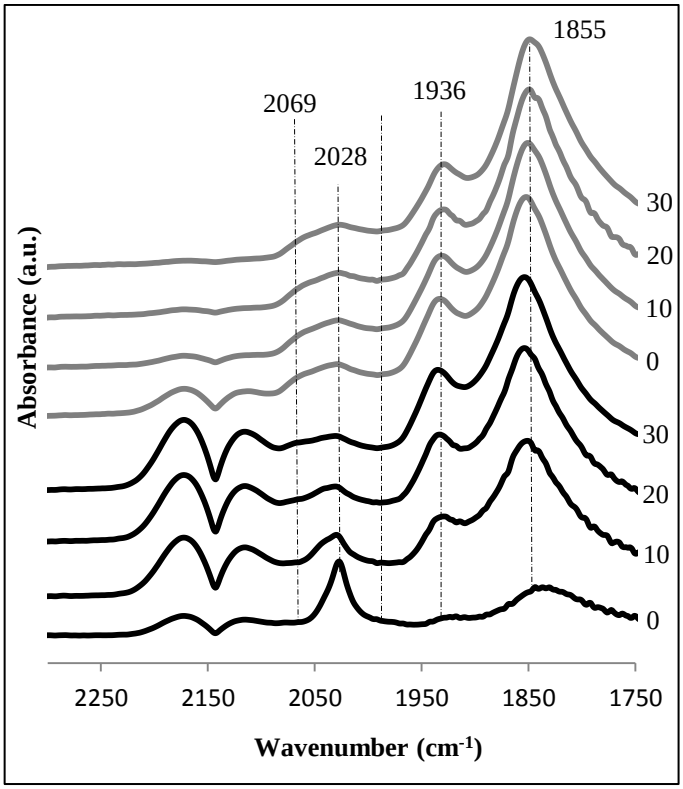

Figure 4.4. Spectra obtained on 0.2Pt15Ni/Al_2O_3 catalyst upon 30 min 1% CO adsorption followed by 30 min He flush at room temperature.

There seemed no difference between two catalysts in terms of the carbonaceous species formed on the surface as those species mostly form on the alumina support. No C-H band was observed around 2900 cm^{-1} revealing that formate species were not formed on the surface (See spectrum d on Figure 4.1). There were two negative peaks in the OH

region at ca. 3731 and 3675 cm^{-1}. These negative peaks were due to the consumption of OH groups of the alumina during the production of carbonate and bicarbonate species.

4.2.2. CO Adsorption Experiments at 300 °C

CO adsorption tests were also conducted at 300 °C and the results are shown for both 0.3Pt10Ni and 0.2Pt15Ni catalysts in Figure 4.5 and Figure 4.6, respectively. First four spectra from the below belongs to the spectrum taken after 0, 10, 20 and 30 minutes of adsorption test; while the other top 4 spectra belongs to the spectra taken after 0, 10, 20 and 30 minutes of He flush.

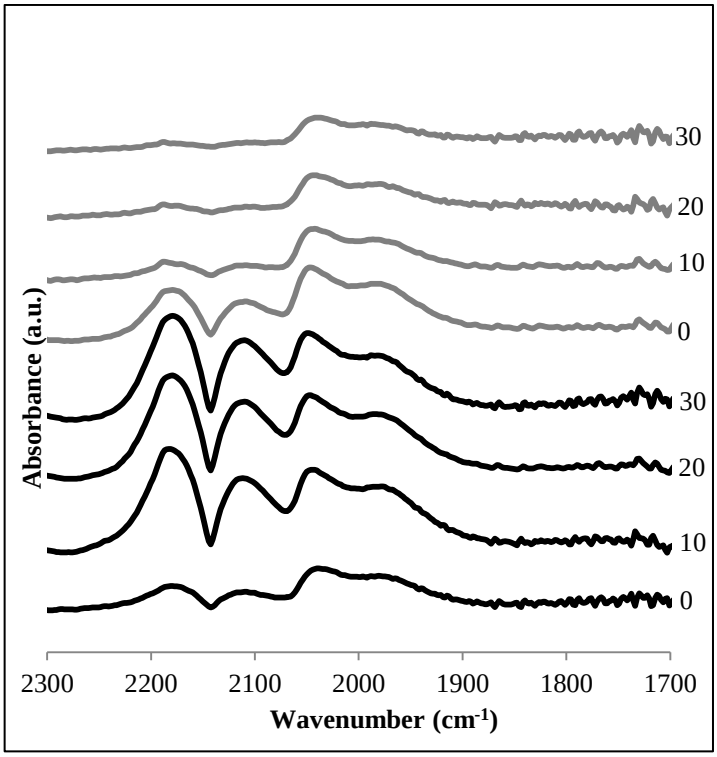

Figure 4.5. Spectra obtained on 0.3Pt10Ni/Al_2O_3 catalyst upon 30 min 1% CO adsorption followed by 30 min He flush at 300 °C.

Upon CO adsorption on 0.3Pt10Ni sample, two wide and strong bands appeared in the metal carbonyl region: one large band centered around 2048 cm^{-1} and one around 1980 cm^{-1}. First one corresponds to the linearly adsorbed CO on Ni metal particles with various

metal particle sizes. Second band corresponds to the bridge bonded CO molecules. Upon He flush, these bands did not vanish, although their intensities decreased in some extent.

CO adsorption on 0.2Pt15Ni sample resulted in a wide band between 1900-2070 cm^{-1}. Linearly bonded CO molecules were observed around 2011 cm^{-1}. This region had a long tail reaching down to around 1900 cm^{-1}showing that there were also some bridge bonded CO molecules on the surface. Upon 30 minutes of helium flow, these bands almost vanished leaving only a very large and weak band.

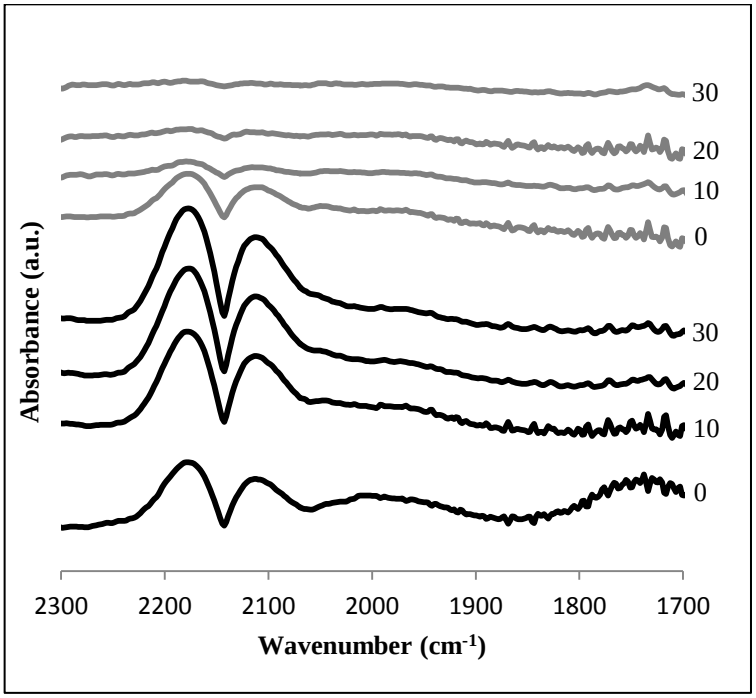

Figure 4.6. Spectra obtained on 0.2Pt15Ni/Al_2O_3 catalyst upon 30 min 1% CO adsorption followed by 30 min He flush at 300 °C.

CO bands on 0.3Pt10Ni sample were definitely stronger than the observed on 0.2Pt15Ni sample. A comparison of the relative intensities by judging from the gaseous CO intensity, which should be same for the same flow, it is obvious that more CO molecules were adsorbed on the 0.3Pt10Ni sample. The most probable reason for this would be the difference in the degree of reduction between those two samples. Better reduction is expected to result in a higher amount of Ni^0 atoms to be available for CO adsorption. As the Pt addition to the Ni metal is known to improve the reducibility of the

catalyst, lower Ni:Pt ratio of the 0.3Pt10Ni sample resulted in a higher extent of reduction. This result was also confirmed by Özkara-Aydinoğlu and Aksoylu who conducted XPS analysis on freshly reduced 0.2Pt15Ni and 0.3Pt10Ni catalysts. They observed that relative intensity of the Ni^{+2} species was 78% for 0.2Pt15Ni sample, while it was 60% for the 0.3Pt10Ni catalyst (Özkara-Aydinoğlu and Aksoylu, 2011). The result obtained from XPS analysis together with the CO adsorption tests performed in this study, clearly shows the beneficial effect of Pt addition to the degree of reduction of the Ni/Al_2O_3 catalyst.

4.2.3. Temperature Programmed CO Desorption Tests

Upon CO adsorption at room temperature, a gradual heating was applied under He flow. Temperature was increased from 25 °C to 100, 200 and 300 °C and at each temperature 30 minutes of inert gas flow was introduced into the system. Figure 4.7 shows the resulting spectra for the 0.3Pt10Ni (left figure) and 0.2Pt15Ni (right figure) samples.

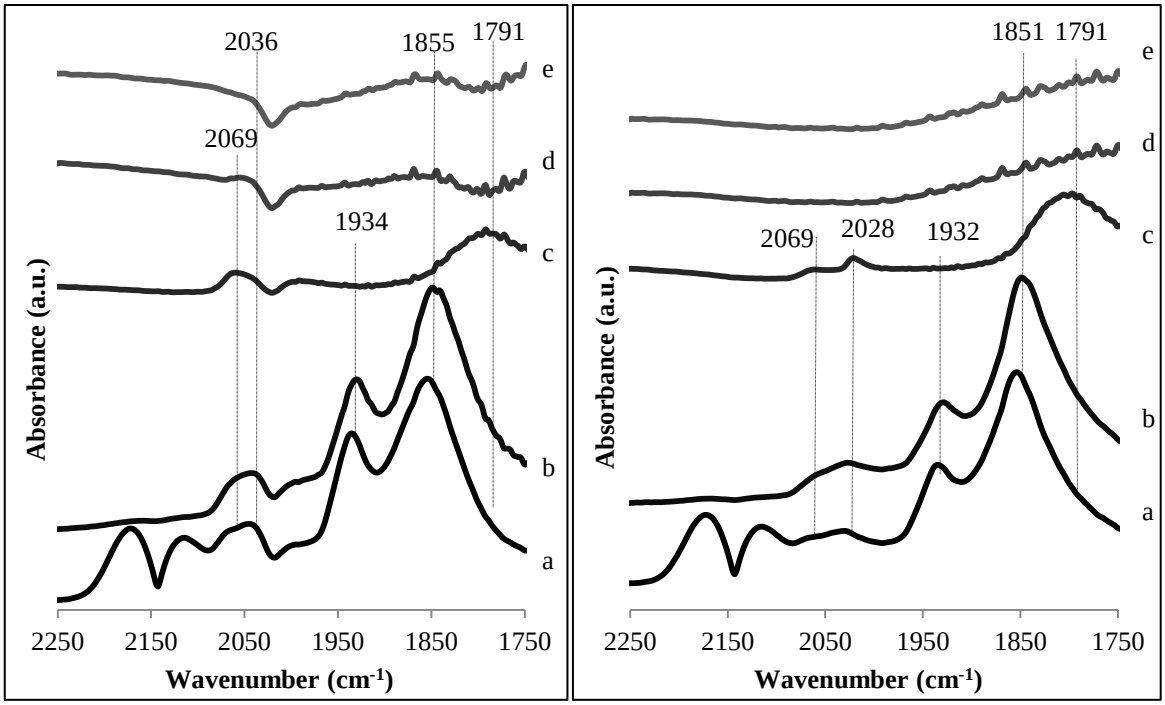

Figure 4.7. Spectra obtained on 0.3Pt10Ni (left) and 0.2Pt15Ni (right) after 30 min CO flow at 25 °C (a), 30 min He flow at 25 °C (b), followed by 30 min He flow at 100 °C (c), at 200 °C (d), and at 300 °C (e).

During the desorption at 100 °C on 0.3Pt10Ni sample, bridge bonded species around 1934 cm^{-1} and multibonded species around 1855 cm^{-1} were gradually vanished and only very small band at 1855 cm^{-1} left after 30 minutes of He flow. Band around 2036 cm^{-1} was also decreased in intensity which could be related with the linearly bonded CO molecules to Ni^0 species. Yet, band related with the linearly bonded CO molecules to the Pt atom, i.e. 2069 cm^{-1}, remained and became more apparent. Furthermore, as the band around 1855 cm^{-1} disappeared, the band at 1791 cm^{-1} could be better resolved in the spectrum. This band is related with the multibonded CO molecules on FCC sites. As desorption temperature was increased to 200 °C, band related with the multibonded CO species on HCP sites (1855 cm^{-1}) could be hardly observed and the band centered around 1791 cm^{-1} was removed to a great extent by forming a deep on the spectra. Only significant bands left on the surface were belonged to the linearly bonded CO molecules. In this region, bands around 2036 cm^{-1} and 2069 cm^{-1} were both decreased in intensity indicating that CO molecules that linearly bonded on Ni and Pt metals were also significantly desorbed from the surface. When the temperature was increased to 300 °C, nearly all bands were removed from the surface only leaving minor peaks which indicated very small surface concentrations.

Same experiment conducted on 0.2Pt15Ni sample showed that, at 100 °C, similar to the 0.3Pt10Ni sample, the band related with the multicentered CO species was appeared at 1791 cm^{-1}. Also, bridge bonded species around 1928 cm^{-1} and multibonded CO species at 1851 cm^{-1} were gradually vanished and only very small band at 1851 cm^{-1} left after 30 minutes of desorption experiment. In the linearly bonded CO region, a band at 2069 cm^{-1} and another centered around 2028 cm^{-1} left on the spectrum. Different form the 0.3Pt10Ni sample, CO species linearly bonded on Ni atoms, at 2028 cm^{-1}, were more apparent than the ones bonded on Pt atoms, at 2069 cm^{-1}. This difference is most likely due to the higher Ni:Pt ratio of the 0.2Pt15Ni sample giving way to the higher amount of Ni atoms are available for the CO molecules to get adsorbed. An increase in temperature to 200 °C, completely removed the CO molecules adsorbed in a linear fashion. This was not the case for 0.3Pt10Ni sample on which there were left some linearly bonded CO both on Ni and Pt atoms after desorption at 200 °C. Furthermore, there was a deep formation on the multicentered CO region of the spectra obtained on 0.3Pt10Ni sample indicating a much

lower surface concentration of this type of species on 0.3Pt10Ni catalyst than the one observed on 0.2Pt15Ni sample at the same temperature.

These differences between the two samples clearly showed that higher amount of Pt addition resulted in a change on the surface structure. The results show that CO species that adsorb in a linear fashion were more thermally stable on 0.3Pt10Ni sample than the ones adsorbed on 0.2Pt15Ni sample. Furthermore, more multicentered CO species remaining on the surface of 0.2Pt15Ni sample after desorption indicates that increase in the Pt:Ni ratio causes a decrease in the thermal stability of these species. Similar results were also found by Parizotto *et al.* who conducted TPD-CO experiments both on Ni/Al_2O_3 and $PtNi/Al_2O_3$ (Parizotto *et al.*, 2009).

In the CO adsorption tests conducted at 300 °C, it was clear that 0.3Pt10Ni sample had more linearly adsorbed CO molecules when compared with the 0.2Pt15Ni sample and this was explained by the higher degree of reduction of this sample. A second reason that can result in this behavior is revealed after FTIR-DRIFTS-TPD-CO experiments. These experiments showed that the sample with higher Pt:Ni ratio favors the stability of the linear bonded CO species whereas it destabilizes the multibonded CO species. As 0.2Pt15Ni sample had lower dispersion and formation of bridged and multibonded CO species are more favored on this sample, it is natural that not as much linear bonded species can be formed on this sample. However, absence of strong bands related with the multibonded CO molecules on 0.2Pt15Ni sample shows that the main reason for the differences between the two catalysts observed in their CO adsorption tests conducted at 300 °C, was due to the differences in their reduction levels.

In Figure 4.8, OCO region of the spectra obtained during the TPD-CO experiment (spectrum d, e and f) is given with the other spectra obtained during CO adsorption experiments at both room temperature (spectrum a and b) and at 300 °C (spectrum c). This comparison is important to differentiate between the carbonaceous species formed during the adsorption tests as these species are known to have different thermal stabilities. CO adsorption test conducted at 300 °C (spectrum c), resulted in much lower concentrations of carbonaceous species than the ones conducted at room temperature. This is due to the much lower stabilities of these species at higher temperatures resulting in less surface

coverages. Hence, in order to observe these carbonaceous species formed in the adsorption test conducted at 300 °C, their intensity values are multiplied by a factor of 3 and an enlarged view of its spectrum was added on Figure 4.8. All the given spectra in Figure 4.8 belong to the 0.3Pt10Ni sample as there was no difference between the two samples in their frequencies observed in the OCO region.

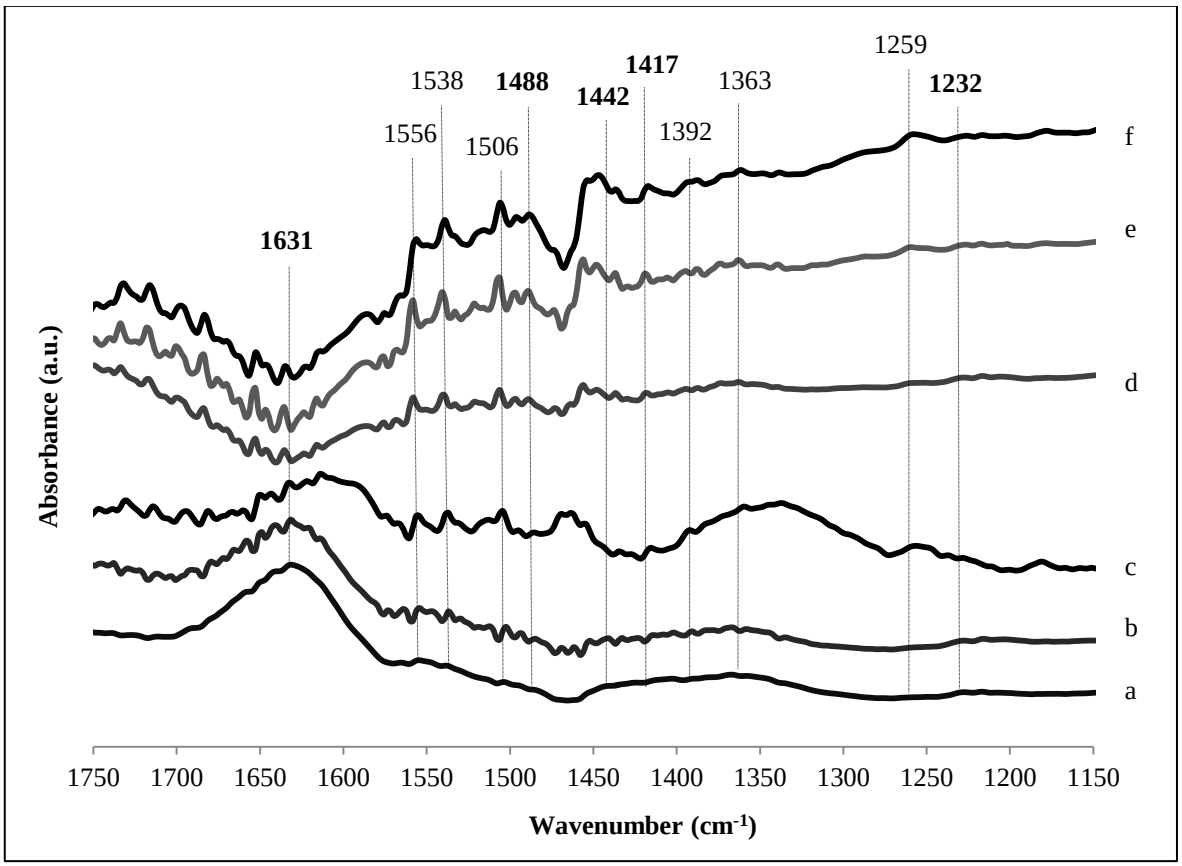

Figure 4.8. Spectra obtained on 0.3Pt10Ni after 30 min 1% CO flow at 25 °C (a), 30 min He flow at 25 °C (b), after 30 min 1% CO flow at 300 °C (c), 30 min He flow at 100 °C (d), at 200 °C (e), and at 300 °C (f).

CO adsorption at room temperature results in bands at 1631 cm^{-1} and 1442 cm^{-1} which can be assigned to the asymmetric and symmetric OCO stretching frequencies of a bicarbonate group. OH bending frequency observed at 1232 cm^{-1} and stretching frequency observed at ca. 3623 cm^{-1} (not shown in Figure 4.8) signifies the formation of bicarbonates on the surface. As the frequency separation between the asymmetric and symmetric bands ($\Delta\nu_3$) is lower than 400 cm^{-1}, these bands cannot belong to a bridged bicarbonate. Hence, it

is either monodentate or bidentate bicarbonate while the exact assignment is not possible as the difference between the two is not straightforward ($\Delta\nu_3$ is lower than 200 cm^{-1} for both of them). Although these bands also appear in the CO adsorption experiments conducted at 300 °C, their relative concentrations were much lower. Additionally, these bands were not thermally stable and rapidly vanished at increased temperatures in the FTIR-DRIFTS-TPD-CO experiments. Especially, the band around 1631 cm^{-1} formed a deep in the spectra and grew in the negative direction as the desorption temperature increased.

Furthermore, bands at 1556, 1537 and 1506 cm^{-1} with bands at 1392 and 1363 cm^{-1} can be assigned to the either bidentate or monodentate carbonate groups. Bands at 1488 and 1417 cm^{-1} can be assigned to the polydentate carbonates due to two reasons: i) they were not vanished upon the TPD-CO test even at 300 °C, ii) and their frequency separation is lower than 100 cm^{-1}. As these species were suggested to be the most thermally stable carbonate species among the carbonates, polydentate carbonate assignment to these bands seems plausible.

4.3. CO_2 Adsorption Experiments

4.3.1. CO_2 Adsorption Experiments at Room Temperature

Spectra obtained upon CO_2 adsorption experiments conducted at room temperature are given in the Figure 4.9 and Figure 4.10 for 2100-1150 cm^{-1} region and 3800-2800 cm^{-1} region for both of the samples, respectively.

Upon CO_2 adsorption on 0.3Pt10Ni and 0.2Pt15Ni samples, there appeared a very small band at 2069 cm^{-1}, which could be assigned to the linearly adsorbed CO molecule. This indicates that CO_2 was dissociated into adsorbed CO and O on the metal surface even at the room temperature. This dissociation is probably induced by Pt metal as it was also observed by Bradford and Vannice on Pt/TiO_2 catalyst at 300 K (Bradford and Vannice, 1999b). This surface CO band, however, was disappeared after 30 minutes of He flush.

Furthermore, there appear large amounts of carbonaceous species in the 1700-1200 cm^{-1} region. By interacting with the surface OH groups and O ions of the alumina, CO_2 is known to produce mostly bicarbonate and carbonate species on the surface (Föttinger *et al.*, 2007). CO_2 adsorption at room temperature resulted in a spectrum very similar to that of obtained on CO adsorption at room temperature. This similarity was also observed by other researchers (Föttinger *et al.*, 2007; Parkyns, 1971). Strong bands at 1631 cm^{-1} and 1442 cm^{-1} can be assigned to the asymmetric and symmetric OCO stretching frequencies of a mono or bidentate bicarbonate group. Also, OH bending frequency observed at 1232 cm^{-1} and OH stretching frequency observed at ca. 3623 cm^{-1}were also present on the surface. Furthermore, bands at 1556, 1537 and 1506 cm^{-1} with bands at 1392 and 1363 cm^{-1}, which were assigned to the either bidentate or monodentate carbonate groups, can be seen on the spectra. Two bands at 1706 cm^{-1} and at 1180 cm^{-1} are indications of a carboxylate group which points out to perturbed CO_2 molecules. Bands at 1488 and 1417 cm^{-1} can be assigned to the polydentate carbonates similar to the bands on CO adsorption spectra.

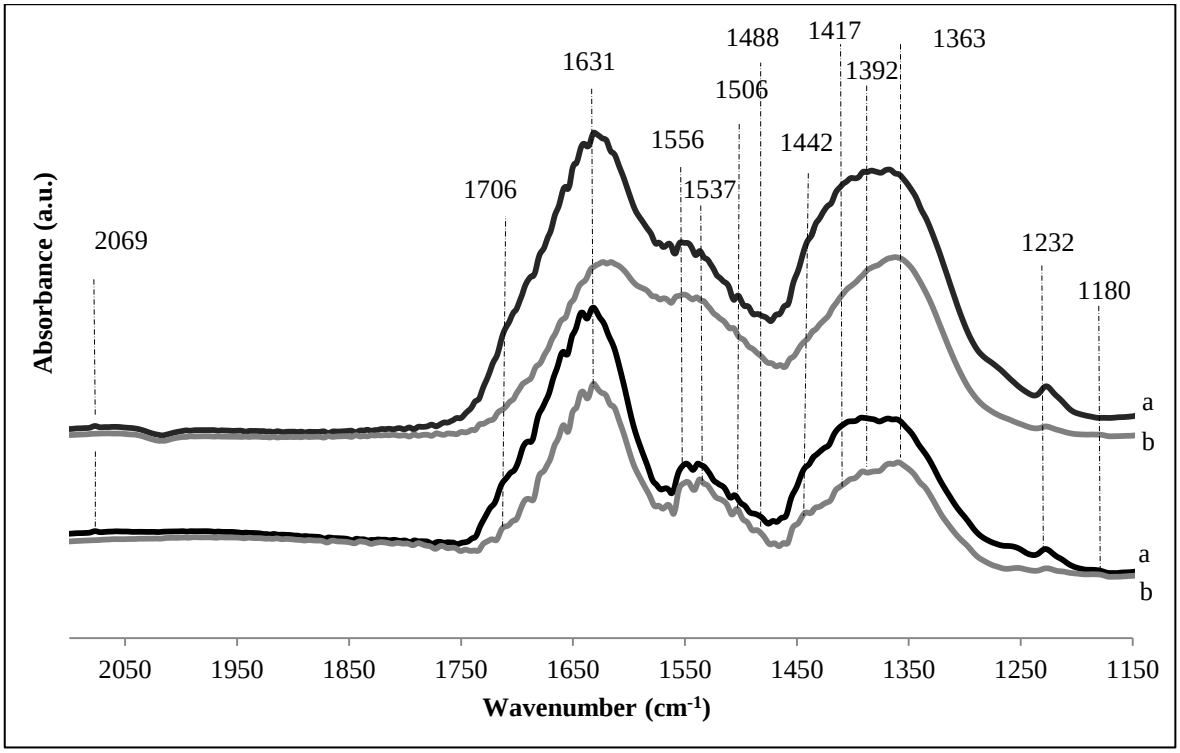

Figure 4.9. OCO stretching region of the spectra obtained on 0.3Pt10Ni (bottom two) and 0.2Pt15Ni (top two) after 30 min 10% CO_2 flow at 25 °C (a), 30 min He flow at 25 °C (b).

Upon He flush, there seems decrease in the intensities of the carbonaceous species, especially for those belonging to the bicarbonate species, yet their positions do not differ. The IR combination bands/overtones of the gas phase CO_2 causes some imperfections around 3715 cm^{-1} and 3612 cm^{-1}, which makes an analysis on this region impossible (Collins *et al.*, 2006). However, after He flush of 30 minutes, band at 3623 cm^{-1} becomes clearer, which were assigned to the OH stretching vibration of the bicarbonates. Although there seems some C-H groups, belonging to the formates, formed on the 0.3Pt10Ni sample around 2960, 2906 and 2867 cm^{-1}, their assignments cannot be performed due to the coverage of their counterparts (asymmetric and symmetric O-C-O stretching vibrations) by the other (bi)carbonates in the 1700-1200 cm^{-1} region. Furthermore, it is reported in the literature that formate formation requires temperatures higher than 175 °C (Korhonen *et al.*, 2008). Hence, assignments of the formate species were neglected.

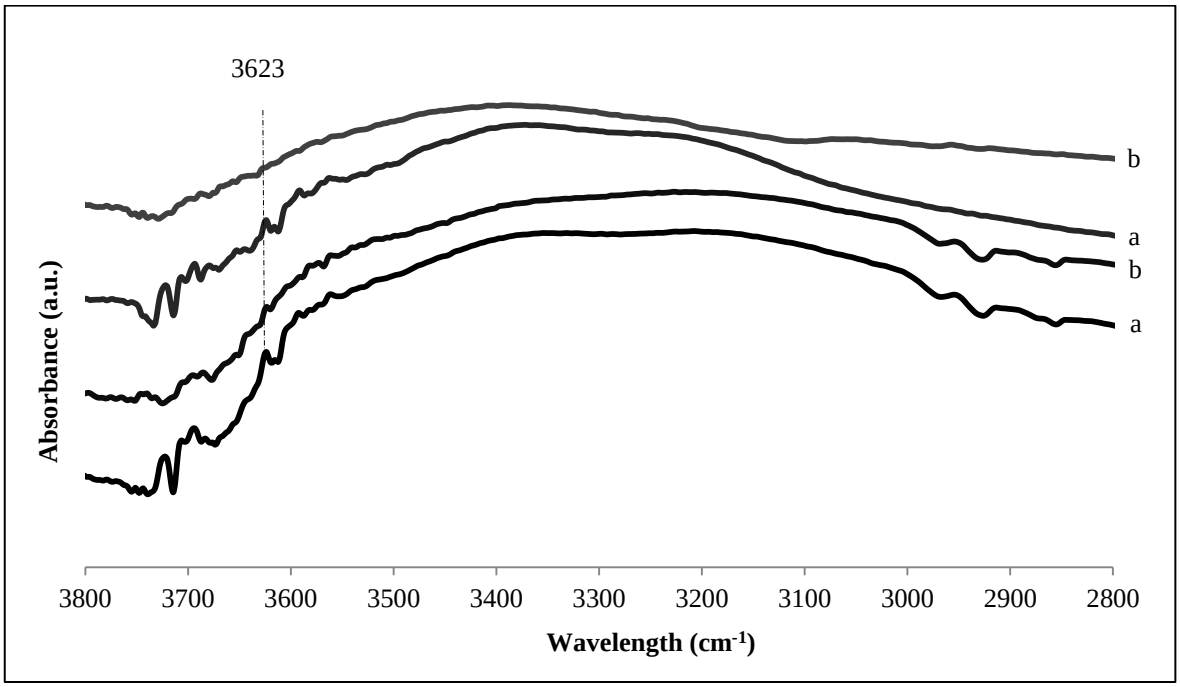

Figure 4.10. C-H and OH stretching region of the spectra obtained on 0.3Pt10Ni (bottom two) and 0.2Pt15Ni (top two) after 30 min 10% CO_2 flow at 25 °C (a), followed by 30 min He flow at 25 °C (b).

4.3.2. CO_2 Adsorption Experiments at 300 °C

Metal-carbonyl region of the spectra obtained upon CO_2 adsorptions at 300 °C on both of the samples are shown in the Figure 4.11.

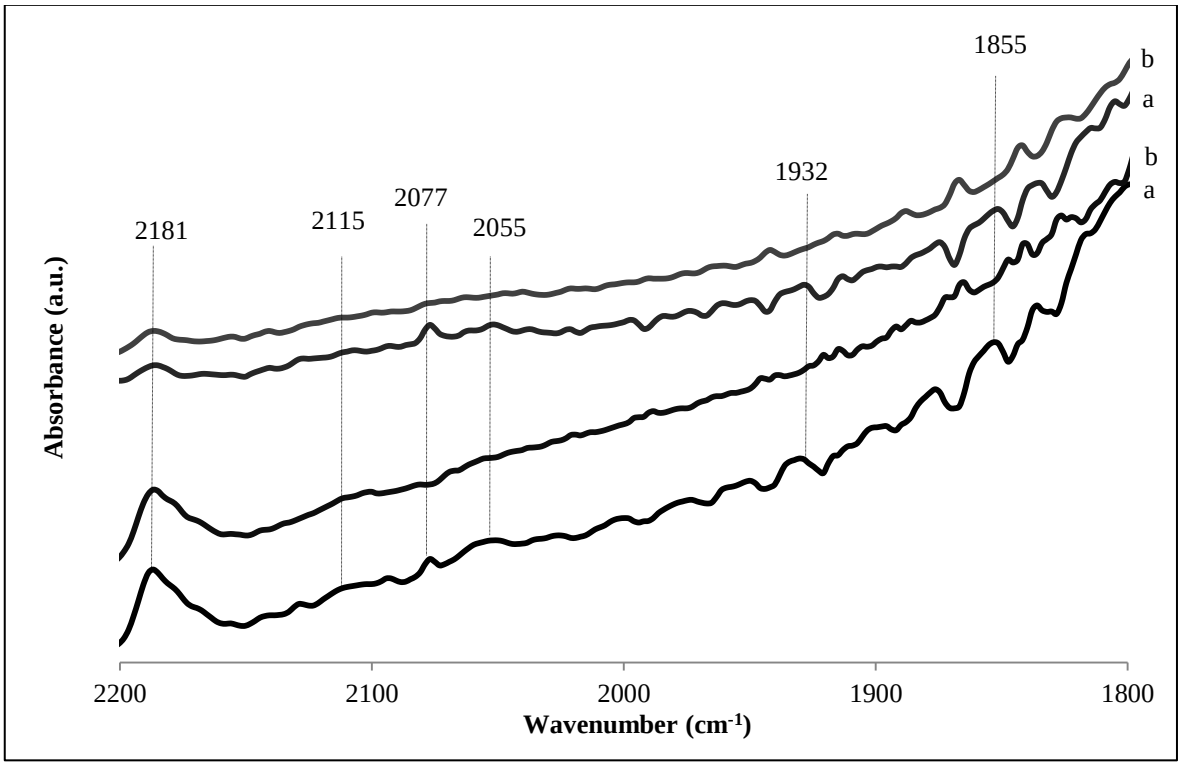

Figure 4.11. Metal carbonyl region of the spectra obtained on 0.3Pt10Ni (bottom two) and 0.2Pt15Ni (top two) after 30 min 10% CO_2 flow at 300 °C (a), followed by 30 min He flow at 300 °C (b).

After 30 minutes of CO_2 flow over the samples, there are gaseous CO bands at 2181 and 2115 cm^{-1} on both spectra. The CO concentration seems to be much larger on the 0.3Pt10Ni sample by judging from its higher intensity. Furthermore, peak observed at 2077 cm^{-1} is common on both of the samples. This shows linearly bonded CO molecule on either Pt metal or on highly dispersed Ni metal. There are also some weaker but wider bands around 2050 cm^{-1} which are also related with the linearly bonded CO molecules. Upon He flush, those peaks signifying linearly adsorbed CO molecules were removed from the surface showing their instability on the surface.

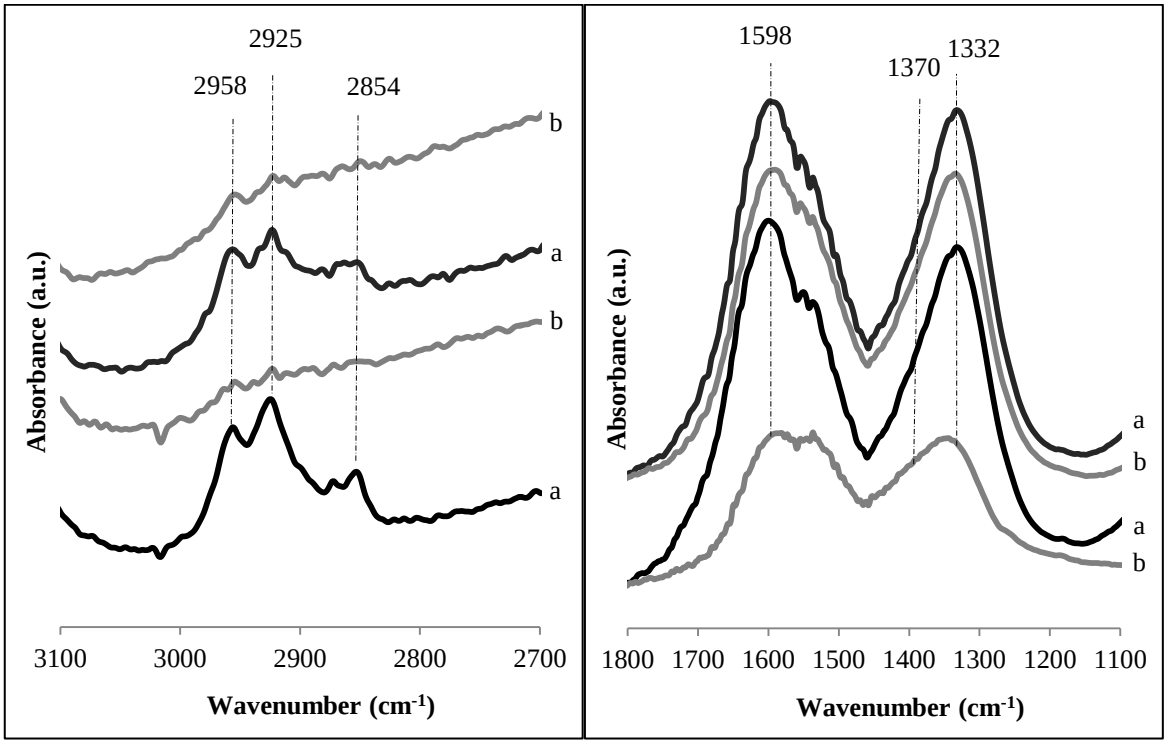

Figure 4.12. C-H stretching region (left) and OCO region (right) of the spectra obtained on 0.3Pt10Ni (bottom two) and 0.2Pt15Ni (top two) after 30 min 10% CO_2 flow at 300 °C (a), followed by 30 min He flow at 300 °C (b).

Peaks at 1932 and 1855 cm^{-1} are also seen on the spectra which were observed at CO adsorption experiments and were assigned to the bridged and multibonded CO molecules on Ni metal, respectively. Those peaks related with the bridged and multibonded CO molecules were also removed upon He flush, but there were some small peaks left on the surface showing their higher stability when compared to the linear bonded CO molecules.

Regions that can elaborate on the carbonaceous species formed during the CO_2 adsorptions are shown in Figure 4.12.

A close inspection into the C-H stretching region reveals strong bands 2958, 2925 and 2854 cm^{-1} which show that there are significant amount of formates formed on the surface during the CO_2 adsorption. The strong band at 1598 and one shoulder at ca. 1370 cm^{-1} shows the formation of formate species on the surface. As the frequency separation is below 250 cm^{-1}, i.e. 228 cm^{-1}, these formate species are probably bidentate formates. Strong band at 1332 cm^{-1} probably belongs to the C-H bending vibrations as it is decreased

in intensity after He flush in accordance with the removal of the C-H stretching bands around 2900 cm^{-1}. Formation of formate species on the surface indicates that there left some hydrogen on the surface after reduction**.** As no band related to the OH bending frequency, δ(OH), of the bicarbonates observed around 1230 cm^{-1}, there are no bicarbonates formed on the surface.

There seems no difference between the two samples in terms of the types of the carbonaceous species formed upon CO_2 adsorption indicating no difference in their CO_2 activation mechanisms. However, intensities of the C-H stretching bands are higher on 0.3Pt10Ni sample. Formate formation is an important step in the CO_2 activation process and its decomposition is reported to result in CO formation (Cheng *et al.*, 2001; Ferreira-Aparicio *et al.*, 2000). Another mechanism which can result in the formation of CO is the dissociation of CO_2 to adsorbed CO and surface O on the active metal surface. As there seems no difference between the two samples in terms of the intensities of adsorbed CO molecules on their surfaces, these adsorption experiments do not yield a certain difference in their CO_2 dissociation rates on the active metal. However, the sample containing a higher proportion of Pt metal produced higher amount of CO. This result is probably due to the existence of higher amount of formate species on this sample which can subsequently decompose into surface OH and gaseous CO.

4.4. CH_4 Adsorption Experiments

4.4.1. CH_4 Adsorption Experiments at Room Temperature

CH_4 adsorption for 30 minutes at room temperature yielded the spectra given in Figure 4.13.

Following the 30 minutes of methane adsorption test, an inert flow of 30 minutes resulted in the spectra given in Figure 4.14. Sharp bands around 3015 and 1305 cm^{-1} are due to the gaseous methane. Methane flow results in the loss of surface hydroxyl species showing the presence of interaction between the alumina support and gaseous methane producing carbonaceous species on the surface observed in 1700-1100 cm^{-1} region. Yet,

gaseous methane bands covered the region around 1400-1300 cm^{-1} making it difficult to comment on the type of the carbonaceous species formed on the surface.

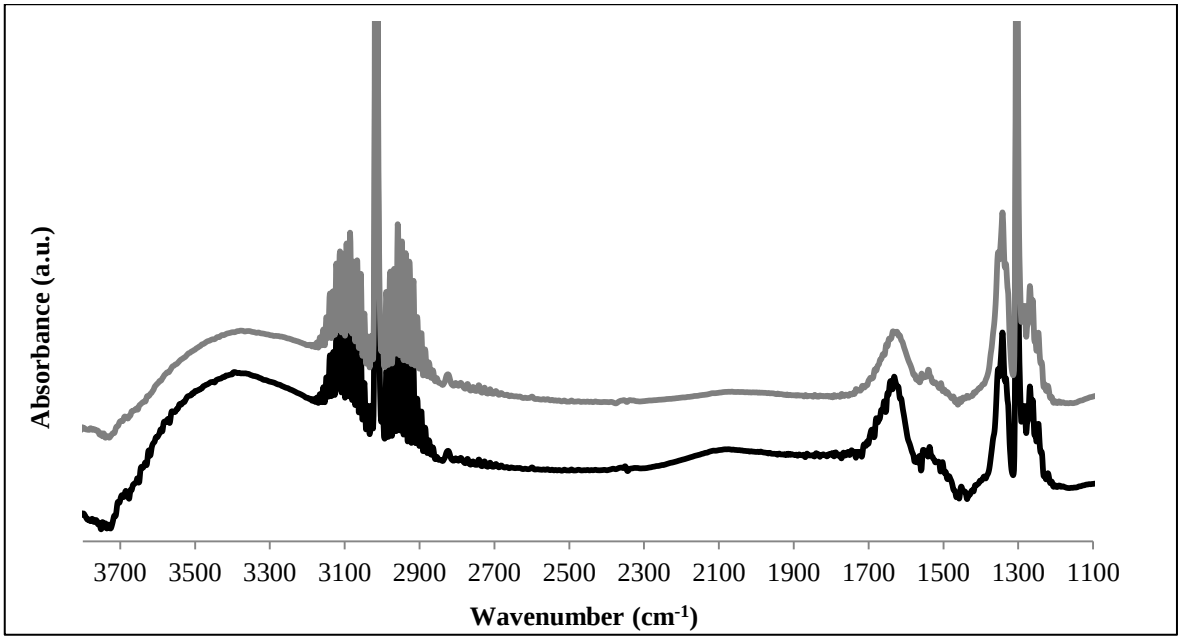

Figure 4.13. Spectra obtained on 0.3Pt10Ni (bottom) and 0.2Pt15Ni (top) after 30 min 10% CH_4 flow at 25 °C.

After 30 minutes helium flow, remaining bands at 3015 and 1305 cm^{-1} show that some physisorbed methane was still desorbing from the surface. Bands in the OCO stretching region (1700-1100 cm^{-1}) are very similar to those of observed on CO adsorption and shows carbonate and bicarbonate type species formed on the surface. Bands at 1631 and 1454 cm^{-1} show the symmetric and asymmetric stretching of a bicarbonate group. Bending OH vibration at 1230 cm^{-1} is very weak probably hindered by the stretching bands of the gaseous methane, which was still desorbing from the surface. Other than that, carbonate species seems to be dominating the spectra which can be inferred by the sharp bands at 1556, 1537 and 1396 cm^{-1}. Bicarbonate peaks are much sharper on 0.3Pt10Ni sample than the ones observed on 0.2Pt15Ni sample.

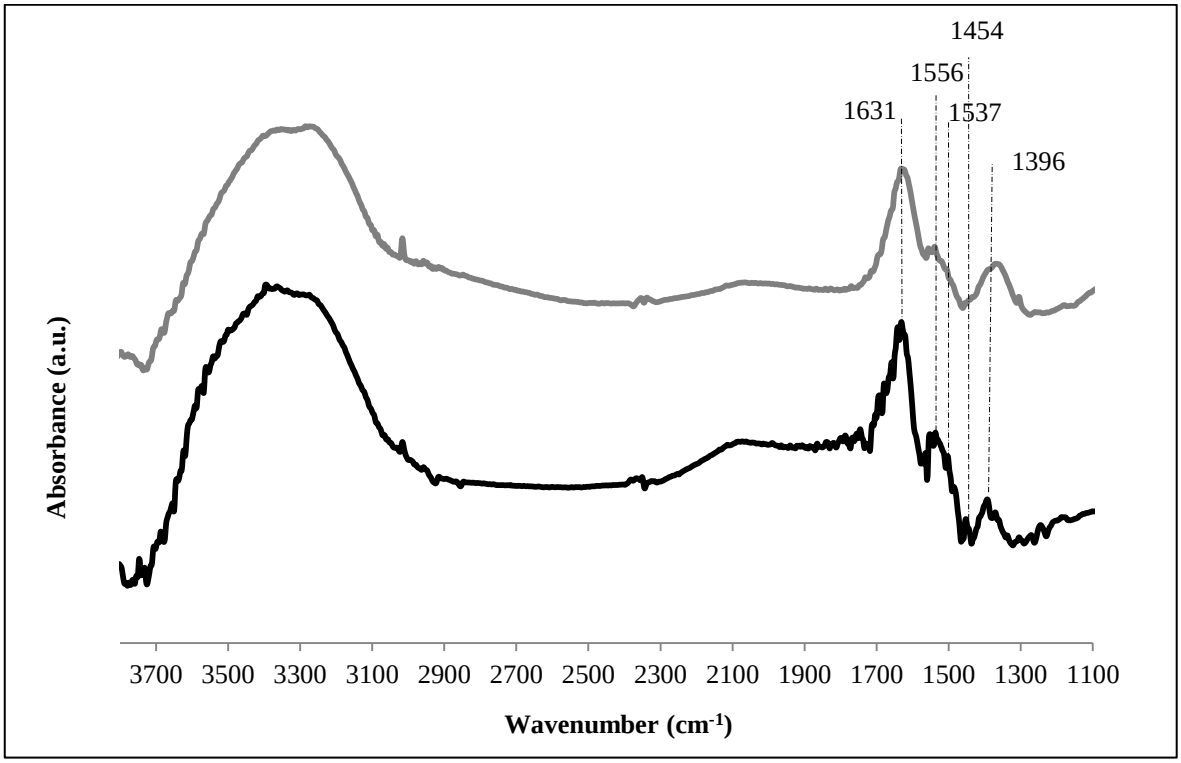

Figure 4.14. Spectra obtained on 0.3Pt10Ni (bottom) and 0.2Pt15Ni (top) 30 min He flow at 25 °C.

4.4.2. CH_4 Adsorption Experiments at 300 °C

CH_4 adsorption on both samples at 300 °C and after a following He flush at the same temperature resulted in the spectra shown in Figure 4.15 and 4.16, respectively.

Band formed at ca. 3650 cm^{-1} is due to the interaction between methane and the surface O groups of alumina. This interaction results in the formation of new OH groups on the alumina support via the additional hydrogen supplied by methane dissociation. This OH band is more apparent on 0.2Pt15Ni sample when compared with the band on 0.3Pt10Ni sample. Higher intensity of this OH band on 0.2Pt15Ni sample shows that there were more hydrogen atoms available on 0.2Pt15Ni sample for the surface OH formation. This is probably due to the higher activity of 0.2Pt15Ni sample in methane decomposition which would result in higher amount of hydrogen atoms to be available to react with the surface O groups of the alumina and produce more surface OH groups.

The most significant result of the adsorption tests conducted at 300 °C is the formation of gaseous CO. As there was no external oxygen source fed into the system, oxygen for the CO should come from the alumina showing the effect of support during the CDRM reaction. In addition, gaseous CO was more apparent in the tests on 0.3Pt10Ni sample when compared to the tests on 0.2Pt15Ni sample. Additionally, a band around 2060 cm^{-1} was observed on 0.3Pt10Ni sample which indicates linearly bonded CO molecule on a highly dispersed metal atom. As CO formation occurs near the metal-support interphase and a bridge or multiple bonding requires close packed structures, it seems plausible that the CO formed at the metal-support interphase adsorbs in a linear fashion which could be observed on either a high dispersed metal surface or on an edge atom positioned at the interfacial region.

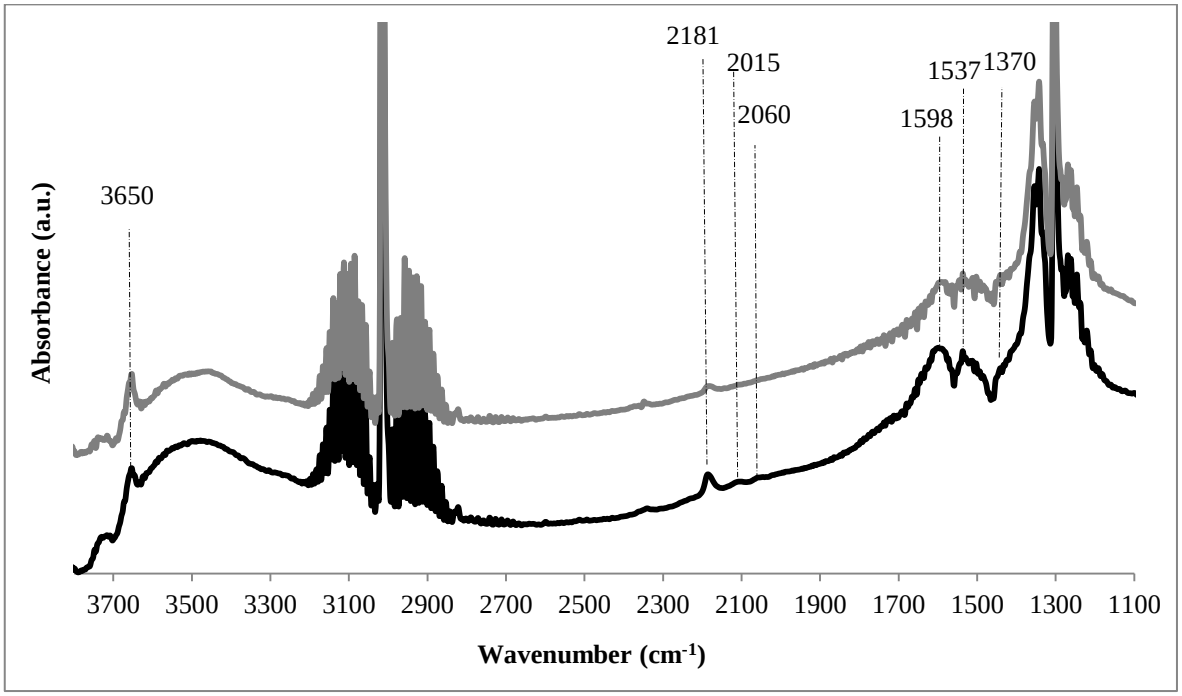

Figure 4.15. Spectra obtained on 0.3Pt10Ni (bottom) and 0.2Pt15Ni (top) after 30 min 10% CH_4 flow at 300 °C.

It is highly probable that carbon formed by methane dissociation is able to reduce the oxide support near the perimeter of the metal particle. This process was also suggested by Staag *et al.* according to their findings in isotopic pulse experiments (Staag *et al.*, 1998). A second possible mechanism of CO formation under methane flow would be via

the dissociation of CH_xO species which can form by the interaction between alumina support and gaseous methane. Bradford and Vannice observed formaldehyde ($H_2C=O$) during the methane flow over Pt/TiO_2 which was decreased in intensity by the formation of CO. Yet, there seems no formaldehyde formation in Figure 4.16 which would be observed around 1690 cm^{-1}. Instead, formate species are observed by using the assignments made on the spectra obtained upon CO_2 adsorptions. These formate species are positioned at 1598 cm^{-1} and 1370 cm^{-1}, while the latter band is covered by the gaseous methane peak.

Upon He flow, some gaseous CO is still present on the surface of the both samples. Linear bonded CO molecule on 0.3Pt10Ni sample can be still observed. This gaseous CO formation is probably due to the decomposition of the formates as their decomposition is known to yield CO.

The reason behind the higher CO produced on 0.3Pt10Ni sample and its higher surface coverage by the adsorbed CO is probably due to the higher metal dispersion obtained on this sample. Higher dispersion is expected to yield higher metal-support interfacial area. As the O for CO comes from the support, and methane decomposition occurs on the active metal; metal support interphase plays an essential role in the CO formation (Bradford and Vannice, 1999). Higher dispersion on 0.3Pt10Ni sample resulted in a higher interfacial area for the C and/or CH_x on metal and O on the support to react on the interphase. Hence, higher CO yields were observed on this sample when compared with the yield on 0.2Pt15Ni sample.

There seems no evidence for C-H species in the 3000-2700 cm^{-1} that could immediately lead to conclusions on the relative activities of the both samples in CH_4 activation. Their presence could not be observed during CH_4 flow as they were covered by gaseous methane. Yet, it is certain that there were some CH_x species formed on the surface as their formation is stated as the methane activation mechanism at lower temperatures (Pakhare and Spivey, 2014). However, formate species were more apparent on 0.3Pt10Ni sample as it can be inferred by the difference in their relative intensities. This may be due to the incomplete dissociation of methane to CH_x species which would result in lower amount of surface C formation and higher amount of CH_x formation on this sample. C formation from methane and/or CH_x species is reported to be depended on the surface

structure. Decomposition of these species to surface C requires a concomitant occupation of the metal sites (Bradford and Vannice, 1998). On the other hand, higher dispersion of 0.3Pt10Ni sample is expected to result in fewer amounts of metal ensembles to be present on the surface. Hence, 0.3Pt10Ni sample is probably less active in C formation that can form by CH_4 and/or CH_x decomposition. Those CH_x species that did not decompose into the hydrogen and surface C, may desorb from the surface or diffuse into the support-metal interphase, where they can interact with the support material, by which more formate, other types of carbonaceous species and further CO would be formed on the support.

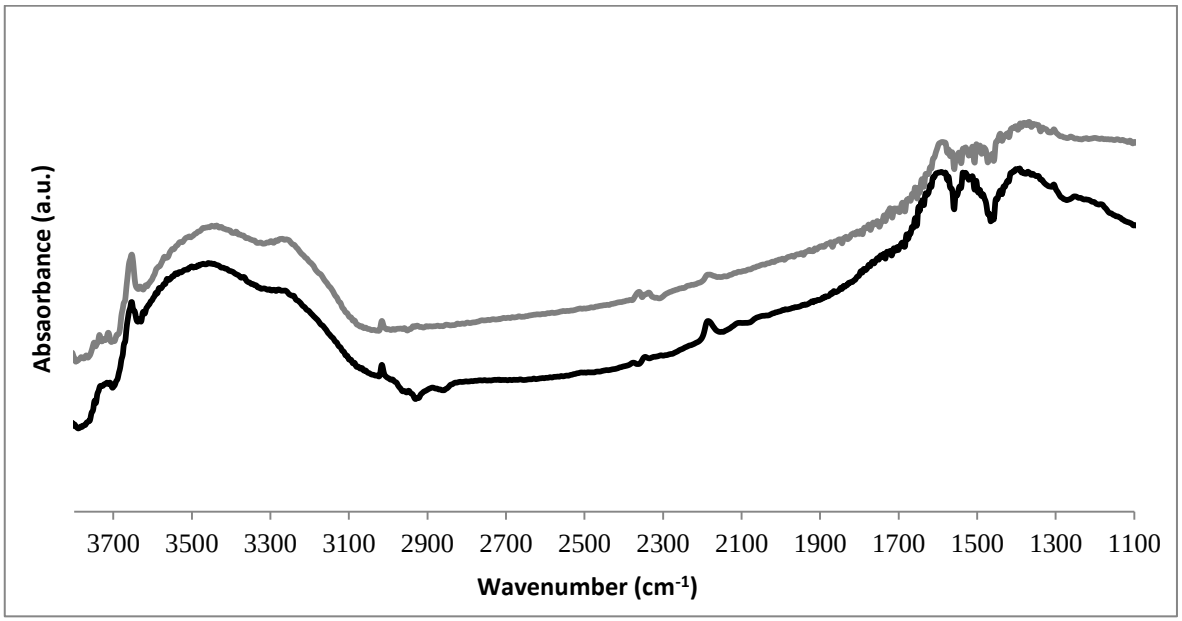

Figure 4.16. Spectra obtained on 0.3Pt10Ni (bottom) and 0.2Pt15Ni (top) after 30 min He flow at 300 °C.

As no any evident CH_x species were observed in the 3000-2700 cm^{-1} region after He flush, these CH_x species do not seem to be stable on the surface and their desorption and subsequent interaction with the support material seems plausible. Additionally, their weak interaction between the metal surfaces may justify a reaction mechanism in which methane is assumed to be weakly adsorbed. In fact, kinetic tests conducted by Özkara-Aydioğlu and Aksoylu on 0.3Pt10Ni sample showed that the model assuming weakly adsorbed methane (model 1) resulted in the lowest squared error among the kinetic models used in their study. On the other hand, this model was not applicable for 0.2Pt15Ni sample which is

probably due to the higher activity of this sample in surface C formation resulting from its lower metal dispersion.

4.5. *In situ* Reaction Experiments

Reaction tests were conducted under a flow of 40% CO_2, 40% CH_4 and 20% He mixture at 300 °C. Higher concentrations than the ones used in the adsorption tests were introduced into the system in order to increase the partial pressures of the reactants and to obtain higher reaction rates.

Metal carbonyl region of the spectra obtained during the reaction experiments is shown in Figure 4.17. First three spectra were taken after 10, 30 and 60 minutes TOS of reaction on 0.3Pt10Ni sample. Fourth spectrum was taken after 30 minutes of He flush which followed the reaction test. Other four spectra on the top are sorted in the same manner and belong to the 0.2Pt15Ni sample.

There appeared gaseous CO bands on both of the catalysts. Furthermore, weak bands around 2077 ad 2050 cm^{-1} show that linearly bonded CO molecules were formed on the active metal surfaces. There are also other bands in the bridged and multibonded CO region indicating CO adsorption on less dispersed metal sites. These species are yielding very similar wavenumbers to those obtained during CO_2 adsorption tests conducted at 300 °C. (Yet, there appear some additional bands below 2000 cm^{-1} in addition to those obtained under 10% CO_2 adsorption tests.) Similar to the both CH_4 and CO_2 adsorption tests, relatively more gaseous CO was formed on 0.3Pt10Ni sample indicating its higher activity in the CDRM reaction when compared with the 0.2Pt15Ni sample.

After 30 minutes of He flow, nearly all bands belonging to the adsorbed CO were removed from the spectra, only leaving some minor peaks, around 1850 and 1791 cm^{-1}, that belong to the multibonded CO species. Absence of linearly bonded CO species after 30 min He flush indicate that CO molecules that were adsorbed linearly on the surface, were not stable on the surface and cannot be involved in determining the rate of reaction. Yet, this result does not exclude the effect of CO on the CDRM reaction rate. As it was found by Özkara-Aydinoğlu and Aksoylu, CO inhibition effect via dissociation of CO to

surface C and O was highly important on the CDRM rates of 0.2Pt15Ni sample (Özkara-Aydinoğlu and Aksoylu, 2013).

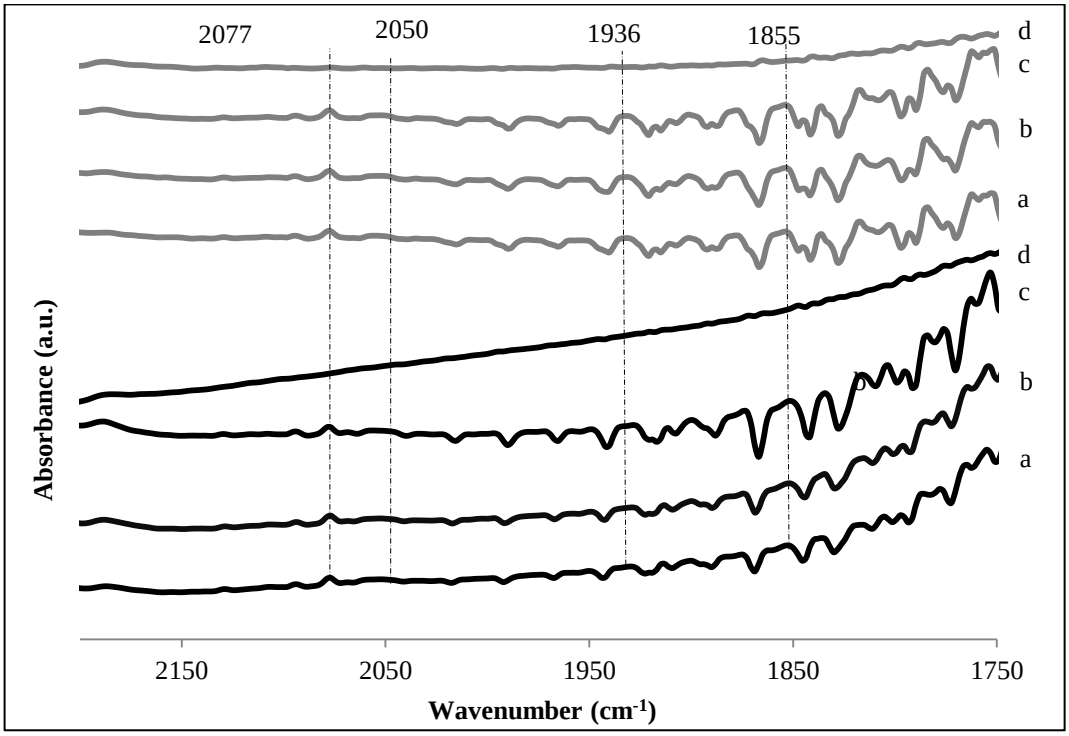

Figure 4.17. Spectra obtained on 0.3Pt10Ni (bottom four spectra) and 0.2Pt15Ni (top four spectra) after 10 minutes (a), 30 minutes (b), 60 minutes of exposure to 40% CO_2 40% CH_4 and 20% He flow at 300 °C (c), 30 minutes of He flow at 300 °C (d).

CO characterization experiments conducted at room temperature revealed that 0.3Pt10Ni sample favors linearly bonded CO molecules more than that of 0.2Pt15Ni sample. Also FTIR-DRIFTS-TPD-CO experiments showed that Pt metal causes a decrease in the stability of the multibonded CO species. When these results are considered with the removal of linearly bonded CO molecules that formed under the reaction conditions upon inert flush, it is clear that 0.3Pt10Ni sample is less prone to CO inhibition that may result from the CO dissociation. It is stated in the literature that CO dissociation requires an ensemble of 4-5 metal atoms to be present on the surface (Bradford and Vannice, 1998). These ensembles are highly likely to be more abundant on the lower dispersed metal surfaces. Higher dispersion observed on 0.3Pt10Ni sample, higher amount of linearly bonded molecules on 0.3Pt10Ni sample and its destabilizing effect on bridged and multibonded CO species indicate that CO inhibition that may result from the CO

dissociation is less likely to have a stronger effect on 0.3Pt10Ni sample than it has on 0.2Pt15Ni sample.

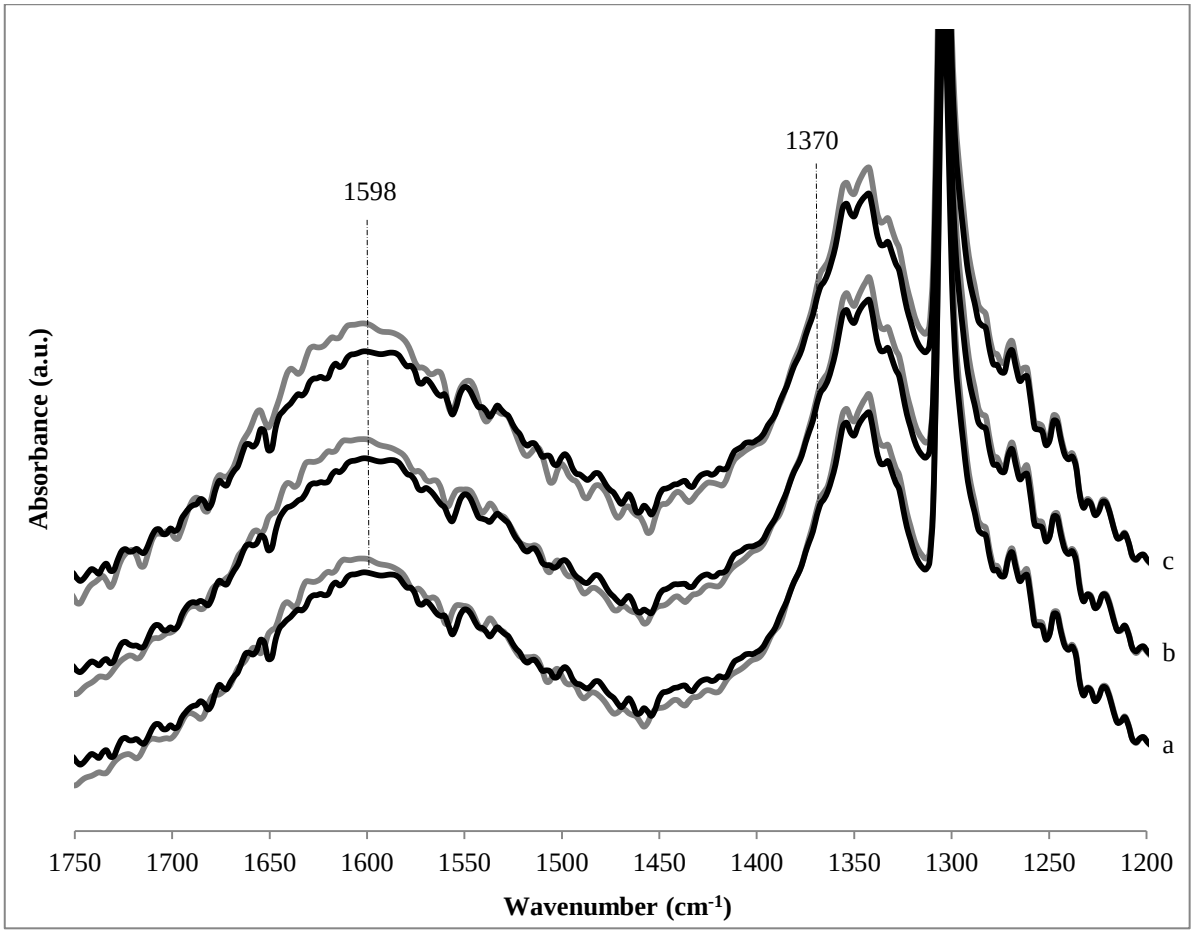

Figure 4.18. Spectra obtained on 0.3Pt10Ni and 0.2Pt15Ni after a) 10 minutes, b) 30 minutes, c) 60 minutes of exposure to 40% CO_2 40% CH_4 and 20% He flow at 300 °C.

Figure 4.18 shows the OCO region of the spectra obtained during the reaction tests. In each couple of spectra, black one belongs to the 0.2Pt15Ni sample whereas the gray one belongs to the 0.3Pt10Ni sample. Since the C-H region does not provide a clear evidence for the formate species due to their coverage by the gaseous methane, OCO region is inspected for the possible formate species. As it can be inferred by the steeper peak formation around 1600 cm^{-1}, more formate species were formed on 0.3Pt10Ni sample. Because both CO_2 and CH_4 adsorption experiments conducted at 300 °C showed higher formate formation on 0.3Pt10Ni sample, this result is actually self-evident.

In the kinetic study performed by Özkara-Aydinoğlu and Aksoylu on 0.2Pt15Ni and 0.3Pt10Ni catalysts the only model that yielded physically meaningful results for both of the samples was the Model 5 which assumed CH_4 and CO adsorbed on the same site whereas CO_2 adsorbed on a different site. In this model, adsorption coefficients increased in the following sequence: $K_{CH4}<K_{CO}<K_{CO2}$ for 0.3Pt10Ni sample and $K_{CH4}< K_{CO2}< K_{CO}$ for 0.2Pt15Ni sample (Özkara-Aydinoğlu and Aksoylu, 2013). For the 0.3Pt10Ni sample, higher K value obtained for CO_2 compared to that of obtained for CH_4 showed that the utilization of CO_2 was strong on this sample. Similarly, CO_2 adsorption tests conducted in this study showed that CO_2 utilization via formate formation was higher for the 0.3Pt10Ni sample when compared with the that of 0.2Pt15Ni sample, which yielded less amount of formate formation. Additionally, methane adsorption tests revealed no CH_x species on the surface after He flush, which may indicate its weak adsorption on the surface. Furthermore, as mentioned above, CO inhibition can be highly restricted on 0.3Pt10Ni sample by its higher dispersion, and destabilizing effect on multibonded CO molecules which may subsequently decompose into C and O. K_{CO} for the 0.2Pt15Ni sample was five times higher than that of 0.3Pt10Ni sample revealing the difference among the samples in their relative vulnerability to CO inhibition. More multibonded CO species left on the surface of 0.2Pt15Ni catalyst in the TPD-CO experiments, and metal dispersion was found to be less on this catalyst. These results may explain why the K_{CO} was 5 times higher on this sample. (Özkara-Aydinoğlu and Aksoylu, 2013).

5. CONCLUSIONS AND RECOMMENDATIONS

5.1. Conclusions

In this study, FTIR-DRIFTS spectroscopy was used in order to gain a deeper insight into the difference between the micro-structural and kinetic properties of two bimetallic catalysts, i.e. 0.3Pt10Ni/Al_2O_3 and 0.2Pt15Ni/Al_2O_3, which have been previously studied in our group and shown to have different kinetic behaviors in CDRM reaction. In this context, CO characterization, CO-TPD, CO_2 and CH_4 adsorption and *in situ* reaction experiments by using FTIR-DRIFTS system were conducted.

CO characterization studies conducted at room temperature revealed that dispersion of Ni on the sample containing higher amount of Pt, i.e. 0.3Pt10Ni, was better than that on the 0.2Pt15Ni sample.

CO adsorption experiments performed at 300 °C showed that the lower Ni:Pt ratio of the 0.3Pt10Ni sample resulted in a higher extent of reduction.

FTIR-DRIFTS-CO-TPD experiments revealed that CO species adsorb in linear fashion were more thermally stable on 0.3Pt10Ni sample than the ones adsorbed on 0.2Pt15Ni sample. Furthermore, more multicentered CO species remaining on the surface of 0.2Pt15Ni sample after desorption indicates that decrease in the Ni:Pt ratio causes a decrease in thermal stability of these species.

CO_2 adsorption experiments conducted at 300 °C revealed that more gaseous CO was formed on the 0.3Pt10Ni sample. Although there seemed no difference between the two samples in terms of CO species formed on their active metal sites, more formate species were formed on 0.3Pt10Ni sample indicating its higher activity in CO_2 utilization.

In the CH_4 adsorption experiments, CO formation was observed on both samples showing that the support also has a role in the course of the CDRM reaction. No CH_x species could be observed upon He flush indicating weak adsorption of methane. Due to

the lower dispersion of 0.2Pt15Ni sample, there formed less amount of formate species on this sample. It is also possible that higher CH_4 decomposition activity of 0.2Pt15Ni sample would lead more surface C and less CH_x species formed on the surface, which would result in formation of fewer amount of formate species.

In situ reaction tests revealed that more gaseous CO and more formate type species were formed on 0.3Pt10Ni sample. Disappearance of adsorbed CO species upon He flush showed that their desorption from the surface cannot be regarded as a rate determining step.

Its higher dispersion and higher amount of linear-CO while less stable multibonded CO adsorption observed on it indicate CO inhibition resulting from CO dissociation should be less pronounced on 0.3Pt10Ni than that on 0.2Pt15Ni.

Differences in the CO adsorption behavior, CO_2 utilization and CH_4 adsorption characteristics of the two samples proves the previous findings on the two catalysts indicating there are significant differences among two samples in terms of the CDRM reaction pathways on them.

5.2. Recommendations

According to results obtained in this study, following points can be recommended for the future research:

- Adsorption and reaction studies can be performed in a wider temperature range in order to obtain a more complete picture on the interaction of the reactants with the catalyst surface as operating temperature is known to have a strong effecton the reaction mechanism.

- If the experiments can be conducted at higher temperatures, an MS coupled FTIR-DRIFTS study will be more fruitful in determining the possible products of the experiment and IR-inactive gaseous species, for instance H_2 and O_2, as well.

- Pulse experiments with isotopic labeled species on MS coupled FTIR-DRIFTS system can reveal much more about the exact mechanism of the interaction of the reactants with catalyst surface and mechanism of the formation of product species.

- Mixed feed experiments, in which products of the CDRM reaction are simultaneously fed to the system together with the reactants, may also be helpful in monitoring the surface species under a more realistic atmosphere.

- In order to observe the possible changes that may be induced by the previous tests on the catalyst surface, it may be helpful to conduct CO or H_2 adsorption studies immediately after the previous test.

- It may be beneficial to perform *in situ* adsorption of one of the reactants on the samples that has the other reactant preadsorbed in following the mechanism of CDRM reaction by FTIR-DRIFTS.

REFERENCES

Akin, A. N., *Development of Coprecipitated Cobalt-Alumina Catalysts for the Production of C_1-C_4 Hydrocarbons by Carbon Monoxide Hydrogenation*, Ph.D. Thesis, Boğaziçi University, 1996.

Akpan, E., Y. P. Sun, P. Kumar, H. Ibrahim, A. Aboudheir, and R. Idem, "Kinetics, Experimental and Reactor Modeling Studies of the Carbon Dioxide Reforming of Methane (CDRM) over a New Ni/CeO_2-ZrO_2 Catalyst in a Packed Bed Tubular Reactor", *Chemical Engineering Science*, Vol. 62, No. 15, pp. 4012-4024, 2007.

Anderson, J. A., M. T. Rodrigo, L. Daza, and S. Mendioroz, "Influence of the Support in the Selectivity of Ni/Clay Catalysts for Vegetable Oil Hydrogenation", *Langmuir*, Vol. 9, No. 10, pp. 2485-2490, 1993.

Ayvaz, M., *The Theoretical Analysis of the Interaction Between Methane Dehydrogenation and Carbon Dioxide Dissociation Products with Ni and PtNi Surfaces*, M.S. Thesis, Boğaziçi University, 2010.

Banares, M. A., "Operando Methodology: Combination of *in situ* Spectroscopy and Simultaneous Activity Measurements under Catalytic Reaction Conditions", *Catalysis Today*, Vol. 100, No. 1-2, pp. 71-77, 2005.

Becerra, A. M., M. E. Iriarte, and A. E. Castro-Luna, "Catalytic Activity of a Nickel on Alumina Catalyst in the CO_2 Reforming of Methane", *Reaction Kinetics and Catalysis Letters*, Vol. 79, No. 1, pp. 119-125, 2003.

Beebe, T. P., D. W. Goodman, B. D. Kay, and J. T. Yates, "Kinetics of the Activated Dissociative Adsorption of Methane on the Low Index Planes of Nickel Single-Crystal Surfaces", *Journal of Chemical Physics*, Vol. 87, No. 4, pp. 2305-2315, 1987.

Bitter, J. H., K. Seshan, and J. A. Lercher, "On the Contribution of X-Ray Absorption Spectroscopy to Explore Structure and Activity Relations of Pt/ZrO_2 Catalysts for CO_2/CH_4 Reforming", *Topics in Catalysis*, Vol. 10, No. 3-4, pp. 295-305, 2000.

Bradford, M. C. J. and M. A. Vannice, "CO_2 Reforming of CH_4 over Supported Pt Catalysts", *Journal of Catalysis*, Vol. 173, No. 1, pp. 157-171, 1998.

Bradford, M. C. J. and M. A. Vannice, "CO_2 Reforming of CH_4", *Catalysis Reviews-Science and Engineering*, Vol. 41, No. 1, pp. 1-42, 1999.

Bradford, M. C. J. and M. A. Vannice, "The Role of Metal-Support Interactions in CO_2 Reforming of CH_4", *Catalysis Today*, Vol. 50, No. 1, pp. 87-96, 1999.

Cheng, Z. X., X. G. Zhao, J. L. Li, and Q. M. Zhu, "Role of Support in CO_2 Reforming of CH_4 over a $Ni/\gamma\text{-}Al_2O_3$ Catalyst", *Applied Catalysis A-General*, Vol. 205, No. 1-2, pp. 31-36, 2001.

Collins, S. E., M. A. Baltanas, and A. L. Bonivardi, "Infrared Spectroscopic Study of the Carbon Dioxide Adsorption on the Surface of Ga_2O_3 Polymorphs", *Journal of Physical Chemistry B*, Vol. 110, No. 11, pp. 5498-5507, 2006.

Çağlayan, B. S., *Design and Development of Catalysts & Adsorbents for CO_x Free H_2 Production*, Ph.D. Thesis, Boğaziçi University, 2011.

Damyanova, S., L. Daza, and J. L. G. Fierro, "Surface and Catalytic Properties of Lantanum-promoted Ni/Sepiolite Catalysts for Styrene Hydrogenation", *Journal of Catalysis*, Vol. 159, No. 1, pp. 150-161, 1996.

De Miguel, S. R., I. M. J. Vilella, S. P. Maina, D. S. Jose-Alonso, M. C. Roman-Martinez, and M. J. Illan-Gomez, "Influence of Pt Addition to Ni Catalysts on the Catalytic Performance for Long Term Dry Reforming of Methane", *Applied Catalysis A-General*, Vol. 435, pp. 10-18, 2012.

De Menorval, L. C., A. Chaqroune, B. Coq, and F. Figueras, "Characterization of Mono- and Bi-Metallic Platinum Catalysts Using CO FTIR Spectroscopy - Size Effects and Topological Segregation", *Journal of the Chemical Society-Faraday Transactions*, Vol. 93, No. 20, pp. 3715-3720, 1997.

Dias, J. A. C. and J. M. Assaf, "Autothermal Reforming of Methane over Ni/γ-Al_2O_3 Catalysts: The Enhancement Effect of Small Quantities of Noble Metals", *Journal of Power Sources*, Vol. 130, No. 1-2, pp. 106-110, 2004.

Fan, M. S., A. Z. Abdullah, and S. Bhatia, "Catalytic Technology for Carbon Dioxide Reforming of Methane to Synthesis Gas", *Chemcatchem*, Vol. 1, No. 2, pp. 192-208, 2009.

Faroldi, B. M., E. A. Lombardo, and L. M. Cornaglia, "Surface Properties and Catalytic Behavior of Ru Supported on Composite La_2O_3-SiO_2 Oxides", *Applied Catalysis A-General*, Vol. 369, No. 1-2, pp. 15-26, 2009.

Ferreira-Aparicio, P., M. Fernandez-Garcia, A. Guerrero-Ruiz, and I. Rodriguez-Ramos, "Evaluation of the Role of the Metal-Support Interfacial Centers in the Dry Reforming of Methane on Alumina-supported Rhodium Catalysts", *Journal of Catalysis*, Vol. 190, No. 2, pp. 296-308, 2000.

Ferreira-Aparicio, P., I. Rodriguez-Ramos, J. A. Anderson, and A. Guerrero-Ruiz, "Mechanistic Aspects of the Dry Reforming of Methane over Ruthenium Catalysts", *Applied Catalysis A-General*, Vol. 202, No. 2, pp. 183-196, 2000.

Ferreira-Aparicio, P., I. Rodriguez-Ramos, and A. Guerrero-Ruiz, "Methane Interaction with Silica and Alumina Supported Metal Catalysts", *Applied Catalysis A-General*, Vol. 148, No. 2, pp. 343-356, 1997.

Föttinger, K., R. Schlogl, and G. Rupprechter, "The Mechanism of Carbonate Formation on Pd/Al_2O_3 Catalysts", *Chemical Communications*, Vol. 3, pp. 320-322, 2008.

Gallego, G. S., C. Batiot-Dupeyrat, J. Barrault, and F. Mondragon, "Dual Active-Site Mechanism for Dry Methane Reforming over Ni/La_2O_3 Produced from $LaNiO_3$ Perovskite", *Industrial & Engineering Chemistry Research*, Vol. 47, No. 23, pp. 9272-9278, 2008.

Garcia-Dieguez, M., I. S. Pieta, M. C. Herrera, M. A. Larrubia, I. Malpartida, and L. J. Alemany, "Transient Study of the Dry Reforming of Methane over Pt Supported on Different γ-Al_2O_3", *Catalysis Today*, Vol. 149, No. 3-4, pp. 380-387, 2010.

Garcia-Dieguez, M., E. Finocchio, M. A. Larrubia, L. J. Alemany, and G. Busca, "Characterization of Alumina-supported Pt, Ni and PtNi Alloy Catalysts for the Dry Reforming of Methane", *Journal of Catalysis*, Vol. 274, No. 1, pp. 11-20, 2010.

Gould, T. D., M. M. Montemore, A. M. Lubers, L. D. Ellis, A. W. Weimer, J. L. Falconer, and J. W. Medlin, "Enhanced Dry Reforming of Methane on Ni and Ni-Pt Catalysts Synthesized by Atomic Layer Deposition", *Applied Catalysis A-General*, Vol. 492, pp. 107-116, 2015.

Gökaliler, F., *Characterization and Performance Analysis of Fuel Flexible OSR-WGS Catalysts*, Ph.D. Thesis, Boğaziçi University, 2012.

Greenler, R. G., K. D. Burch, K. Kretzschmar, R. Klauser, A. M. Bradshaw, and B. E. Hayden, "Stepped Single-crystal Surfaces as Models for Small Catalyst Particles", *Surface Science*, Vol. 152, No. 1, pp. 338-345, 1985.

Hattori, H. and Y. Ono, *Solid Acid Catalysis – From Fundamentals to Applications*, Pan Stanford Publishing Pte. Ltd., Singapore, 2015.

Holmgren, A., B. Andersson, and D. Duprez, "Interactions of CO with Pt/Ceria Catalysts", *Applied Catalysis B-Environmental*, Vol. 22, No. 3, pp. 215-230, 1999.

Hou, Z. Y., O. Yokota, T. Tanaka, and T. Yashima, "A Novel KCaNi/α-Al_2O_3 Catalyst for CH_4 Reforming with CO_2", *Catalysis Letters*, Vol. 87, No. 1-2, pp. 37-42, 2003.

Hu, Y. H. and E. Ruckenstein, "Isotopic Study of the Reaction of Methane with the Lattice Oxygen of a NiO/MgO Solid Solution", *Catalysis Letters*, Vol. 57, No. 4, pp. 167-169, 1999.

Ivanova, A. S., E. M. Slavinskaya, R. V. Gulyaev, V. I. Zaikovskii, O. A. Stonkus, I. G. Danilova, L. M. Plyasova, I. A. Polukhina, and A. I. Boronin, "Metal-Support Interactions in Pt/Al_2O_3 and Pd/Al_2O_3 Catalysts for CO Oxidation", *Applied Catalysis B-Environmental*, Vol. 97, No. 1-2, pp. 57-71, 2010.

Kester, K. B., E. Zagli, and J. L. Falconer, "Methanation of Carbon Monoxide and Carbon Dioxide on Ni/Al_2O_3 Catalysts: Effects of Nickel Loading", *Applied Catalysis*, Vol. 22, No. 2, pp. 311-319, 1986.

Knözinger, H. and P. Ratnasamy, "Catalytic Aluminas: Surface Models and Characterization of Surface Sites", *Catalysis Reviews-Science and Engineering*, Vol. 17, No. 1, pp. 31-70, 1978.

Korhonen, S. T., M. Calatayud, and A. O. I. Krause, "Structure and Stability of Formates and Carbonates on Monoclinic Zirconia: A Combined Study by Density Functional Theory and Infrared Spectroscopy", *Journal of Physical Chemistry C*, Vol. 112, No. 41, pp. 16096-16102, 2008.

Köck, E., M. Kogler, T. Bieltz, B. Klötzer, and S. Penner, "In situ FT-IR Spectroscopic Study of CO_2 and CO Adsorption on Y_2O_3, ZrO_2, and Yttria-Stabilized ZrO_2", *Journal of Physical Chemistry*, Vol. 117, No. 34, pp. 17666-17673, 2013.

Kroll, V. C. H., H. M. Swaan, S. Lacombe, and C. Mirodatos, "Methane Reforming Reaction with Carbon Dioxide over Ni/SiO_2 Catalyst - II. A Mechanistic Study", *Journal of Catalysis*, Vol. 164, No. 2, pp. 387-398, 1996.

Li, B. T., S. Kado, Y. Mukainakano, T. Miyazawa, T. Miyao, S. Naito, K. Okumura, K. Kunimori, and K. Tomishige, "Surface Modification of Ni Catalysts with Trace Pt for Oxidative Steam Reforming of Methane", *Journal of Catalysis*, Vol. 245, No. 1, pp. 144-155, 2007.

Lonergan, W. W., D. G. Vlachos, and J. G. Chen, "Correlating Extent of Pt-Ni Bond Formation with Low Temperature Hydrogenation of Benzene and 1,3-Butadiene over Supported Pt/Ni Bimetallic Catalysts", Journal of Catalysis, Vol. 271, No. 2, pp. 239-250, 2010.

Mahoney, E. G., J. M. Pusel, S. M. Stagg-Williams, and S. Faraji, "The Effects of Pt Addition to Supported Ni Catalysts on Dry (CO_2) Reforming of Methane to Syngas", *Journal of CO_2 Utilization*, Vol. 6, pp. 40-44, 2014.

Miyao, T., W. H. Shen, A. H. Chen, K. Higashiyama, and M. Watanabe, "Mechanistic Study of the Effect of Chlorine on Selective CO Methanation over Ni Alumina-Based Catalysts", *Applied Catalysis A-General*, Vol. 486, pp. 187-192, 2014.

Moradi, G. R., M. Rahmanzadeh, and S. Sharifnia, "Kinetic Investigation of CO_2 Reforming of CH_4 over La-Ni Based Perovskite", *Chemical Engineering Journal*, Vol. 162, No. 2, pp. 787-791, 2010.

Nandini, A., K. K. Pant, and S. C. Dhingra, "Kinetic Study of the Catalytic Carbon Dioxide Reforming of Methane to Synthesis Gas over Ni-K/CeO_2-Al_2O_3 Catalyst", *Applied Catalysis A-General*, Vol. 308, pp. 119-127, 2006.

Ni, J., L. W. Chen, J. Y. Lin, M. K. Schreyer, Z. Wang, and S. Kawi, "High Performance of Mg-La Mixed Oxides Supported Ni Catalysts for Dry Reforming of Methane: The Effect of Crystal Structure", *International Journal of Hydrogen Energy*, Vol. 38, No. 31, pp. 13631-13642, 2013.

Osaki, T., T. Horiuchi, K. Suzuki, and T. Mori, "Kinetics, Intermediates and Mechanism for the CO_2-Reforming of Methane on Supported Nickel Catalysts", *Journal of the Chemical Society-Faraday Transactions*, Vol. 92, No. 9, pp. 1627-1631, 1996.

Özkara-Aydinoğlu, S. and A. E. Aksoylu, "Carbon Dioxide Reforming of Methane over Co-X/ZrO_2 Catalysts (X = La, Ce, Mn, Mg, K)", *Catalysis Communications*, Vol. 11, No. 15, pp. 1165-1170, 2010.

Özkara-Aydinoğlu, S. and A. E. Aksoylu, "CO_2 Reforming of Methane over Pt-Ni/Al_2O_3 Catalysts: Effects of Catalyst Composition, and Water and Oxygen Addition to the Feed", *International Journal of Hydrogen Energy*, Vol. 36, No. 4, pp. 2950-2959, 2011.

Özkara-Aydinoğlu, S. and A. E. Aksoylu, "A Comparative Study on the Kinetics of Carbon Dioxide Reforming of Methane over Pt-Ni/Al_2O_3 Catalyst: Effect of Pt/Ni Ratio", *Chemical Engineering Journal*, Vol. 215, pp. 542-549, 2013.

Özkara-Aydinoğlu, S., E. Ozensoy, and A. E. Aksoylu, "The Effect of Impregnation Strategy on Methane Dry Reforming Activity of Ce Promoted Pt/ZrO_2", *International Journal of Hydrogen Energy*, Vol. 34, No. 24, pp. 9711-9722, 2009.

Pakhare, D. and J. Spivey, "A Review of Dry (CO_2) Reforming of Methane over Noble Metal Catalysts", *Chemical Society Reviews*, Vol. 43, No. 22, pp. 7813-7837, 2014.

Pan, Q. S., J. X. Peng, T. J. Sun, S. Wang, and S. D. Wang, "Insight into the Reaction Route of CO_2 Methanation: Promotion Effect of Medium Basic Sites", *Catalysis Communications*, Vol. 45, pp. 74-78, 2014.

Parizotto, N. V., D. Zanchet, K. O. Rocha, C. M. P. Marques, and J. M. C. Bueno, "The Effects of Pt Promotion on the Oxi-Reduction Properties of Alumina Supported Nickel Catalysts for Oxidative Steam-Reforming of Methane: Temperature-resolved XAFS Analysis", *Applied Catalysis A-General*, Vol. 366, No. 1, pp. 122-129, 2009.

Parkyns, N. D., "Influence of Thermal Pretreatment on Infrared Spectrum of Carbon Dioxide Adsorbed on Alumina", *Journal of Physical Chemistry*, Vol. 75, No. 4, pp. 526-531, 1971.

Pawelec, B., S. Damyanova, K. Arishtirova, J. L. G. Fierro, and L. Petrov, "Structural and Surface Features of PtNi Catalysts for Reforming of Methane with CO_2", *Applied Catalysis A-General*, Vol. 323, pp. 188-201, 2007.

Poncelet, G., M. A. Centeno, and R. Molina, "Characterization of Reduced α-alumina-supported Nickel Catalysts by Spectroscopic and Chemisorption Measurements", *Applied Catalysis A-General*, Vol. 288, No. 1-2, pp. 232-242, 2005.

Rege, S. U. and R. T. Yang, "A Novel FTIR Method for Studying Mixed Gas Adsorption at Low Concentrations: H_2O and CO_2 on NaX Zeolite and γ-Alumina", *Chemical Engineering Science*, Vol. 56, No. 12, pp. 3781-3796, 2001.

Rethwisch, D. G. and J. A. Dumesic, "Effect of Metal Oxygen Bond Strength on Properties of Oxides - 1. Infrared Spectroscopy of Adsorbed CO and CO_2", *Langmuir*, Vol. 2, No. 1, pp. 73-79, 1986.

Ruckenstein, E. and Y. H. Hu, "Role of Lattice Oxygen During CO_2 Reforming of Methane over NiO/MgO Solid Solutions", *Catalysis Letters*, Vol. 51, No. 3-4, pp. 183-185, 1998.

Ryczkowski, J., "IR Spectroscopy in Catalysis", *Catalysis Today*, Vol. 68, No. 4, pp. 263-381, 2001.

Seets, D. C., C. T. Reeves, B. A. Ferguson, M. C. Wheeler, and C. B. Mullins, "Dissociative Chemisorption of Methane on Ir(111): Evidence for Direct and Trapping-Mediated Mechanisms", *Journal of Chemical Physics*, Vol. 107, No. 23, pp. 10229-10241, 1997.

Son, I. H., S. J. Lee, and H. S. Roh, "Hydrogen Production from Carbon Dioxide Reforming of Methane over Highly Active and Stable MgO Promoted Co-Ni/γ-Al_2O_3 Catalyst", *International Journal of Hydrogen Energy*, Vol. 39, No. 8, pp. 3762-3770, 2014.

Stagg, S. M., E. Romeo, C. Padro, and D. E. Resasco, "Effect of Promotion with Sn on Supported Pt Catalysts for CO_2 Reforming of CH_4", *Journal of Catalysis*, Vol. 178, No. 1, pp. 137-145, 1998.

Steinhauer, B., M. R. Kasireddy, J. Radnik, and A. Martin, "Development of Ni-Pd Bimetallic Catalysts for the Utilization of Carbon Dioxide and Methane by Dry Reforming", *Applied Catalysis A-General*, Vol. 366, No. 2, pp. 333-341, 2009.

Sutthiumporn, K., T. Maneerung, Y. Kathiraser, and S. Kawi, "CO_2 Dry-Reforming of Methane over $La_{0.8}Sr_{0.2}Ni_{0.8}M_{0.2}O_3$ Perovskite (M = Bi, Co, Cr, Cu, Fe): Roles of Lattice Oxygen on C-H Activation and Carbon Suppression", *International Journal of Hydrogen Energy*, Vol. 37, No. 15, pp. 11195-11207, 2012.

Vindigni, F., M. Manzoli, T. Tabakova, V. Idakiev, F. Boccuzzi, and A. Chiorino, "Gold Catalysts for Low Temperature Water-Gas Shift Reaction: Effect of ZrO_2 Addition to CeO_2 Support", *Applied Catalysis B-Environmental*, Vol. 125, pp. 507-515, 2012.

Walter, K., O. V. Buyevskaya, D. Wolf, and M. Baerns, "Rhodium-Catalyzed Partial Oxidation of Methane to CO and H_2 – In situ DRIFTS Studies on Surface Intermediates", *Catalysis Letters*, Vol. 29, No. 1-2, pp. 261-270, 1994.

Wang, S. B., G. Q. M. Lu, and G. J. Millar, "Carbon Dioxide Reforming of Methane to Produce Synthesis Gas over Metal-supported Catalysts: State of the Art", *Energy & Fuels*, Vol. 10, No. 4, pp. 896-904, 1996.

Wang, H. and C. Au, "CH_4/CD_4 Isotope Effects in the Carbon Dioxide Reforming of Methane to Syngas over SiO_2-supported Ni catalysts", *Catalysis Letters*, Vol. 38, No. 1-2, pp. 77-79, 1996.

Wang, S. and G. Q. Lu, "A comprehensive Study on Carbon Dioxide Reforming of Methane over Ni/γ-Al2O3 Catalysts", *Industrial & Engineering Chemistry Research*, Vol. 38, No. 7, pp. 2615-2625, 1999.

Wei, J. M. and E. Iglesia, "Isotopic and Kinetic Assessment of the Mechanism of Reactions of CH_4 with CO_2 or H_2O to Form Synthesis Gas and Carbon on Nickel Catalysts", *Journal of Catalysis*, Vol. 224, No. 2, pp. 370-383, 2004.

Yang, R. Q., C. A. Xing, C. X. Lv, L. Shi, and N. Tsubaki, "Promotional Effect of La_2O_3 and CeO_2 on Ni/γ-Al_2O_3 Catalysts for CO_2 Reforming of CH_4", *Applied Catalysis A-General*, Vol. 385, No. 1-2, pp. 92-100, 2010.

Yates, J. T. and C. W. Garland, "Infrared Studies of Carbon Monoxide Chemisorbed on Nickel and on Mercury-poisoned Nickel Surfaces", *Journal of Physical Chemistry*, Vol. 65, No. 4, pp. 617-624, 1961.

Zecchina, A., E. E. Platero, and C. O. Arean, "Low Temperature CO Adsorption on Alum-Derived Active Alumina: An Infrared Investigation", *Journal of Catalysis*, Vol. 107, No.1, pp. 244-247, 1987.

Zhang, J. G., H. Wang, and A. K. Dalai, "Development of Stable Bimetallic Catalysts for Carbon Dioxide Reforming of Methane", *Journal of Catalysis*, Vol. 249, No. 2, pp. 300-310, 2007.

Zhang, Z. and X. E. Verykios, "Mechanistic Aspects of Carbon Dioxide Reforming of Methane to Synthesis Gas over Ni catalysts", *Catalysis Letters*, Vol. 38, No. 3-4, pp. 175-179, 1996.

Zhu, X. L., P. P. Huo, Y. P. Zhang, D. G. Cheng, and C. J. Liu, "Structure and Reactivity of Plasma Treated Ni/Al_2O_3 Catalyst for CO_2 Reforming of Methane", *Applied Catalysis B-Environmental*, Vol. 81, No. 1-2, pp. 132-140, 2008.